Università degli Studi di Torino
Doctoral School of the University of Torino
PhD Programme in Chemical and Materials Sciences XXXIII Cycle

Development of multifunctional materials for aesthetical and smart automotive components.

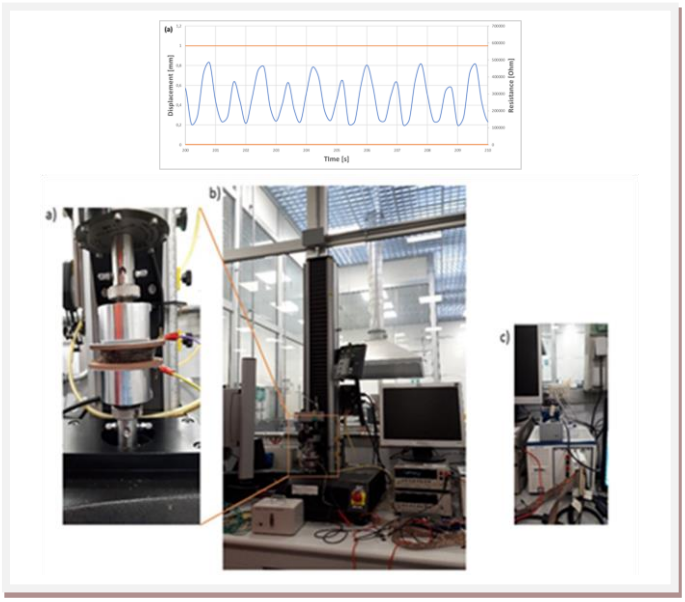

Enea De Meo

Supervisor:
Prof. Marco Zanetti

Abstract

Nanocomposite polymers with electrical properties are interesting academic and industrial field. In particular, CNT and other carbonaceous filler added to functional polymer as polyurethane both thermoplastic and thermosetting have been explored in this project resulting from the collaboration between Fiat research center and chemistry department of the University of Turin. Piezoresistive behaviour of different nanocomposite material was characterized in order to understand their suitability in automotive field for smart component.

Chapter 1 describes the main characteristics of the CNT and the polyurethane with particular attention to the automotive scenario. The percolation theory and the piezoresistive effect, which are the fundamental physics phenomena investigated, is detailed described and literature reference of the main theory are reported for each argument. The aim of this work has been developing a simple method for piezoresistive polyurethanes/CNT sensors and achieving multifunctional properties in a single mono material component. Chapter 2 shows the state of the art for these materials and the main production methods. Moreover, dispersion methods for obtaining multifunctional polymers are described and compared in order to have a clear understanding of strengths and weaknesses of the different methodologies.

This project was developed in two different activities, the first dedicated to the development of three kind of PU-CNT foams: PU-CNT 1.5%, PU-CNT-COOH 1.0 %, and PU-CNT-COOH 1.5 % and carried out in the laboratories of Fiat Research center and the department of chemistry of the university of Turin. Materials, developed production method, detailed description of the testing facilities are deeply described in Chapter 3.1 to 3.2. The second part, which is dedicated to the piezoresistive characterization of thermoplastic polyurethane skin loaded with GNPs, is described in subparagraph 3.2.6. The TPU/GNP skin was produced by an important nanotechnology industry named Avanzare (Spain). The goal of the project was to characterize the skin produced in Graphene core 2 in order to understand their applicability as a piezoresistive sensor. The sample preparation and the electromechanical characterization of the skin were performed at the ICE/HT department of University of Patras. Results of all these activities is shown in Chapter 4.

In particular, Subparagraphs 4.1.1 4.1.2 and 4.1.3 shows the chemical and morphological characterization of the PU/CNT and PU/CNT-COOH produced samples. Moreover, the subparagraphs 4.1.4 and 4.1.5 describe the piezoresistive behaviours obtained respectively from PU and CNTs foam composites and TPU/GNP skin. We observed that Polyurethane with CNT-COOH showed an insulating-conductive transition phenomenon when the foam reaches the 80% of its compression strain with a gauge factor (Gf) of about 30. Instead, PU-CNT showed conductivity only at 1.5% of filler concentration and a steady piezoresistive behaviour with a Gf of 80. However, this samples did not show the insulating-conductive transition. Instead, we discovered that the best condition of use for obtaining the best performance of TPU/GNP skin are deformation rate of 0.5 Hz and maximum displacement of 1 mm. The obtained samples show also a steady long-term performance up to 1000 of cycles.

The results show that having improved the electromechanical properties of final nanocomposite polyurethane foam with different fillers, CNT and CNT-COOH, demonstrates that the proposed method can be applied differently for design sensors and switches. Moreover, the result achieved with TPU/GNP skin ensure its applicability as a control switch for automotive dashboard.

The outlook in Chapter 5 describes improvements for smart polyurethane foam and skin reached with this work. The results of this work will be the starting point for the evaluation of new types of matrices, with a view to environmental sustainability. Eventually, it will be necessary to address the issue from an economic point of view and establish if the higher cost of CNTs could be afford by future profit that will come from better customer perceived quality. For the economic point of view seems more interesting the application of GNP instead of CNT for lower cost and improved production method. Another interesting aspect that emerged from this work is the behaviour of CNT and CNT-COOH of the final nanocomposite properties. Further study could investigate and better understand the percolation mechanisms of different carbonaceous fillers. Finally, more effort should be done for obtaining materials with tuneable and more homogenous properties.

Figure index

Index

Acronym

CB	carbon black
CNT	carbon nanotube
CNTs	carbon nanotubes
GNPs	graphene nanoplatelets
GF	gauge factor
HMI	Human machine interface
MDI	methylene diphenyl diisocyanate
MWCNTs	mutli-walled carbon nanotube
PU	polyurethane
rGO	reduced graphene oxide
SWCNT	single walled carbon nanotube
SHM	structural health monitoring
SEM	scanning electron microscopy
TEM	transmission electron microscopy
TGA	thermogravimetric analysis
TPU	thermoplastic polyurethane
XRD	x-ray diffraction

1 Chapter 1: Introduction

1.1 Smart Materials and automotive scenario

Research in material science involve not only discovering novel properties or materials but also including multiple and unique functionalities in the same object. Usually, materials that shows more than one functionality like piezoresistivity, piezoresistivity, special mechanical properties (i.e. pseudoelasticity, etc) are called smart materials. In general, smart materials are composite materials made with a matrix that is usually polymeric loaded with a filler. In this context, automotive materials research is changing in the direction of smart vehicles where inter-vehicle communication systems support applications related to safety, comfort, info-mobility and passenger entertainment. The current production of cars is subjected to implementation requests in terms of amount and typologies of human-machine interface (HMI), e.g. switches and adjustment knobs, placed mainly in the dashboard or door panels. However, the environmental limitations imposed by European Commission and governments concern the reduction of non-renewable materials and the emission limitation that can be reached only lowering the weight of the final vehicle. The prevalent strategy for obtaining the environmental compliance goals is removing metal elements such as metal wires and heavy metal parts and replacing them with polymeric based smart materials. Furthermore, multifunctional materials could incorporate several properties of non-renewable materials and also have a lower weight respect them. Nowadays, automotive tools are complex system made with different materials and interconnected with metal wires the whole system represent the on-board vehicle electronic systems. The command button, sensors and connection wires are typically implanted in the plastic dashboard and this step increases manufacturing time and cost. Differentiation of non-renewable materials and plastic component for recycling is also a costly process. Several strategies have been attempted to get nanocomposite with different properties like conductivity and piezoresistivity (electrical wiring). Researchers found that the addition of carbonaceous nano-filler (graphene nano platelets (GNP) , or carbon black (CB) or carbon nanotubes (CNT)) to commercial polymer composites can

improve the mechanical behaviours [1,2], thermal conductivity [3–5], electric conductivity [5–8] and piezoresistive behaviour [7,9–11].

The infotainment systems are also composed of complicated parts whose are made up of several materials (silicon, rare metals, polymers, copper). Figure 1 shows the body computer of the vehicle, which has the same feature of a normal computer, and it is placed just behind the dashboard. Moreover, the system manages the window lifter, mirrors, door locks, starting, anti-theft alarm, steering switch. The principal electric command are seats, hoods, sunroofs, keys, remote controls. Figure 2 shows an example of configuration of the navigator and radio system.

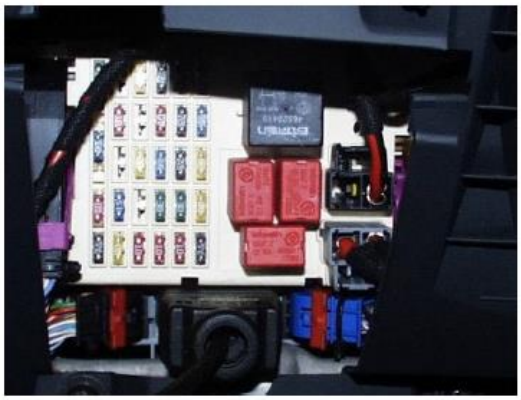

Figure 1 The body computer of the vehicle.

Figure 2 Digital entertainment system of vehicles.

1.2 Polymer Nanocomposites

Polymer nanocomposites have been extensively studied because of their versatility in terms of properties, fields of application and very high workability. The first application of bending polymers with nanofillers started in 1990 within automotive field with the sol-gel process discovered by Japanese researchers. The novel idea was to obtain functional and structural properties with the same material in order to simplify and improve the operation and capability of the final device/application. Moreover, nanomaterials have had a great impact in all field that is medicine [12], engineering [13–16], chemistry [13,17,18] and physic [19–21]. For instance new polymer nanocomposites are developed in order to improve human body compatibility for implant [22]. Polymer nanocomposites showed also multifunctional properties including electromechanical and electrochemical [23,24]. The goal of this study is to investigate and obtain polymers loaded with carbonaceous fillers and evaluate their electromechanical behaviour.

1.3 Polyurethanes

The basic discovery of Polyurethane was made by Wurtz in 1849. In fact, he obtained an aliphatic isocyanate with an organic sulphate and a cyanate. Furthermore, the first industrialization has been fine-tuned by DuPont only in 1950 and DuPont sold the first polyurethane in 1956. The family of polyurethanes includes a long list of different polymers that have in their formula urethane links. Figure 3 shows the generic formula of a polyurethane with the urethane group.

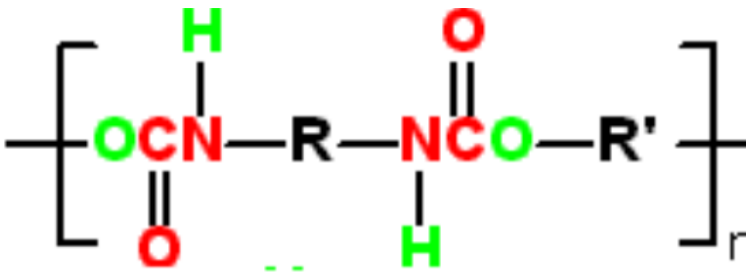

Figure 3 Polyurethane formula

The reaction between an isocyanate and a polyol is the basis to produce polyurethane. Furthermore, additives as catalysts and surfactants are added to control the reaction. Expanding agent is also an important ingredient in order to have and control the final foam structure of expanded polyurethanes. Polyols are a chemical species that have in their formula one or more hydroxy groups (*OH) and are a fundamental component in the polyurethane reaction formation. The chemicals that could be classified as a polyol are different. For instance, some of these are erythritol, xylitol, sorbitol, mannitol, maltitol, isomaltose, lactitol, polyglycitol. Moreover, isocyanate are chemical species that have in their formula the isocyanate group (-N-C-O). The most used isocyanate is methylene diphenyl diisocyanate (MDI), toluene diisocyanate (TDI), hexamethylene diisocyanate (HDI) isophorone diisocyanate (IPDI). Every possible combination of polyol and isocyanate generates a different polyurethane. The final structure of a polyurethane could be schematized as a chain of soft segment (polyol) and hard segment (isocyanate). The different behaviour of these two parts is related to glass transaction. In fact, soft segments have a lower glass-transaction temperature than hard segments, which is higher than the application temperature. In thermosetting polyurethanes, cross linking also takes place chemically, for this to be possible the functionality of the monomers must be greater than 2. During the reaction, the isocyanate could react with water (H_20) and forming new chemical species that is amine and carbon dioxide. The CO_2 remain trapped inside the polyurethane structure and forms cells and struts that is the typical structure of the polyurethane foams. There are two types of polyurethane foam: open cell and closed cell. Each of these two different materials has characteristics and properties that are ideal in particular applications. The closed cell polyurethane foam, commonly called "spray polyurethane" is a semi-rigid product with variable density from $1*10^{-5}$ kg/cm^3 up to over 100 kg/cm^3. Its mechanical resistance, usually proportional

to the density, makes it perfect in the construction of foundations for floors, protection, and insulation of walls in contact with the ground, for some types of waterproofing and roofing as well as in an infinite number of industrial applications from boating to automotive. Closed cell polyurethane has a completely different property. In fact, the closed-cell foam, like PVC foam, are waterproof because the fluid can not to penetrate inside the structure. Moreover, the mechanical behaviour is more elastic than open-cell structured polyurethane [25]. Figure 4 shows a digital image with the two polyurethane different structure: open-cell and closed-cell polyurethane.

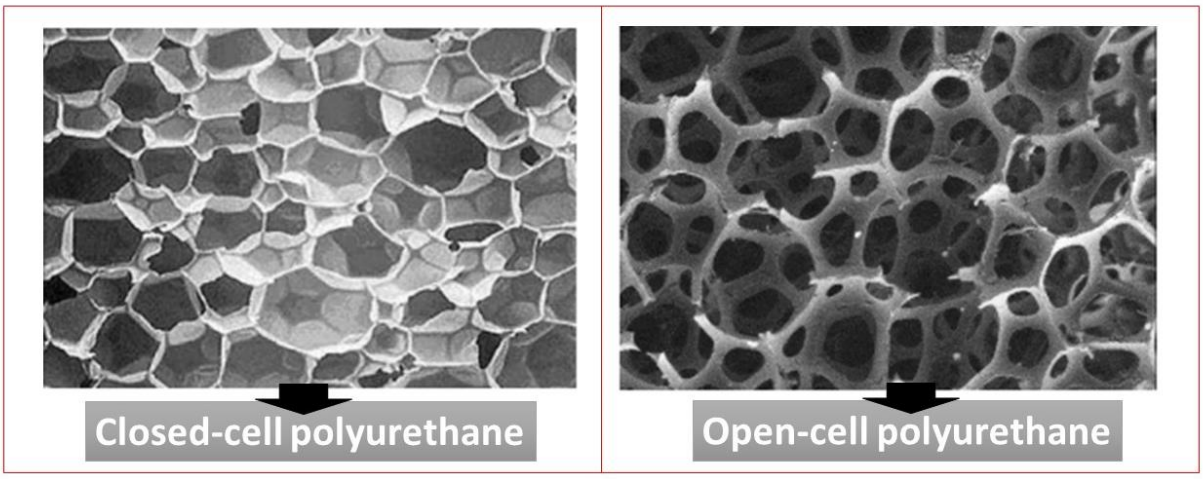

Figure 4 Different image representation of polyurethan cell structure, closed-cell and open-cell.

1.4 Carbonaceous structures

Carbon is an element known since ancient times. Carbon gets its name from the Latin word “carbo”, which meaning is charcoal or coal, that is one of the fundamental materials that has allowed the evolution of the humankind thanks to important energy stored in its structure. The natural materials in that carbon that could be find as a single constituent element are three: graphite, diamond, and fullerene. Moreover, each structure is representative of typical hybridizations of the carbon atom orbitals. The hybridization of carbon atoms inside graphite structure are sp^2. Carbon atoms inside diamond structure have a hybridization of sp^3. Fullerene is a particular configuration of carbon atoms gradually increasing the C number the final structure tends to a balloon shape. This particular configuration weakens the π bond and at the same time requires a re-hybridization of the atomic orbitals p, incorporating a partial

contribution of s character. The result is atomic orbitals p of character $s^x p$ (with x << 1). Figure 5 shows the three allotropic form of the carbon atom.

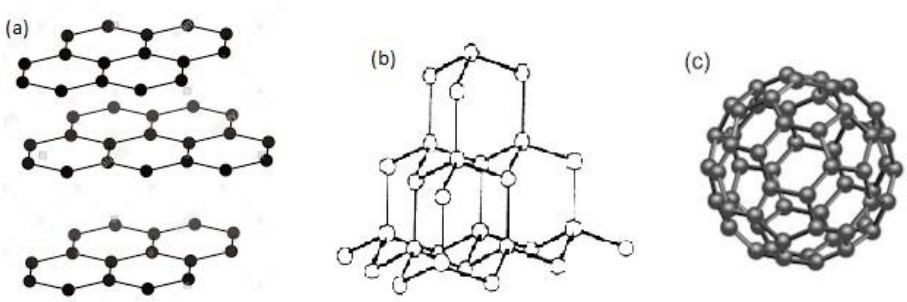

Figure 5 Allotropic structure of carbon atoms.

Moreover, chemists discovered and produced new carbon allotropic forms. The most important are carbon nanotubes (CNT) and Graphene. The property of this new material is completely different from the common allotropic structure. After that several studies discovered their property and their potential application.

1.5 Carbon nanotubes (CNT)

Different method has been developed to obtain new kind of carbon allotropic structures. One of the first and most known and studied is surely carbon nanotubes. The chemist Richard E. Smalley after the discovered of fullerene noticed also that the carbon atoms after a while tends to roll up in a cylindric structure. Sumo Iijima thanks to TEM microscope saw for the first time CNT structure. The hybridization of carbon atoms in CNT is always sp^2, the same of graphite. In fact, it is possible to think at CNT as a rolled graphene sheet. Moreover, the properties of CNT was discovered an excellent diversified application assets [26]. Figure 6 shows a graphical image of CNT structure.

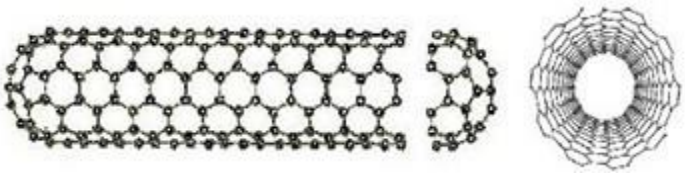

Figure 6 Nanotube with a single wall.

CNT could have one or more wall and several production methods for obtaining single wall CNT (SWCNT) and multi wall CNT (MWCNT) were established. Chemical Vapor Deposition (CVD) is one of the best strategies for creating CNT without defects and with higher electrical and mechanical properties [27]. Metal catalyst foil or particle, which could be Nickel or Cobalt, have been placed inside a chamber in which a mixture of acetylene and hydrogen have been fluxed at pressure of 20 kPa for 2 hours. The dimensions and the structure of CNT strongly depends on the metal catalyst and on the process conditions. Figure 7 shows the results obtained in [28] where it is possible to see how the morphologies of CNT varies with the temperature of the process.

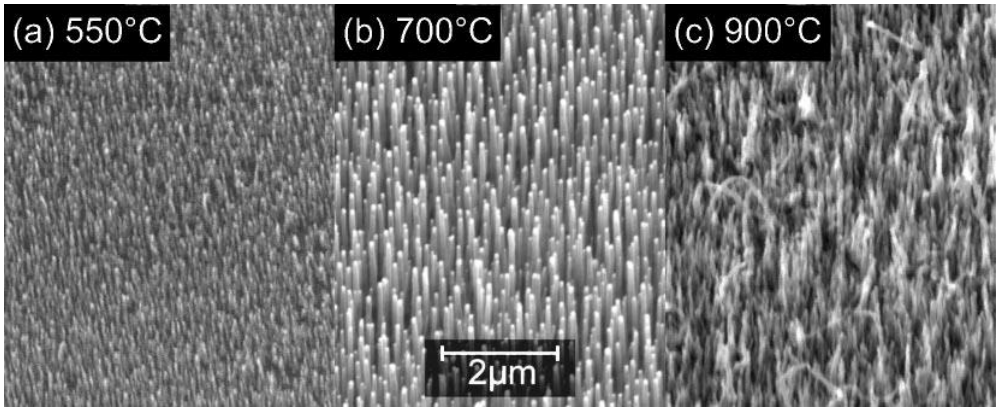

Figure 7 Image of CNT growth with different temperature of the process, [28].

CNT showed remarkable values of mechanical and electrical properties i.e Young's modulus of 1 TPa, tensile strength of 100 GPa and electrical conductivity upper than 100 S/m [29]. Peculiar and interesting aspect of CNT are not only the high electrical conductivity but also the very high aspect ratio until to

132,000,000:1 [30] that leads a very minimal percolation threshold when added in a matrix. Furthermore, embedding of CNTs produced stress sensitivity capability to the nanocomposite polymers, called piezoresistive material, which can be used for pressure sensors or structural health monitoring (SHM) [31]

.

1.6 Interesting properties of CNT

CNT are the strongest materials discovered in terms of tensile strength and elastic modulus. This high mechanical properties outcomes from the covalent sp^2 bonds formed between the individual carbon atoms. MWCNT was assessed to have a tensile strength of 63 GPa [32]. However, the weak interaction among walls of CNT dramatically reduce the tensile strength of the CNT bundle[33]. Table 1 shows mechanical and physical properties of CNT.

Mechanical properties	MWCNT	SWCNT
Elastic modulus	0.28-1 TPa	1 TPa
Elongation at bk	N.F	59%
Tensile strength	10-60 GPa	100-500 GPa
diameter	10-80 nm	1-3 nm
Lenght	10-100 μm	50 μm

Table 1 Mechanical and physical properties of CNT.

Having a structure similar to graphene, CNT possess also a very high conductivity. However, the peculiar structure of the CNT dramatically affects the value of electrical conductivity. As in the graphene, the carbon atoms are arranged in hexagonal structures but in the realization of the tubular shape this hexagon can be arranged with different orientation leading to a different chiral structure. Armchair CNT share electrical properties similar to metals while the zigzag and chiral CNT possess electrical properties similar to semiconductors [34]. Table 2 showed the overall electrical and thermal properties of CNT.

Mechanical properties	MWCNT	SWCNT
Electrical conductivity	10^4-10^8S/m	10^4-10^8S/m
Thermal conductivity	1500 W/m-k	1500 W/m-k
Thermal stability	750°C (air)	750°C (air)

Table 2 Electrical and thermal properties of CNT.

Theoretical studied showed that conductive nanotubes can carry an electric current density of 4×10^9 A/cm^2 that is more than 1,000 times bigger than metals could reach (copper), the current densities in this metals are limited by electromigration [35]. The mechanism of electron conduction inside CNT are widely studied. Furthermore, the electron transport inside the CNT could be explained only with the quantum channelling theory. The dimension of CNT diameter is in the order of few nanometre and the electrons must propagate only through the length of the CNT shape. The maximum electrical conductance of a single-walled carbon nanotube is $2G_0$, where $G_0 = 2e^2/h$ is the conductance of a single ballistic quantum channel [36]. Figure 8 explain a visual concept of the quantum tunnelling effect. The probability of finding the electron beyond on higher potential barrier is not zero as in the classical physics but decreases with the distance.

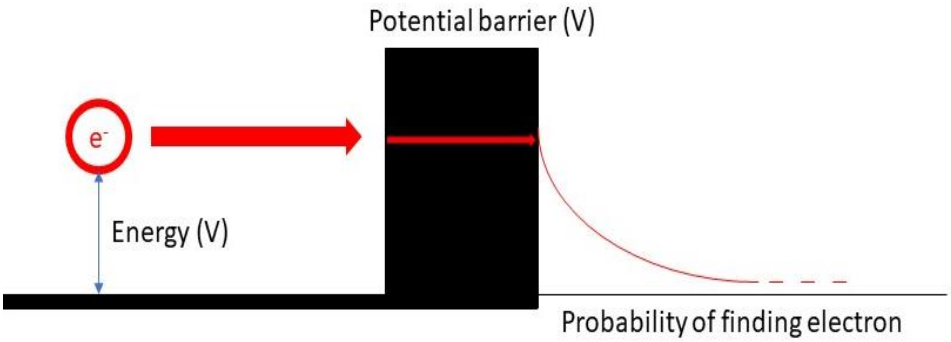

Figure 8 Graphical representation of quantum channel effect.

This model could also explain how it is possible the electrical transport of electron inside a continuous network of CNT. The quantum tunnelling effect could explain how the electron current could flow from one CNT to others. The mathematical formula which describes the probability of tunnelling is $P= Ge^{-2kL}$ where G and k are two factors which depends on the energy of the potential barrier and the electron energy and L is the length of the tunnelling distance.

1.7 Percolation Theory

The network formation and the dynamics of that have been extensively explored and a detailed theory was found to explain the behaviour on CNT inside a polymer matrix. Network could be described as bond and nodes between objects or entities. In the material science field, we find several cases in which the formation of a network is observed. For example, the nucleation of crystals, the dispersion of fillers inside a matrix etc. The first approach to network formation and percolation problem was given by Broadbent & Hammersley in 1957. The problem addressed in their studied involved the path creation of a fluid (filler) inside a medium (matrix). Given the probability for a fluid particle to fill a position inside a path. They tried to define a statistical function which describe the probability of finding a percolation path defined as the

path which allowed to completely cross the medium [37]. Research in Nanocomposite material started from the common percolation problem to develop models with the aim of define a specific concentration value reaching the percolation inside the matrix and this has allowed to obtain material with interesting properties such as electric conductivity and piezoresistivity. Moreover, the conductivity of a nanocomposite material filled with conductive nanoparticles, such as CNT, is commonly described by [38,39]:

$$\sigma = \sigma_0(\rho - \rho_c)^t$$

Where σ_0 is the conductivity of the filler, ρ is the volumetric fraction of the filler, ρ_c is the volumetric fraction at the percolation and t is the critical exponent. The critical concentration of CNT for reaching percolation inside a matrix is a complex problem and it depends on dispersion degree, interaction between CNT, surface tension. When the percolation is reached, we can assume a continuous network of CNT inside the material which could carry electron. The overall resistance of nanocomposite material is composed by several contributions. Firstly, the fundamental resistance of CNT that depends only on CNT and their structure. Secondly, the resistance due to CNT-CNT interaction that depends on CNT contact resistance and tunnelling resistance. The generalized formula of tunnelling resistance is widely described by [20] in all cases we can derive:

$$R_T\ (V, S, \varphi)$$

Where R_T is the tunnel resistance and V is the applied voltage, S is the gap in Amstrong between adjacent CNT and φ is the height of the potential barrier. This resistance will tend to infinity when the gap tends to micron and the barrier tend to infinity. Furthermore, the existence of tunnelling resistance is due to quantum channel effect and strongly depends on the gap between CNT. In particular, the variation of tunnelling resistance exponentially depends on the CNT gaps. Figure 9 is an example of percolation curve; the chart shows a typical behaviour of nanomaterials loaded with different weight percentage of CNT.

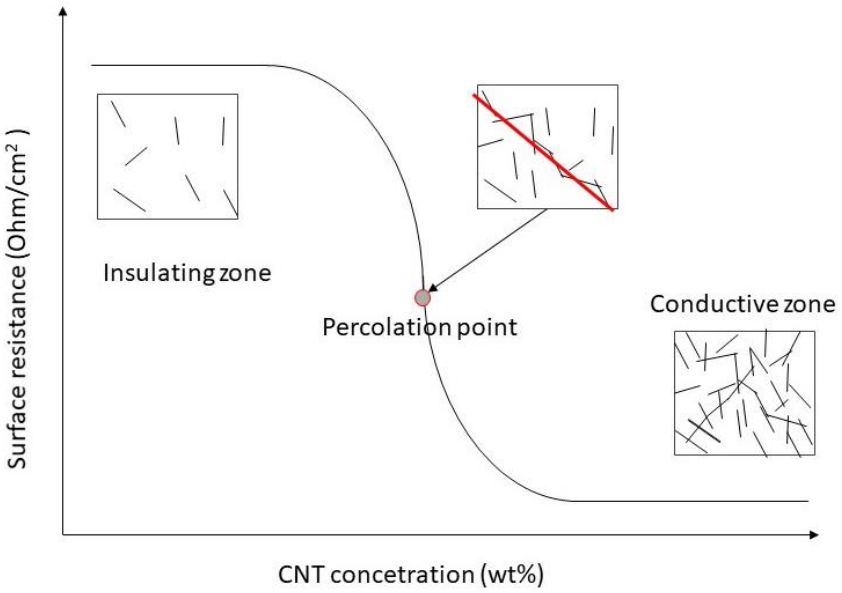

Figure 9 Percolation curve of a nanomaterial load with different percentage of CNT.

In the first part of the curve in Figure 8 the quantity of filler is too low to form a CNT conductive network therefore is not possible to see any effect on the electric resistance of the composite material. As the amount of CNT increases, conductive paths begin to form, the CNTs approach each other and the contact area between the particles increases and when the first path could be formed that concentration is called percolation threshold consequently the resistance of the nanocomposite starting to decrease, and the current could flow through the material. Beyond the concentration threshold, the tunnel resistance and the contact resistance between CNT reach their minimum value and therefore an increase in conductivity is not obtained even by further increasing the concentration [40].

1.8 Piezoresistivity

The piezoresistive effect is the modification of the electrical resistivity of a material when mechanical strain is applied on it. Therefore, the major parameters that must be monitored during piezoresistive tests are the mechanical deformation and the electric resistance. The mechanical deformation depends on the imposed pressure above the specimen and it can be defined as the ratio between the elongation and the initial dimension of piezoresistive specimen as it is showed in the following formula (in this case the deformation is expressed in percentage):

$$\varepsilon = \frac{elongation(l)}{length\ (l_0)} \cdot 100$$

A piezoresistive nanocomposite must change in its resistance, and resistivity after a mechanical deformation for being classified as it is. These two physical parameters are related through the Ohm second low:

$$R = \rho \cdot \frac{l}{A}$$

Where R is the resistance, ρ is the resistivity and l is the length of the specimen and A is the section surface. The resistivity, which is expressed in Ω·cm, is an intrinsic property of a specific material that quantifies how strongly a given material opposes the flow of the electrical current.

Piezoresistive materials have some free electric charges that allows the electric transport. Therefore, when a piezoresistive material is integrated into an insulating matrix it creates conductive paths inside the matrix and it leads to a big variation of the resistivity of the nanocomposite with small pressure.

The main parameter used for evaluating the piezoresistive response is the Gauge Factor which is usually expressed as *GF* or *Q*:

$$GaugeFactor(GF) = \frac{R - R_0 / R_0}{L - L_0 / L_0} = \frac{R - R_0}{R_0 \varepsilon} = \frac{\Delta R}{R_0 \varepsilon}$$

Where R_0 is the unstrained material electric resistance, R is the material electric resistance when a specific strain is applied and ε is the strain of the material which leads to a specific resistance value (L_0 is the initial length of the sample and L is the length after a deformation).

When the variation of the electric resistance of the material is the highest with the lowest deformation the Gauge Factor is maximum. In this way, we can use the piezoresistive effect with the minimal deformation, otherwise with minimal stress.

The piezoresistivity is a complex physical phenomenon because depends on several parameters such as the structural properties and the charge transport inside the material. The piezoresistive effect of our piezoresistive materials is due to the graphene network inside the matrix. The aspect ratio is one of the most important parameters for the piezoresistive behaviour. It is also important to consider the matrix properties as well as the intrinsic resistivity (ρ_{polym}) and the resistivity that can be due to some fillers (for instance additives, carbon black, oxides, etc.) inside the matrix (ρ_{add}). Furthermore, the types of graphene structures and matrices selected as well as the mixture phases, like the percentage (i.e., the volumetric fraction, ν) and the level of dispersion inside the matrix are all crucial factors. The electric resistance change is mainly due to the conductive network. In particular, CNT are linked thanks to the insulating polymer matrix, when a mechanical stress appears and the matrix is deformed, the GNPs are moved away from each other and the resistivity of the material change dramatically due to a rearrangement of the conductive network. The resistance of the material must be in the order of 1-1000kΩ. In fact, nanocomposites with this resistance value have a highly deformable conductive network and this ensure the highest variation of resistance and therefore the highest GF.

2 Chapter 2: State of the art

Considerable number of substances have been tested to produce CNT/nanocomposites with piezoresistive properties, but more and not exotic polymers, fillers and filler/matrix combinations should be investigated to target industrial applications, starting from polymers already widely used in automotive industry.

2.1 Polyurethane/CNT

Different methods for obtaining polyurethane/CNT nanocomposite with interesting properties have been developed so far. The main strategy for fabricating nanocomposite sensors made with polyurethane and carbonaceous fillers could be divided in two different approaches: the direct melt-compounding of the filler with the molten polymer and the dispersion of the filler in a polymer solution with the need to remove the solvent at the end of the dispersion process. The most common strategy reported in literature for PU consist of a coating process that involves a carrier solvent that allows the deposition of CNT. A particularly illustrative example for this approach is certainly the work published by Amit Tawari and co-workers [41]. They produced a piezoresistive polyurethane sponge by dipping a commercial PU sponge into a rGO/MWCTN ink. Two type of carbonaceous fillers MWCNT, reduced Graphene Oxide and commercial polyurethane foam were retained. The first step was the production of an Ink made with hydrazine monohydrate and a dual component additive composed of benzisothiazoline and methylisothiazolinone (5:1 ratio by volume) in which MWCNT and rGO was dispersed by ultrasonication. The ink was used to dip a commercial polyurethane foam and then the sample has been dried in vacuum oven at 70°C. Figure 10 shows the scheme proposed in the article which explain the production process and the set-up for testing piezoresistivity.

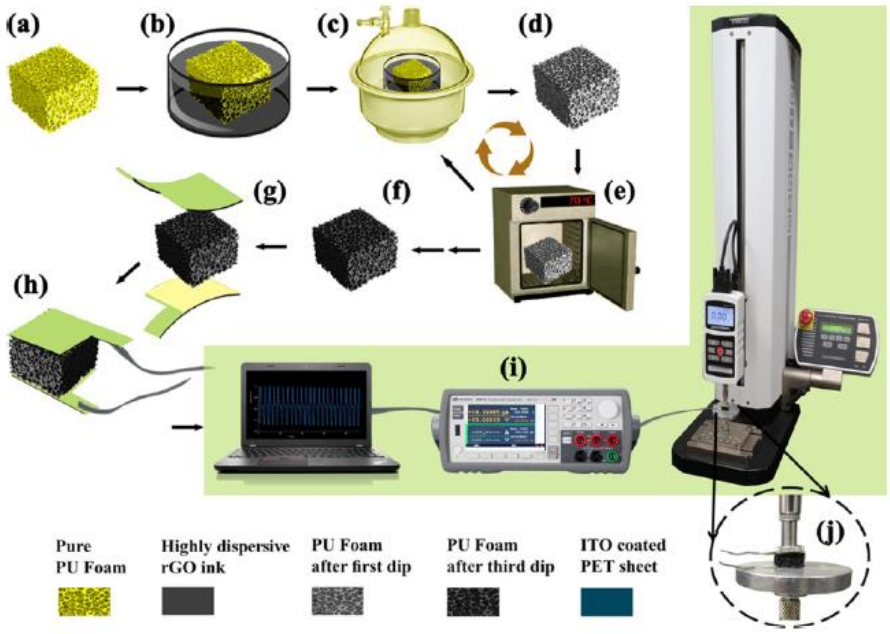

Figure 10 The process proposed by Amit Tawari [41] *for the production of nanocomposite polyurethane foam for pressure sensing application.*

The produced PU/CNT-rGO foam was placed between two ITO coated PET electrodes and then characterized with a tensile testing machine and a multimeter for measuring deformation and resistance, respectively. The samples also showed conductivity and excellent piezoresistive behaviour. Figure 11 showed the results of electromechanical characterization, published by Amit Tawari, of the nanocomposite sensors. In particular, the piezoresistive behaviour could be clearly seen after 52% of the strain with a Gauge factor of -2.13. Moreover, the sample was subjected to several cycles to understand the reliability of the piezoresistive response. Researchers also demonstrated the possibility of acquiring vital signal from the human body. These results clearly shown that the PU/MWNT-RGO has ability to detect strain and therefore information from the human body. The major problem of this technology is the reproducibility is very difficult to obtain samples with the same characteristics. Moreover, the use of solvent is not convenient in terms of environmental safety and for the economical point of view. This kind of procedure is not suitable in a large-scale production.

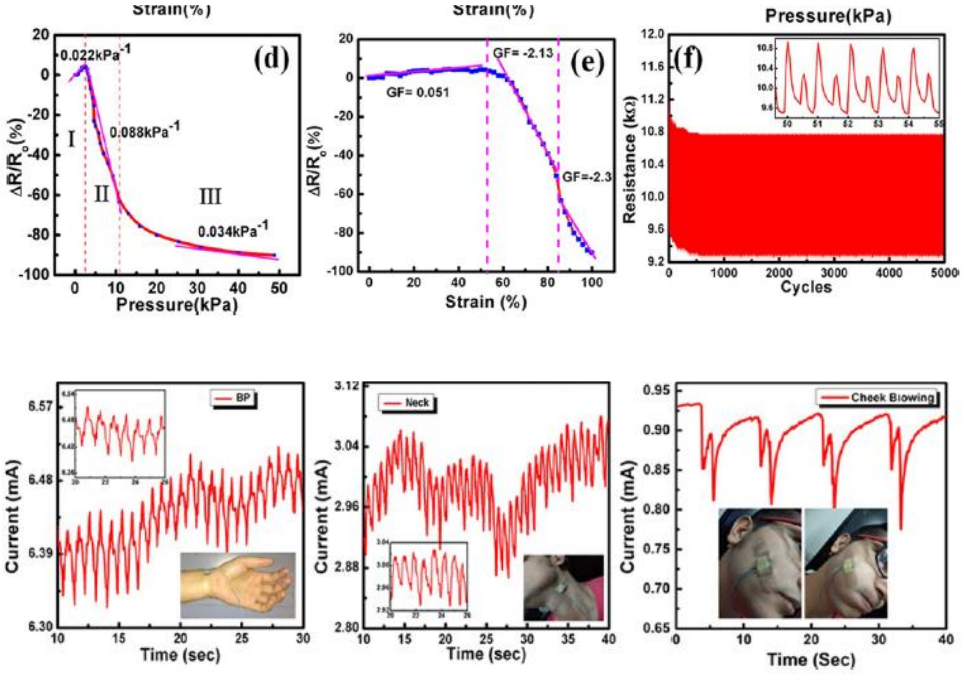

Figure 11 Results of piezoresistive characterization obtained in [41]

The second strategy for obtaining piezoresistive sensors with nanocomposite material concern the dispersion of CNT directly into the polymers or one of the main components without solvent evaporation. Xiang-Bin Xu and co-workers developed an innovative method for producing PU/CNT foam dispersing CNT directly into the polyol solution and then adding isocyanate for producing conductive nanocomposite foam [42]. The MWNT used in this study have a diameter of 20 to 40 nm and a length of 30 micron. The components for the synthesis of PU included polyether polyol and polyisocyanate, additives and distilled water. The purified CNTs were mixed with polyether polyol in the vessel. The vessel was immersed in a water bath at 100°C. After that the CNT dispersion obtained with an ultrasonic bath. Finally, the isocyanate was added to the solution and placed in a closed mould for obtaining the final nanocomposite foam. The characterization of the expanded foam was performed with SEM microscopy for morphology and the electrical conductivity with multimeter. Figure 12 shows the percolation curve, and the SEM images of the sample with 2% of CNT.

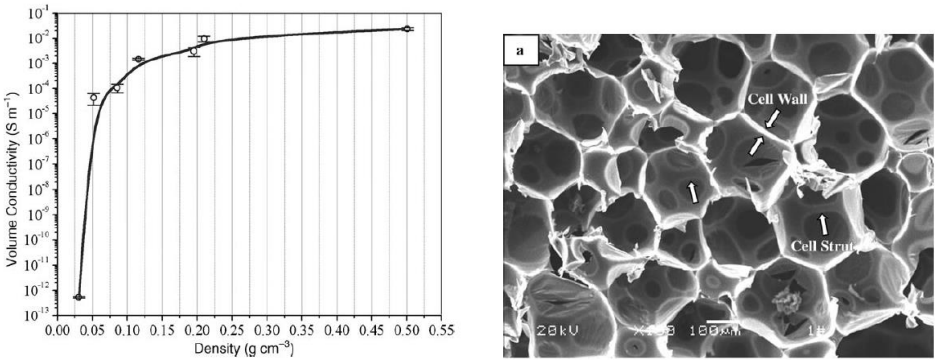

Figure 12 The percolation curve and SEM image of PU/CNT 2%.

In this study a conductive polyurethane foam was produced with only 2%wt of CNTs. Moreover, they noticed that the electrical conductivity changed considerably with the density of the final foam. This phenomenon could be explained with the modification of the cell structure. In fact, foam with lower density showed bigger air bubble and smaller junction among them. Hereupon, CNTs are placed mainly in the cell strut reducing their number inside the junction road. Consequently, foams with lower density showed less probability to have percolation path inside the nanocomposite reducing the conductivity of the final samples. In conclusion, Xiang-Bin Xu and co-workers produced an ultralight conductive polymers with a weight-reduction of 92 % [42]. Moreover, they observed for the first time a conductor-insulator transition controlled by the density of the final nanocomposite foam. The percolation of the polyurethane foam strongly depends on the morphological and structural property of the cell the cell-strut network.

Tianliang Zhai and co-workers [43] obtained a piezoresistive polyurethane foam by mixing the polyol solution with CNTs and final adding the PM-200 diisocyanate. The dispersion methods utilized for obtaining a fine dispersion of CNT was the ball milling method. The PU/CNT composite foam showed enhanced electromechanical properties, piezoresistive properties, stress and strain sensitivity. The nanocomposite foam has also better compression strength compared to standard PU. The resistance response of samples under cyclic compressive loading was reliable during time. Different CNT samples concentration were achieved: unfilled foam 0%, foams with 0.3 %, foams with 0,5%, foams with 1,0%, foams with 1,5 % and 2%. The nanocomposite foams were characterized at mechanical and electrical level. Figure 13 showed the results of the compression tests on PU/CNT foam with different CNT

concentration. Figure 14 shows the set-up used by Tianliang Zhai and co-workers for characterize electromechanical and piezoresistive properties of nanocomposite foams.

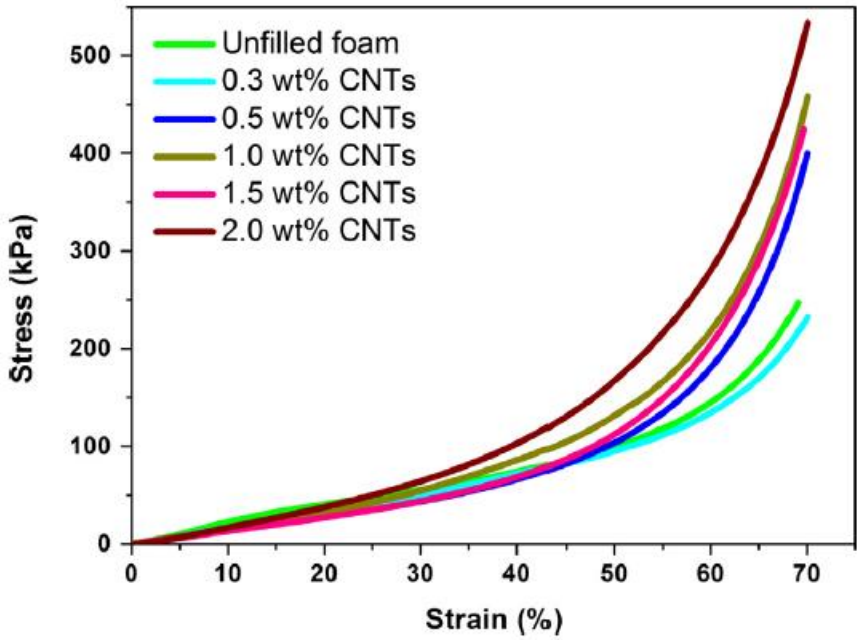

Figure 13 Results of compression tests, obtained in [43]*, on PU/CNT sample at different concentration from 0 to 2%.*

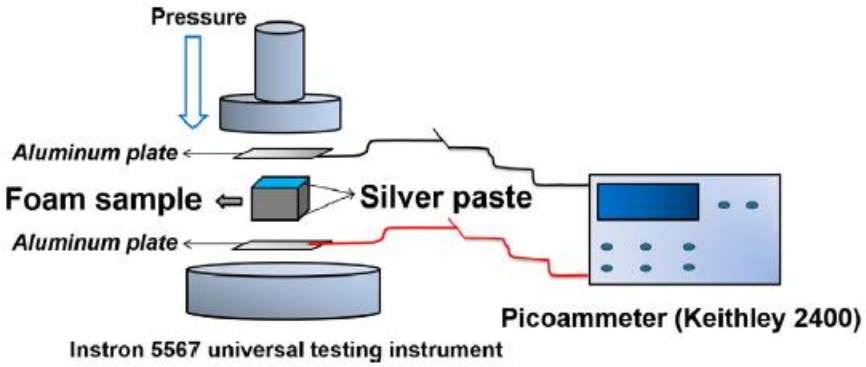

Figure 14 The set-up for piezoresistive characterization used by Tianliang Zhai and co-workers.

The results of compression tests showed clearly that the increasing of CNTs is responsible for hardening of the final nanocomposite sample. The sample with 2.0% of CNT is the hardest reaching 500 kPa that is

150 kPa higher than unfilled foam. The nanocomposite foam containing 0.5% of carbon nanotubes showed the largest strain sensitivity for the resistance. The PU/CNT foams were characterized under cyclic deformation for measure piezoresistive behaviour. Figure 15 shows the cyclic deformation together with the electric resistance of the PU/CNT sample with 0.5%.

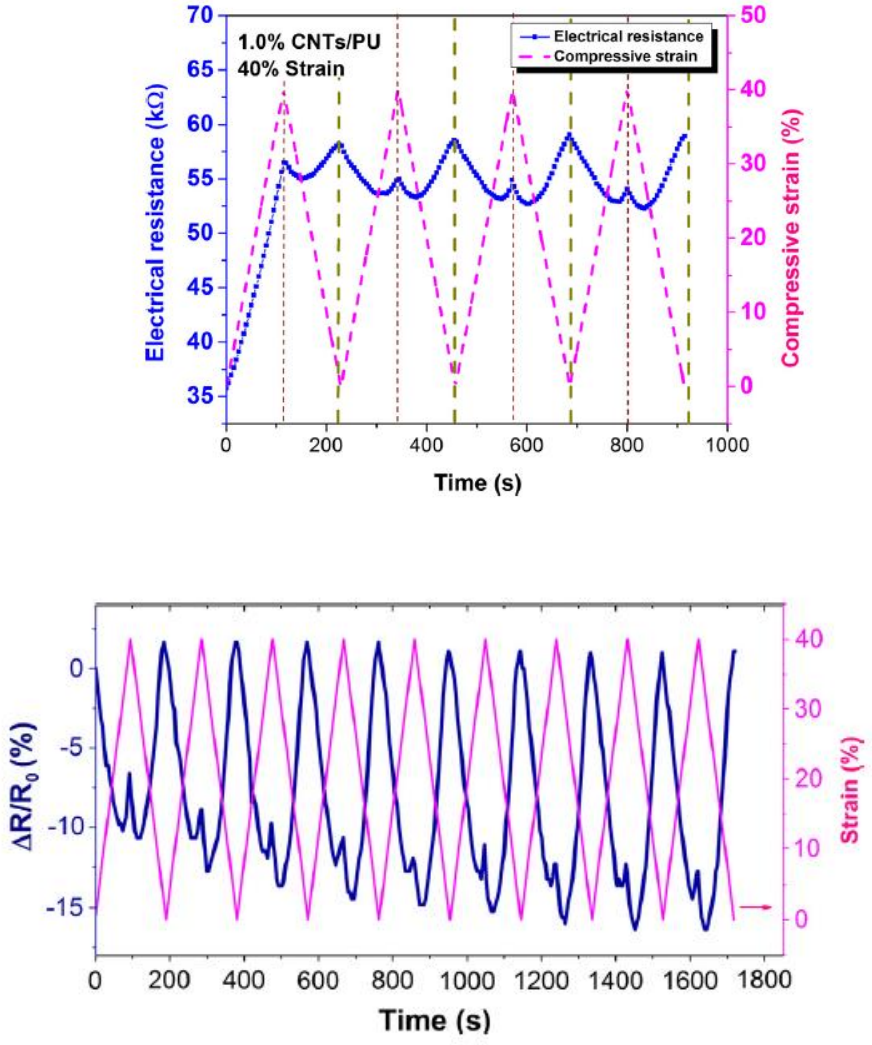

Figure 15 Results of piezoresistive tests, obtained in [43]*, on PU/CNT 1%.*

A negative pressure coefficient was observed. Moreover, the PU/CNT samples showed a continuously decreasing of electric resistance when a pressure was applied on the edge of the samples. As described

before the piezoresistive effect is due mainly to the modification of the percolative CNT network inside the material. Therefore, the CNTs inside the material become more closely and the tunnelling resistance decrease with the average CN-CNT distance. Another important effect showed by PU/CNT sample is a resistance relaxation phenomenon. The samples not immediately recovered the initial value of electrical resistance because of internal relaxation of struts. This behaviour is very similar to the viscoelasticity of elastomeric polymers. Pure elastic polymers when subjected to a loading-unloading cycle immediately recover the unstrained shape following the same stress and strain curve without any deviation. Furthermore, elastomeric polymers during a deformation-relaxation cycle do not follow the same stress and strain curve but they show a hysteresis loop that represents the energy lost as heat during the experiment. Figure 16 shows the results of loading-unloading cycle obtained with PU/CNT foam and a comparison among curves acquired with pure elastomeric polymer.

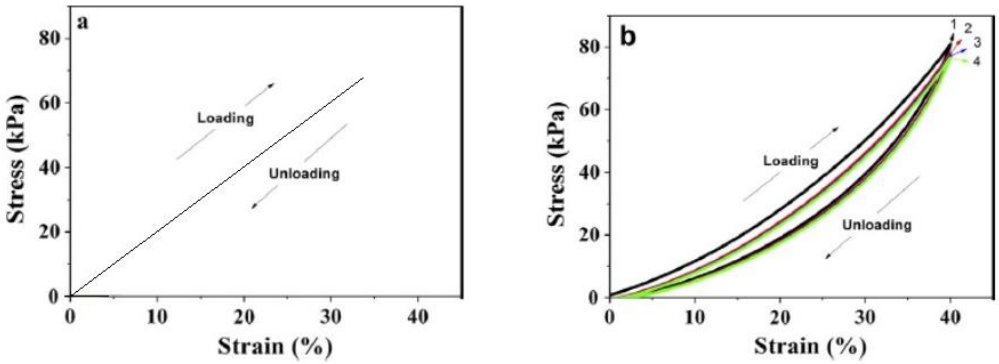

Figure 16 Comparison between a loading-unloading curve obtained with a pure elastic polymer (a) and the same curve obtained with the PU/CNT samples.

The stress relaxation inside a viscoelastic polymer strongly depends on the time. This means that the recovering process is not an instantaneous process but the stress starting to decrease exponentially after the force removal from the sample. The formula proposed by [43] is:

$$\sigma(t) = \sigma_1 t^{-n}$$

Where t is the time in minute, σ_1 is the stress after 1 minute of relaxation and n is the relaxation index of the material. Similarly, to the stress relaxation phenomenon is showed also the electrical resistance. Therefore, the electric resistance decreasing with the time after removing the stress as showed for the stress itself. Moreover, the proposed formula is very similar to the stress time dependence:

$$R(t) = R_1 t^{-n'}$$

Where t is the time in minute, R_1 is the stress after 1 minute of relaxation and n' is the resistance relaxation index of the material. Moreover, the stress relaxation and resistance relaxation follow different mechanisms. The decreasing of stress inside the material is always higher than the recovery of resistance. In other words, the characteristic of resistance relaxation of CNT/PU composite foam is different from the stress relaxation due to the different relaxation mechanism. During compressive stress relaxation, the CNT/ PU foam composites have excellent resistance recoverability while poor stress recoverability.

2.2 Dispersion methods

The major problem related to the fabrication of polymer nanocomposites is the nanofiller dispersion inside the polymeric matrix. CNTs are generally produced and sold as a complex powder in which CNTs

are strongly interconnected each other forming agglomerates. Since the aim is to obtain nanocomposite with smart functionalities with a relatively low concentration of CNTs uniformly distributed it is important to mechanically disaggregate and disperse CNT inside the polymer as best possible as possible. Several methods were experimented to obtain this result. However, the objective of obtaining a homogenous CNTs distribution is not related only to the used method but also with the compatibility between filler and matrix. For example, some solvents are more effective for the CNTs dispersion for their molecular structure which can penetrate inside the CNT agglomerates and promote the deagglomerations. The parameter that indicates the solubility of one material in other is called Hansen parameter. The CNTs have strong Van der Walls interaction among them and they tend to merge in agglomerates also after a strong dispersion process. The most known CNT dispersion techniques are: ultrasonication, high shear mixing, ball milling, calendering. A way to enhance the dispersion is to improve the interaction between the polymer matrix and the filler trough a chemical functionalization of the CNT.

2.2.1 Ultrasonication

Ultrasonication mechanism concerns ultrasound energy to stir entire particles in a mixture. Usually, this process required an ultrasonic bath or an ultrasonic horn, also known as a sonicator. Figure 17 shows a digital image of this instrument. The theory of this practice is that when ultrasound spreads through a series of compression, reduced waves are induced in the nanoparticles through which it passes. The production of these shock waves supports the ‘‘peeling off” of individual nanoparticles located at the external part of the nanoparticle bundles, or agglomerates, and thus results in the separation of individualized nanoparticles from the bundles. Ultrasonication is one of the most used and reliable method to obtain a very good CNTs dispersion in liquids substances: dimethylformamide (DMF), ethanol, water and acetone. However, polymers have a very high viscosity, completely different from common solvents, and one strategy could be adding solvent with CNT dispersion in molten polymer and then drying the solvent. Sonicators have a power of about 100W at 20–23 kHz. Horn sonicators have an adjustable amplitude ranging from 20% to 70% and a power until 1500 W [44–47]. However, the duration and the power of such technique could damage CNTs and reduce the average length of CNT [48].

Figure 17 Example of ultrasonication instruments for laboratory dispersion of nanofillers.

2.2.2 High shear mixing

High shear mixing technique is used for dispersing nanofillers directly into high viscosity polymers. The main parameters controlled by high shear mixing procedure is the round per minute of the blade and the shape of stator and blade. This instrument is not suitable for low viscosity fluid as solvents. The objective is to destroy agglomerate with shear forces and homogenize the final solution polymer/nanofiller [47,49,50]. The negative aspect of high shear mixer is that the treated solution incorporates a lot of air and another vacuum treatment is necessary in order to extract the trapped air form the final material. Moreover, the duration and the power of such technique could damage CNTs and reduce the average length of CNT [48]. Figure 18 shows a digital photo of the high shear mixer. The particles go through shear forces when one area of liquid goes with a different relative rate to a contiguous part. The velocity of the external part of the blade will be higher than the velocity of the stator and this differential will generates shear forces.

Figure 18 High shear mixer.

2.2.3 Three roll mills

Another interesting method for dispersion of nanoparticles as CNTs is called calendering. The name of the instrument used for this method is called three roll mills. This method is inspired to the process for smoothing the paper or metal sheet. The working principle is the production of high pressure between rotating rollers. The solution with polymers and CNT goes through a series of rotating rollers with a very small gap between them[51,52] . The pressure and the rotating forces induce inside the fluid high shear forces that cause the rupture of agglomerates. The efficiency of the process could be measured with the area ratio between area of CNTs agglomerates and the total visible area. If the ratio decrease more effective is the dispersion process. This method showed good results in dispersing CNT inside polycaprolactone (PCL) and ethylene–vinyl acetate (EVA) and polypropylene (PP) [53]. Three roll mills

dispersion method demonstrated also high degree of dispersion. The principal effect of finite dispersion is the enhancement of mechanical properties such as the fracture toughness[54]. Well dispersed CNTs showed also high adhesion level with the matrix confirmed by the absence of pull-out phenomenon[54]. Moreover, the final composite with less than 0,1 % of CNT showed conductivity so a well stabilised percolation network[54]. Figure 19 shows a digital image of three roll mills machine.

Figure 19 Three roll mill.

2.2.4 Ball milling

Ball mill is an instrument composed by hard metal balls with different diameters placed inside a rotating or shaking metal cylinder. Originally ball milling was used for griding coal. Furthermore, the same approach could be successfully used for griding many various fillers such as pigment, additives, powder. Firstly, the method was applied to reduce the granulometry of fillers. Secondly, the method showed good

results also in homogenize solid or liquid dispersions. The first step is to place material and fillers inside the metal cylinder with metal balls, the polymer matrix is inserted from the left (cone 60°) instead the powder enters on the right (cone of 30°). Figure 20 shows a technical draft of the ball milling machine. Subsequently, the cylinder starts to rotate on the central axis. The rolling motion drags the metal balls in the upper side of the cylinder and the gravity force causes these objects to impact on the materials. The consistent elements in between the balls and ground are reduced in size resulting from these collisions. Moreover, the fillers mechanically infiltrate the matrix guaranteeing a good cohesion. However, dispersed fillers showed seriously modification caused by the action of metal balls. The energetic process could promote the broken end of nanofiller such as CNTs under the action of the impact of steel balls by ball milling processing. The degradation of CNT was noticed after long lasting treatments and the treatment induces other carbon structure such as fullerenes [55].

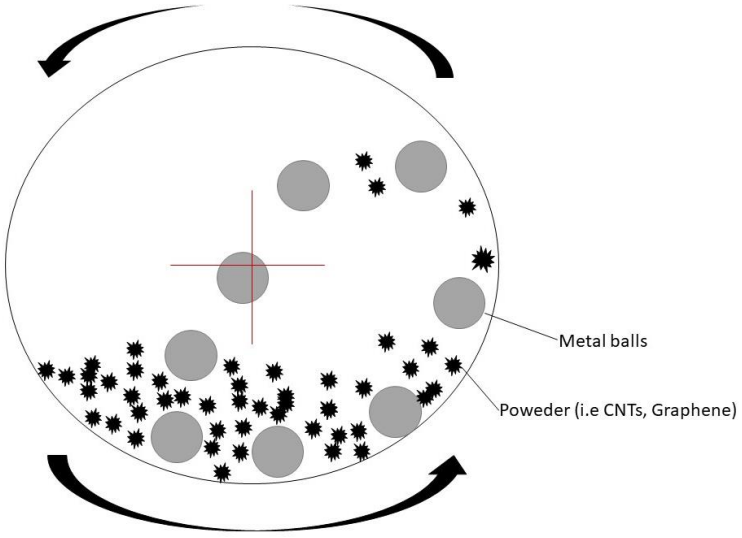

Figure 20 Ball milling machine and working principle.

2.2.5 Dispersion improvement: Functionalization and Hansen parameter.

Mechanical dispersions are very effective methods and could be applied almost in any case. However, the major limitation to apply this method alone without other strategies is represented by the different chemical nature of materials. In fact, dispersing one substance in another is not only question of

mechanical homogenization, according to Hansen theory, but the chemical affinity of different species is also fundamental for obtaining a stable solution. The methods that could be choose for homogenize the final mixture there are several strategies for achieving better dispersion that could be applied in parallel despite the choice of the dispersion methods. Therefore, it is advantageous to overcome the chemical compatibility problem with the chemical functionalization. The novelty of this approach consists of modifying the interaction surface between matrices and fillers. Moreover, the crucial point is reducing the cohesion forces among fillers (Van Der Waals forces for CNT) to having more significant interactions, such as hydrogen bonding, with the polymeric matrix. Therefore, the best strategy is to modify the surface of the fillers. The functionalization is a valuable method for improving the chemical compatibility that could support the main dispersion method but does not represent a method for obtaining the dispersion alone. In fact, functionalization is a second step strategy after choosing the most appropriate mechanical dispersion method.

The method for obtaining chemical functionalization of fillers such as CNTs could be divided in two categories: chemical and physical methods. Chemical methods concern the alteration of carbon chemical bonds. In particular, the hybridization of the C atoms from sp2 to sp3 in order to grab functional group otherwise the defect transformation. The advantages of this approach consist in avoiding agglomeration inside the matrix, good interaction bond with specific polymers. However, this method could not be easy to use specially in the functionalization phase and the CNT could be damaged and loss their peculiarities. Physical modification technique is represented by polymer wrapping ($\pi-\pi$ bonds), surfactant absorption (Physical absorption) and endohedral method (capillarity effect). The main characteristic of all physical method is avoiding the CNTs damage. Generally, this technique is easier to use respect to chemicals. However, the interaction forces are not to strong and the CNTs could agglomerate inside the polymer. Better dispersion was reached also with both methods. Nanda Gapol Shaoo and co-workers developed a method to disperse functionalised CNTs with carboxylic group (COOH) inside the DMF and surfactant solution with ultrasonication method. The solution was added into polyurethane and then stirred for solvent evaporation. The final PU sample showed an increasing of tensile strength and modulus of about

750% [56]. SEM characterization showed also better adhesion respect to non-functionalised CNT. The functional groups on the CNTs surface promote and accelerate the dispersion of nanofillers. Moreover, surface connection among CNTs and polyurethane chain was improved with the use of surfactant. Figure 21 showed the scheme of CNT-polyurethane interaction and the improvement obtained with functionalized CNT obtained in [56].

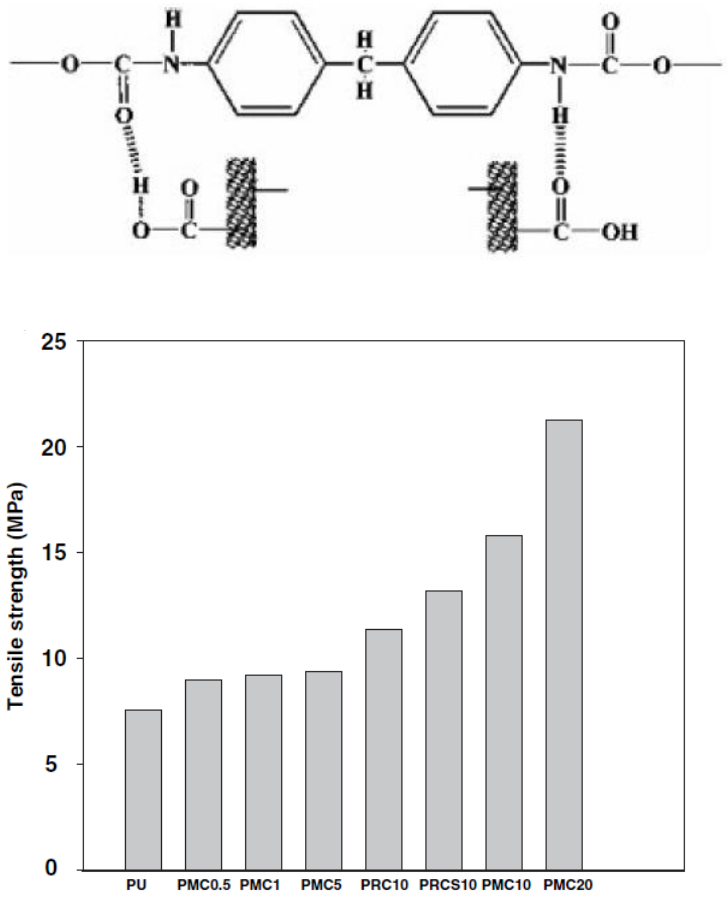

Figure 21 Schematic molecular representation of PU/CNT-COOH and results of mechanical characterization of PU and PU/CNT-COOH (PM and PRC).

Functionalization of CNT with carboxyl group is not suitable in any case. In fact, CNT without functionalization dispersed in thermoplastic polyurethane with high shear methods showed better performance and lower percolation threshold (2,5%) compare to CNT-COOH 5%. This is mainly due to higher defects induced in CNT-COOH respect to CNT [57].

2.3 Aim of the work

The ground-breaking objectives of this doctoral project entail the creation of several functionalities embedded in a single component by developing smart nanocomposite components and industrial exploitation of the process in automotive case. New way of manufacturing components allowing new opportunities for aesthetic design. The main goal of the project is going to a complete integration of devices and electrical circuits on interiors parts of the vehicle, (e.g. dashboard modules or door panels) that allows new possibilities of design with piezoresistive switches and/or capacitive knobs harmoniously integrated on interior automotive components surface without adding any mechanical switches or knobs. The components or their composite suitable as a part of conductive circuits purpose, on the rear of the dashboard that are not visible to the consumer, are approximately near the percolation threshold that it is not reached when the composite is produced. In fact, the main breakthrough of the project consists in the production of materials that can be electrically active with an external pressure. The entire industrial production process could be simplified avoiding extra-material component and create “in situ” sensors. The “in situ” processed devices will be interfaced with electronic devices. Other conductive nanocomposites will be exploited for sensing purpose. The main activities during the first year was aimed to acquire knowledge on the nanocomposites suitable for automotive use case and on the comprehension of piezoresistive mechanism in terms of the interaction nanofiller and polymer substrate. Information and materials harvested during the first year was essential for the activities of the second year. Several attempts were done in order to investigate fillers and matrices. Polyurethanes resulted as the most interesting for piezoresistive application because their high deformability which resulted in biggest sensitivity. Furthermore, the most promising nanocomposites was subjected to mechanical and chemical characterization. In particular CNTs, CNT-COOH and GNP were investigated and studied in order to obtain a suitable production method for industrial use case. The effect of the major parameter of piezoresistive application was studied and related for optimizing the conductive samples on the dashboard component. During the last year all the experimental activities related to chemical-physical characterization of smart nanocomposite polymers was carried out. In particular, Thermogravimetric Analysis (TGA) and electron

microscopy (SEM) was performed to better understand the working principle and properties of the new materials.

3 Experimental section

3.1 Materials and method

Polyurethane

The components for the synthesis of Polyurethane (PU) foam included polyether polyol and isocyanate were kindly furnished by BASF (Germany). The PU utilized was the same adopted on the FCA dashboard which name is ELASTOFLEX E. The main components of this commercial product are: (i) polyether polyol based on: Polyol, catalyst, additives. (ii) isocyanate, PMDI = iso 133/6. For the technical information we referred to the Technical Data sheet shown on Figure 22. Important data was the density, the component temperature, and the free rise density. The last information describes the final density of the foam and give us an indication about the ratio of expansion in order to calculate the possibility of percolation threshold inside a foam structure. Moreover, the density allowed us to estimate the CNT percentage for obtaining the percolation compare to the polyurethane foam produced within the state of the art. Another important aspect to consider is the ratio between polyol and isocyanate for obtaining the same quality, aspect and rigidity of the foam already used in a modern automotive dashboard.

Technical Data Sheet

Elastoflex® E 3595/101

BASF
The Chemical Company

Application

Polyurethane (PUR) semi rigid foam for the production of instrument panels for the automotive industry.

Chemical Characteristics

Polyol-Component: Preparation based on: polyol, catalyst, additives
Iso-Component: Preparation based on: P-MDI = Iso 133/6

Supply

The type of supply for the components will be decided after consultation with our Sales Office.

Storage, Preparation

Polyurethane components are moisture sensitive. Therefore they must be stored at all times in sealed , closed containers.The A-component (Polyol) must be homogenised by basic stirring before processing.More detailed information should be obtained from the separate data sheet entitled "Information for in-coming material control, storage, material preparation and waste disposal" and from the component data.

Possible Hazards

The B-component (Isocyanate) irritates the eyes, respiratory organs and the skin. Sensitisation is possible through inhalation and skin contact. MDI is harmful by inhalation. On processing these, take note of the necessary precautionary measures described in the Material Safety Data Sheets (MSDSs). This applies also for the possible dangers in using the A-component (Polyol) as well as any other components.See also our separate information sheet " Safety- and Precautionary Measures for the Processing of Polyurethane Systems."
Use our Training Programme " Safe Handling of Isocyanate."

Waste Disposal

More detailed information is provided in our country -specific pamphlet.

Consumer articles, medical products

There are national and international laws and regulations to consider if it is intended to produce consumer articles (eg articles that necessitate food or skin contact,toys etc.) or medical objects out of BASF Polyurethanes GmbH products. Where these do not exist , the current legal requirements of the European Union for consumer articles as well as medical products should be sufficient. Consultation with our Sales Office and our Ecology and Product Safety Department is strongly recommended.
.

PU Solutions
Elastogran

Component Data

Characteristics	Unit	Polyol-Comp	Iso-Comp.	Method
Density (25°C)	g/cm³	1.03	1.21	G 133-08
Viscosity (25°C)	mPa·s	1300	155	G 133-07
Shelf-life	months	6	6	
Recommended storage temperature	°C	≥ 20	≥ 20	

Typical Processing Data

Cup Test

Characteristics	Unit	Value	Method
Component temperature	°C	23	
Weight	g	A = 100 B = 56	
Start time	s	11	G 132-01
Rise time	s	84	
Free rise density	kg/m³	48	

Machine Processing

Characteristics	Unit	Value	Method
Mixing ratio	parts per weight	A = 100 B = 56	
Processing temperature	°C	25 - 35	
Mould temperature	°C	40 - 50	

BASF
The Chemical Company

Typical Physical Properties

Characteristics	Unit	Measured value	Method
Density	kg/m³	102	DIN EN ISO 845
Tensile strength	kPa	352	DIN EN ISO 1798
Elongation at break	%	83	
Compression stress (40 %)	kPa	44,8	DIN EN ISO 3386

BASF Polyurethanes GmbH
Postfach 1140
49440 Lemförde
Germany

Tel.: +49 (0) 5443/12-0
Fax: +49 (0) 5443/12-2020
Mail: pu-spezialsysteme@basf.com
Internet: www.pu.basf.eu

PU Solutions
Elastogran

Figure 22 Thecnical data sheet of the polyurethane used for the production of pizoresistive CNT foam.

CNT

The multi-walled CNTs, CNT-OH and CNT-COOH with a purity of >95 wt.-% with a diameter of 8 nm and a length of about 10-30 um were purchased from NanoAmor Nanostructured & Amorphous Materials, Inc. (USA). Figure 23 shows the Energy Dispersive X-Ray spectroscopy results given by the producer.

Components	Contents (%)
C	97.46
Al	0.19
Cl	1.02
Co	1.09
S	0.24

Components	Contents (%)
Multi-walled nanotubes	> 95
-OH	3.52-3.89
C	Bal.
Al	0.03
Cl	0.09
S	0.12

Components	Contents (%)
Multi-walled nanotubes	> 95
-COOH	2.43-2.67
C	Bal.
Al	0.03
Cl	0.09
S	0.12

Figure 23 Results of Energy Dispersive X-Ray spectroscopy furnished by Nanoamor.

Sample preparation

The sample preparation was made by firstly dispersing the CNT or CNT-COOH inside the polyol solution with different strategies for improving the filler dispersion. After several attempts we found that the

composition of the polyol mixture undergoes to chemical variation due to volatile component (the components of the polyol mixture cannot be revealed due to agreement with BASF). The only way to preserve the integrity of polyol solution was to reduce the working-time at max 2 hours and avoiding thermal heating steps. Therefore, the final procedure resulted from a compromise between dispersion of CNT and final quality of the polyol mixture, which resulted in a high quality of polyurethane foam. Firstly, Polyol/CNT solutions were prepared with different dispersing strategies to obtain the best CNT dispersion. The selected procedure consisted in adding and dispersing 4 wt% to polyol solution. The polyol masterbatch was diluted for obtaining different weight percentage of CNT and CNT-COOH. The final Polyol/CNT or CNT-COOH solution was mechanically stirred with a 4-blade stirrer at 1500 rpm for 2 hours. After the dilution, the polyol/CNT solutions and the PMDI were mixed at the ratio of 1:5,6, as described in the technical data sheet (Figure 22). The PU composite foam resulted from this process was named PU/CNT 1%, PU/CNT 1.5%, PU/CNT-COOH 1% %, PU/CNT-COOH 1.5%. Figure 25 shows a digital image of the PU/CNT composite sample obtained with this technique. The entire process is described in Figure 24.

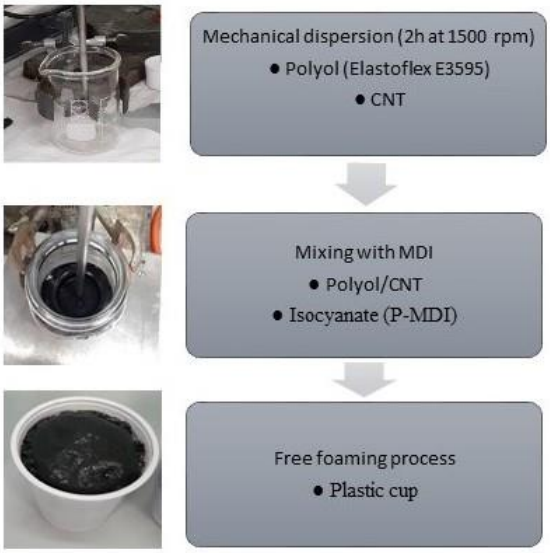

Figure 24 Scheme of the process studied for producing polyurethane/CNT foam for an automotive dashboard.

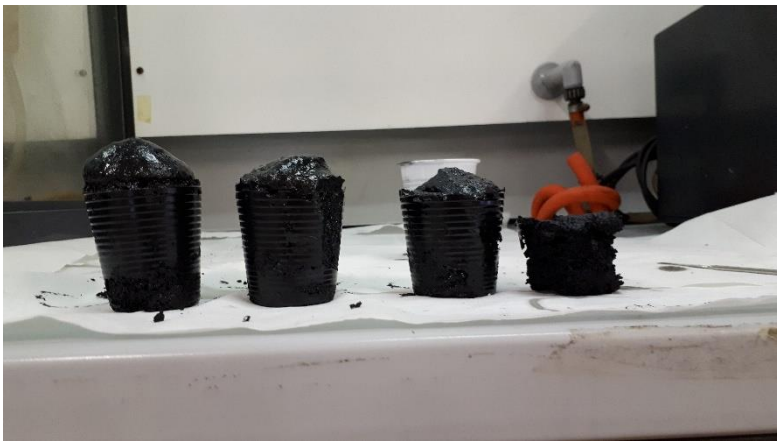

Figure 25 Shows the sample made with the selected strategy.

All the sample produced are very similar to the image in Figure 25 and the only way to distinguish them is with a label. The foams were cut and tested in Fiat Research Center (CRF) laboratories. The final samples have the same dimension: diameter of 4,5 cm and 1 cm of height. The height of sample has been chosen very similar to the operative component inside an FCA automotive dashboard. Figure 26 shows how we obtained the final samples to be tested from one cup of the same material with a specific concertation of CNTs. Moreover, little fragments of material have been obtained from the remaining pieces of the specimen. These fragments were used for TGA analysis and SEM analysis. In particular, the material used for SEM characterization was obtained by frizzing the material with liquid nitrogen to have brittle fracture in which CNTs are clearly visible without alteration of the matrix.

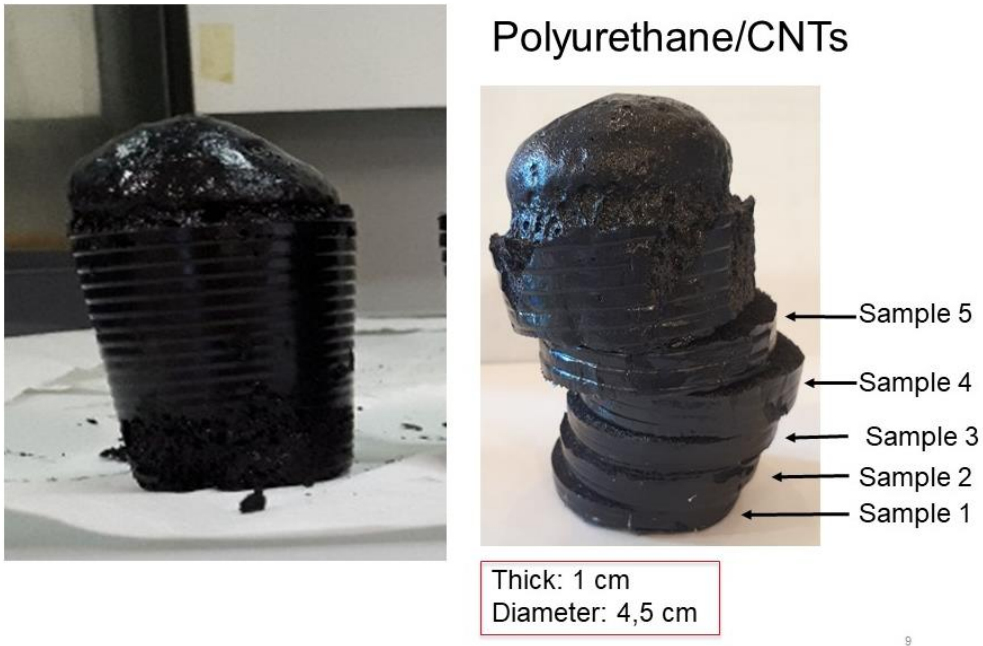

Figure 26 The PU/CNT foam and the samples obtained by one cup of material.

3.2 Mechanical and piezoresistive characterization

The piezoresistive response of the polyurethane composites was tested with an Instron tensile testing machine and two self-made copper electrode discs. A dedicated instrumental setup has been realized in order to measure the electromechanical properties of the samples. The instrument layout has been designed to evaluate the variations of the electrical resistance of the specimens (measured with a digital multimeter) caused by an imposed cyclic mechanical deformation.

3.2.1 Data acquisition hardware

The system has been realized with the following instruments:

- Tensile Testing Machine (Instron 5544, 2kN load cell)
- Digital multimeter (Keithley KE2700)
- Potentiometer (Gefran PY1 C 50)

- Dedicated acquisition system (PXI chassis with DAQ AI and AO modules)

The Instron (Figure 27b) has a particular system which allows it to perform tensile test, bending test and compression test. Moreover, it is equipped with compression test set-up (metal cylinders Figure 27a) a load cell which operates from 0N to 2kN.

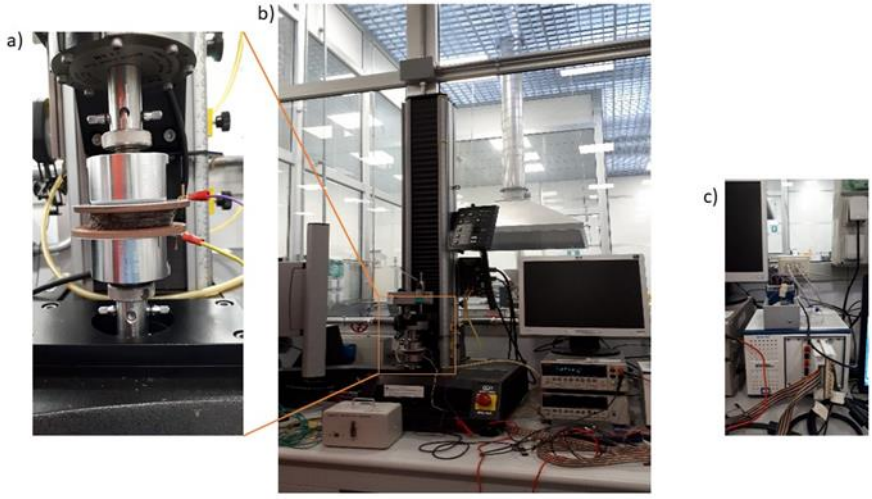

Figure 27 The instrument set-up for piezoresistive tests. a) the load cell with a sample between two self-assembled copper electrodes. B) the tensile testing machine with the acquisition system. C)The data acquisition system PXI box of national instrument.

The Instron has a specific software (Blue Hill 3.0) which allows us to change the parameter configuration for the different tests.

The potentiometer measures the imposed deformation of the specimens. The data acquisition tool PC-USB (National Instruments cDAQ-9178) has been connected to the potentiometer and to the data acquisition system for processing the electric output of the instrument. The electronic interface cDAQ-9178 has also equipped with two modules for acquiring data from the potentiometer and the thermocouple for the measuring of the temperature during the test:

- NI-9263: analog-output controller
- NI-9223: analog-input controller

The digital multimeter has been linked to the data acquisition system, with LabVIEW, through an adapter National instrument GPBI-USB, and it has allowed to acquire the variation of the electric resistance of the sample on time. This system has also allowed to combine the resistance variation with the imposed mechanical deformation (Figure 28).

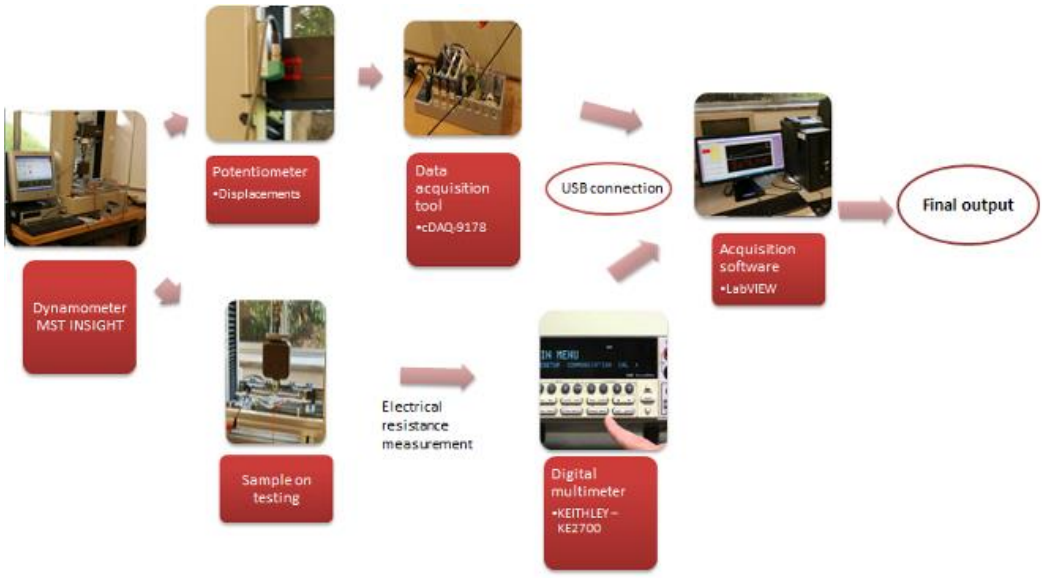

Figure 28 Instrumental setup for piezoresistive characterization

A device for multiplexed acquisition has been linked to the digital multimeter. Moreover, the electrodes deposited on the specimen will be linked to this device through some copper wires. This kind of measuring system is able to measure more than one resistance simultaneously. In fact, the digital multimeter, through the device for multiplexed acquisition, elaborates all the resistances of the specimen that must be measured. Furthermore, in our case the device was settled to measure only one resistance. The main physical parameters which are involved in the characterization of the piezoelectric properties have been defined and. In conclusion, a customized measuring system has been designed and realized in order to measure the electric resistance and the deformation in a proper way. The same layout is also able to synchronize the data to get the resistance-displacement graph and the main parameter such as GF.

3.2.2 Data processing software

The instruments have been programmed in order to allow us the elaboration and the acquisition of the resistances and displacement coming from the digital multimeter and the potentiometer. Moreover, it has been necessary to write a computer code using the National Instruments LabVIEW programming language. The LabVIEW software elaborates the data coming from the digital multimeter (resistance) and the potentiometer (displacement) and it gives us the resistance-displacement charts. Figure 29 shows how the software acquires and elaborates the data.

The computer code, which has been written in LabVIEW language (flow-chart in Figure 29), is able to acquire simultaneously until 9 multiplexed resistance channels and the displacement of the sample. This system can acquire different signals in sequence and to transmit to the software the different measures separately. Therefore, it will we be able to measure up to 9 different resistances of the sample.

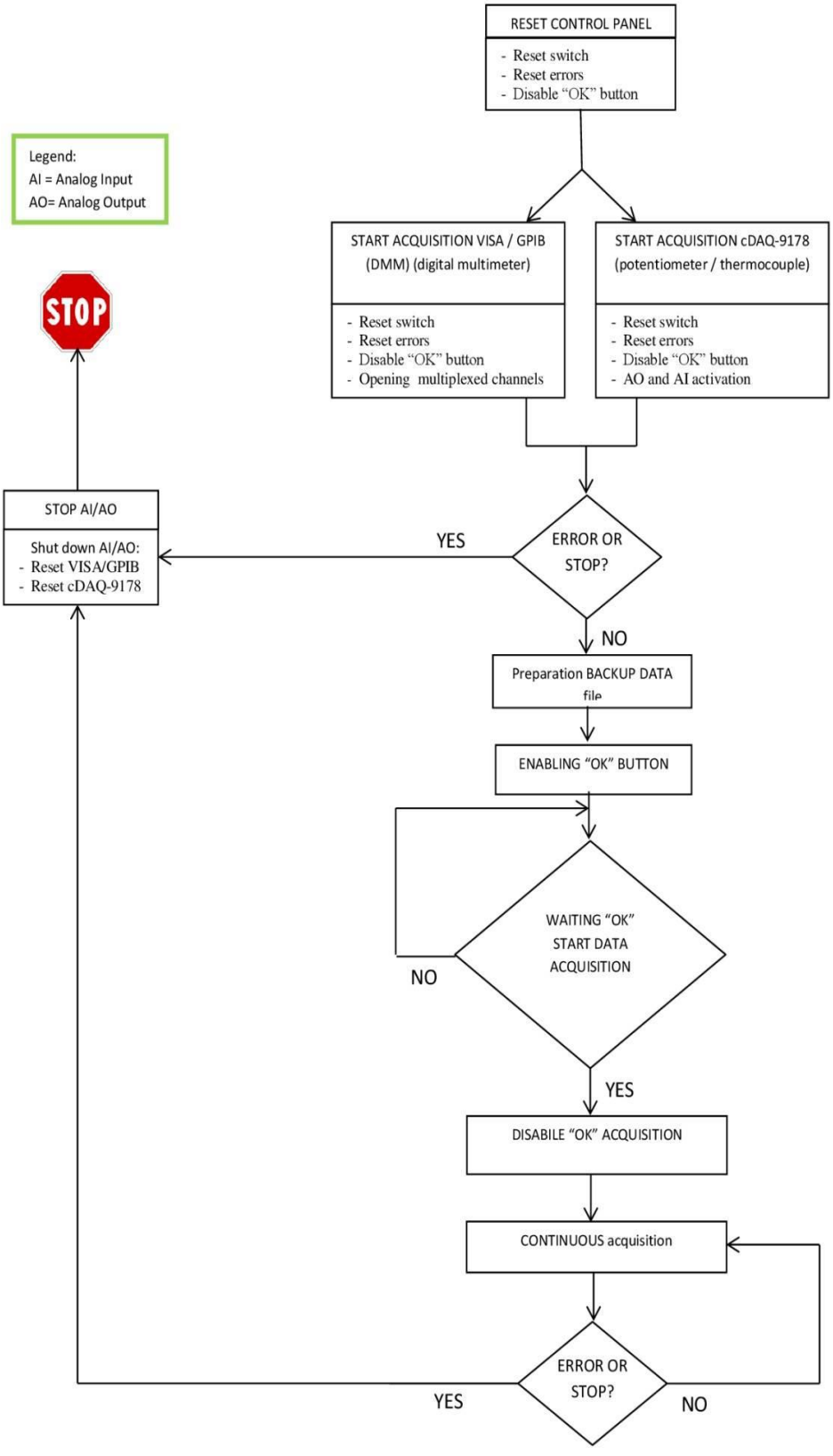

Figure 29 The flow-chart shows how the LabView code acquires the data (resistance/displacement/temperature).

3.2.3 Designed PU/CNT testing procedure for mechanical and piezoresistive compression characterization.

The samples obtained from PU/CNT foams have been prepared to mechanical and piezoresistive tests. The mechanical characterization was performed with the foam as prepared was locked between the compression set-up inside the tensile testing machine. During the mechanical characterization, the Blue Hill software acquired simultaneously the load (N) and the imposed compression (mm). Furthermore, the preparation for piezoresistive characterization was more complex and required several steps. Firstly, two copper discs were locked with riveted screw to metal wires. The metal wires are directly connected to the digital multimeter. The contact between copper disc and metal wire were measured in order to have a negligible contact resistance. Secondly, the copper disks were externally covered with an insulating layer made with Myalr (polyester PET) in order to guarantee also mechanical performance to compression. The Mylar film avoided in each compression phase electrical short cut. Moreover, the compression contribution of Mylar thin film is absolute negligible. Thirdly, the PU/CNT foam was placed between the copper disks. Figure 30 shows the instrument outline with a sample inside the two copper electrodes.

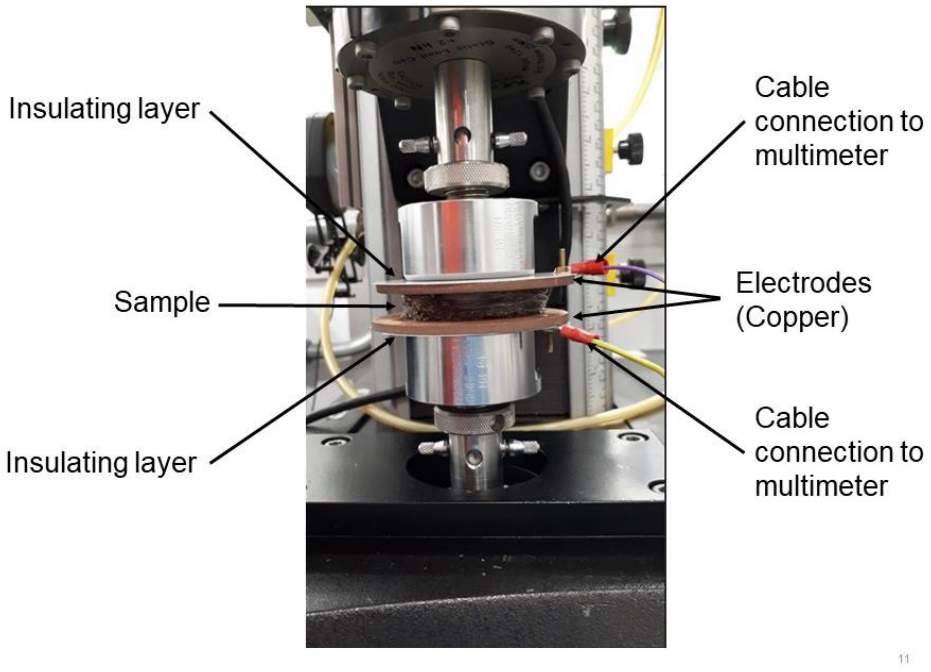

Figure 30 Digital image and schematic representation of piezoresistive set-up used for the characterization of PU/CNT foam.

3.2.4 TGA analysis

Thermogravimetric analysis (TGA) is an analytical technique for the thermal classification of materials. The technique consists in the continuous measurement over time of the mass of a polymeric fragment as a function of time or temperature during an heating ramp, in conditions of controlled atmosphere (air or nitrogen). The result of this analysis, generally referred to as a Thermogram or Thermal Decomposition Curve, is a graph showing the weight variation (Y axis), in absolute or percentage value, as a function of time or temperature (X axis). Figure 31 shows the TGA Q500 - TA instrument used for performing TGA characterization in this study. The parameter used were heating ramps of 10 ° C / min between 30 ° C and 700 ° C. The final thermogram shows the percentage weight loss (%) of the sample as a function of the temperature (° C). The thermograms were processed with the dedicated software: TA Universal Analysis by TA instruments.

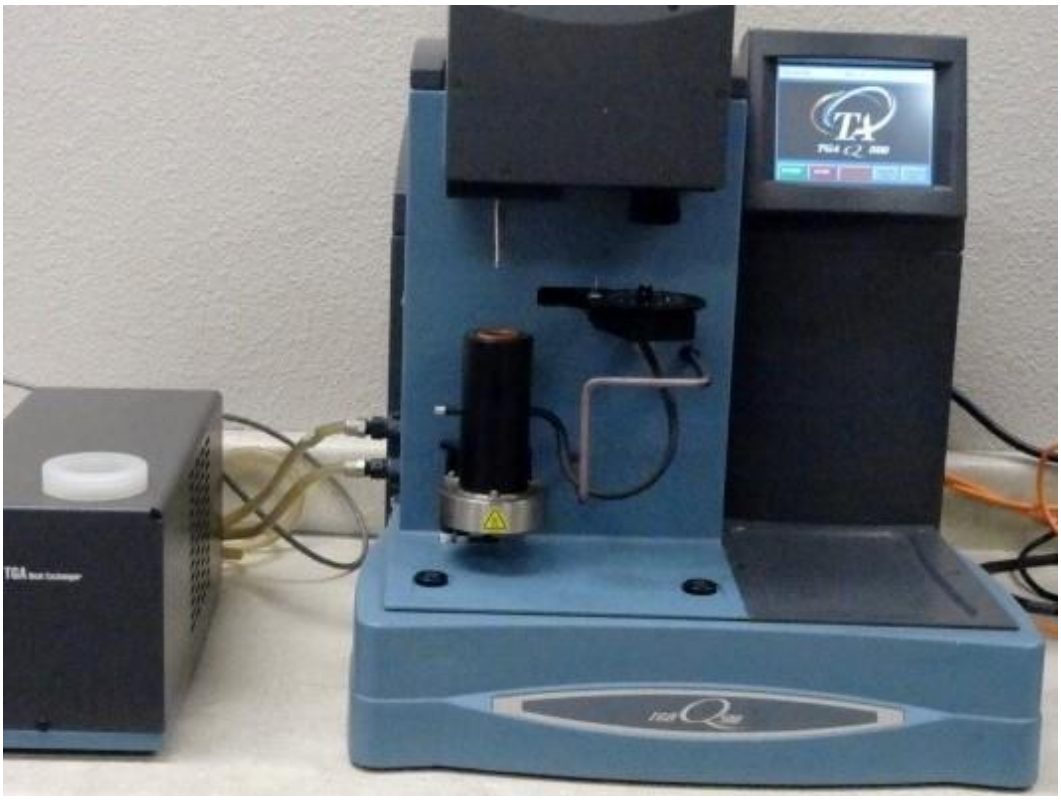

Figure 31 TGA Q500 the model of TGA used for thermal analysis.

3.2.5 SEM characterization

SEM analysis was used to analyse the distribution and agglomeration of CNTs inside the composite foams. The samples were first subjected to cryofracting and the braking surface was sputtered with gold nanoparticle. This process was performed with BAL-TEC 050, with a sputtering current of 60 mA for 40 second. The SEM images were collected by using both the secondary electron and the backscattered electron detectors. The electron microscope used for this purpose was the Leica Stereoscan 410 - Oxford Instrument, and the Zeiss EVO 50 XVP-LaB6 (Figure 32). The instruments are part of the equipment owned by the chemistry department of University of Turin (Center for nanostructured interfaces and surfaces - NIS lab).

Figure 32 SEM Zeiss EVO 50 XVP-LaB6.

3.2.6 Characterization of thermoplastic polyurethane with reduced graphene nanoplatelet (TPU/GNP)

The following activities were performed in FORTH laboratories in Greece within a collaboration between CRF and FORTH ICE-HT department (European project: Graphene Core 2). The aim was to characterize a BASF thermoplastic polyurethane (TPU) loaded with reduced graphene nanoplatelets (GNP). The blend and the fillers are produced by AVAZARE which is a graphene producer and compounder companies placed in Spain. The material was designed and produced entirely by AVANZARE. The purpose was to investigate TPU/GNP at piezoresistive level to understand if this can be used as an automotive aesthetic skin for dashboard. The idea was to use TPU/GNP skin together with polyurethane foam for making smart nanocomposite structure to replace metal wires, buttons, and sensors. Avanzare and FORTH (Foundation for Research & Technology – Hellas) are partners of CRF inside the graphene flagship and more specific in Core 2 Wp14 “Polymer composites”.

3.2.6.1 Preparation of graphene/TPU nanocomposites by AVANZARE

The TPU/GNP nanocomposites were prepared by melt extrusion in a counter rotating twin screw micro-laboratory extruder Rondol 10 mm LD20 at a screw speed at 30 rpm. The process temperature in the different barrels in either extrusion processes are presented in Table 1.

After pelletizing TPU/GRM composite are processed in a hot press at to produce the TPU/GRM laminates (Figure 33), and in a hot roll-pressing 160ºC 5 min. All these activities were designed and performed by AVANZARE with BASF thermoplastic polyurethane.

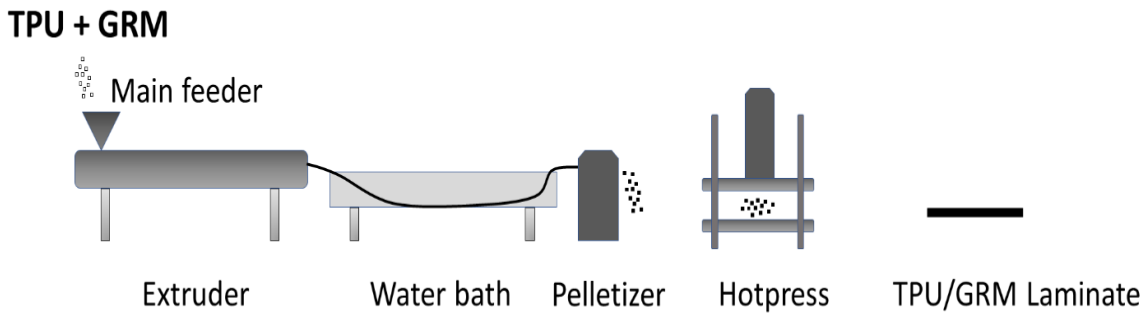

Figure 33 Scheme of the process used by AVANZARE to produce the laminates.

Table 1 Temperature profiles used for the GRM/TPU extrusion.

Extruder zones	***Die***	***Z4***	***Z3***	***Z2***
Temperature ºC	150	150	140	120

Avanzare developed different grades of TPU ELASTOLAN ES.OFT 45A 12 P000/graphene with a circular shape and a different graphene filler. Figure 34 shows the original shape of the materials produced by Avanzare and sent to FORTH laboratories. Table 2 summarizes the main information of the TPU prepared grades.

Figure 34 Example of specimen produced by Avanzare sent to FORTH laboratories.

Table 2 Main information of TPU/graphene composites prepared by Avanzare.

Name	Type of Grapehene	Load (%wt)	Production method	Preliminary electrical measurement (linear)	Preliminary electrical measurement (volume)
SN-1487-A	AVAFLG18	12.5	Industrial extruder	0.1-1 GΩ	3-4 MΩ
SN-1487-B	AVAFLG18	15	Industrial extruder	250 kΩ	236 kΩ

The sample named SN-1487-A showed a very high value of electric resistance (higher than 120 MOhm). That value is not suitable for electronic car equipment and therefore this material was not tested.

3.2.6.2 Sample preparation for piezoresistive characterization

The shape selected in order to test and compere the data with our measuring system, is a rod shape of 40 mm length 12 mm width and 1 mm thickness. Figure 35 shows a sketch of the obtained samples.

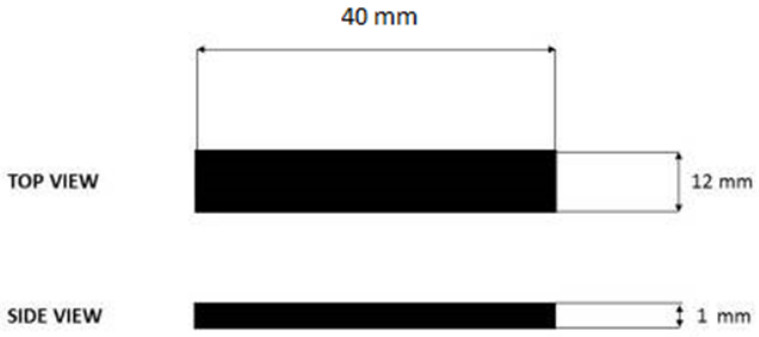

Figure 35 Ideal specimen shape used for testing the materials.

The tested specimens were cut from the samples sent by Avanzare made up of TPU ELASTOLAN ESOFT 45A 12 P000 loaded with GNP produced by AVANZARE (AVAFLG18). The digital image in Figure 36 shows the samples obtained by cutting the main sheets of composite material.

Figure 36 Composite material sample after cutting.

Two electrical wires were placed at the two ends of the sample spaced 2 cm of the useful region. The wires have been bound softening the polymer with a hot tip and incorporating them on sample surface. Furthermore, two metal electrodes were painted on the surface near the wires with a silver paint on the rod specimens in order to obtain the two electrodes from which the resistance signal was detected. This paint is applicable with a small brush and took 10 minutes to dry and 30 minutes to be conductive. The electrodes were made paying attention to get all the electrodes in the same shape and size and placed at the same distance for all the samples. The dimension of each electrode is 1x1 cm, the distance between them is 2 cm. Figure 37 shows a digital image of the sample.

Figure 37 Specimen with two painted electrodes.

3.2.6.3 Instrumental set-up for piezoresistive characterization of TPU/GNP skin.

A dedicated instrumental setup has been realized in FORTH to measure the electromechanical properties of TPU/Graphene samples. The instrument layout has been designed to evaluate the variations of the electrical resistance of the specimens (measured with a digital multimeter) caused by an imposed mechanical deformation (linear or cyclic).

Data acquisition hardware

Electromechanical properties of TPU/GRM composites have been investigated by using a custom-made experimental setup in order to measure the variations of the electrical resistance caused by an imposed mechanical tensile deformation (linear or cyclic).

Prior to testing, the electrical resistance of all the specimens has been measured by using a digital multimeter (Keithley 2420). Then, the strain dependence of resistivity was measured using a four-contact measurement system under a constant applied voltage of 10V on the specimens subjected to mechanical loading. In particular, monotonic tensile loading was applied by using a micro-tensile tester (MT-200, Deben UK Ltd, Woolpit, UK) equipped with a 210 N load cell and with custom-made isolating clamps necessary to avoid current leakages showed in Figure 38. In this configuration, all test specimens were loaded with a crosshead displacement speed of 1.5 mm min−1 (corresponding to a test specimen strain rate of 0.075 s−1). Cyclic tests were performed by using a Universal Servo-hydraulic Testing Apparatus (MTS 858 Mini Bionix 848 Figure 39), equipped with a 10kN load cell.

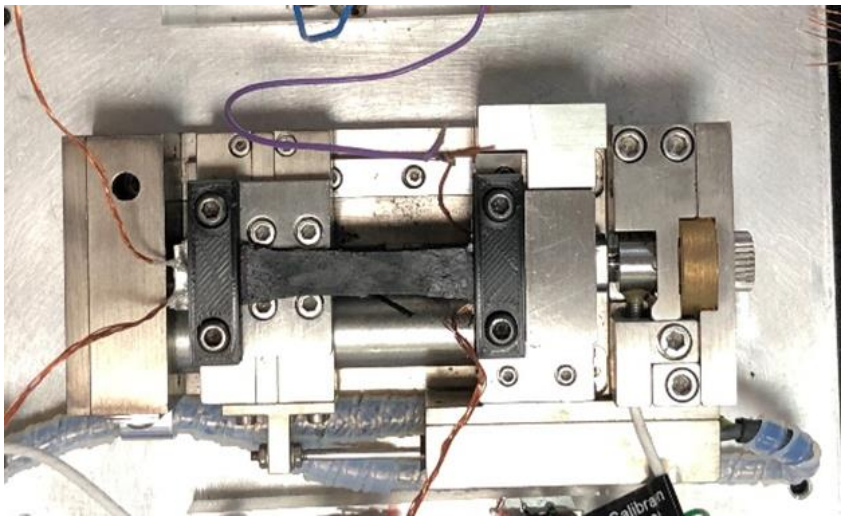

Figure 38 MT-200, Deben UK Ltd, Woolpit, UK FORTH laboratories.

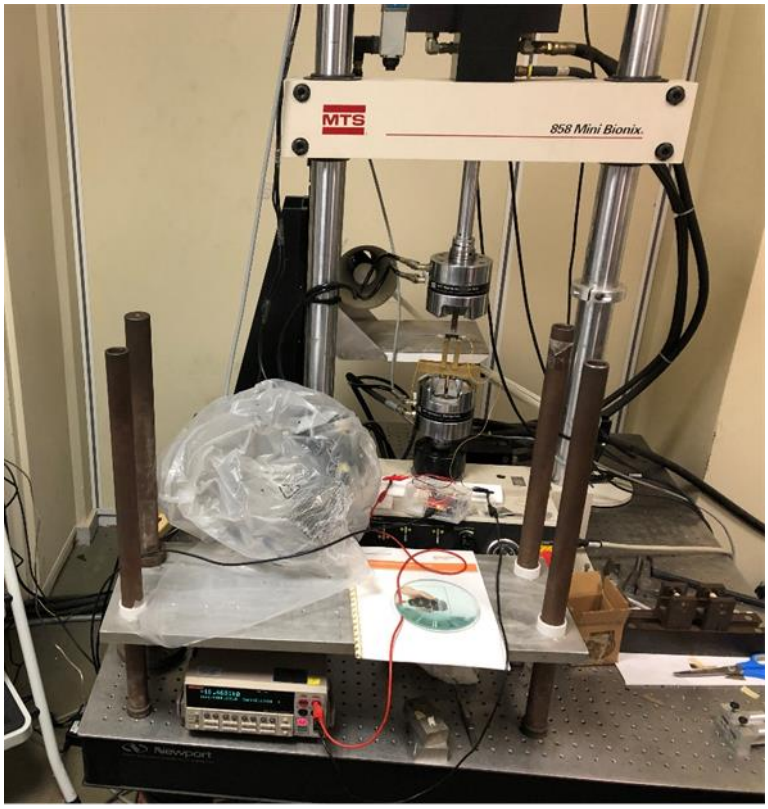

Figure 39 Tensile testing machine MTS 858 Mini Bionix 848 used for cyclic characterization of TPU/GNP.

3.2.6.4 Programmed piezoresistive tests characterization

The purpose of these tests was to characterize the composite material named SN-1487-B as a sensor at mechanical level and at piezoresistive level. As a first tensile test it was crucial to define the elastic range in order to assume a specific range on which cyclic test could be done without permanent deformation. However, to assure an appropriate electrical response the resistance variation inside this range should be large enough, at least 3% of the initial resistance variation. Consequently, the cyclic tensile tests have been planned based on the failure test results. The tensile cyclic tests were scheduled with the aim of exploring two main different parameters (deformation rate and maximum elongation) in order to obtain the best electrical response in terms of quality of the signal and consistency. TTest-2, TTest-3 and TTest-4 have been planned to investigate the reproducibility of the electromechanical behaviour of the material with a fixed maximum elongation, established by TTest-1, and three level of deformation rate. TTest-5, TTest-6 have been done with the fixed best deformation rate, which has been determined from previous tests, and a two different level of maximum elongation. In conclusion, TTest-7 has been done to demonstrate reproducibility of the signal with the most appropriates parameter after many cycles (1000). The Table 3 shows the scheduled tests.

Table 3 Scheduled Tensile cyclic test

TESTS	**SAMPLES**	**Deformation rate (Hz)**	**Maximum elongation (mm)**	**Number of cycles**
TTest - 1 (failure test)	Sample 1	N.A.	N.A.	N.A.
TTest - 2	Sample 2	1 Hz	1	100
TTest - 3	Sample 3	2 Hz	1	100
TTest - 4	Sample 4	0.5 Hz	1	100
TTest - 5	Sample 5	0.5 Hz	2	100
TTest - 6	Sample 6	0.5 Hz	0.5	100
TTest - 7	Sample 7	0.5 Hz	1	1000

The stress and strain were calculated through the machine-recorded force and displacement based on the initial cross-section area and gauge length, respectively.

4 Results and Discussion

4.1.1 Mechanical results

Figure 40 shows a digital image of an Alfa Romeo dashboard cross section, the polyurethane foam layer has a different thickness depends on the position. The upper layer is a synthetic skin which has aesthetics purpose and for masking the colour of the polyurethane. The sample preparation and tests have been taken inspiration on the production process of the dashboard and the main functionality of the foam. Figure 41 shows a compression stress-strain curve of the neat polyurethane foam. To test the mechanical properties of solid polyurethane foams, compression tests are normally used: the sample is placed between two pistons connected to a tensile testing machine and the applied pressure (σ) is measured as a function of the deformation (ε).

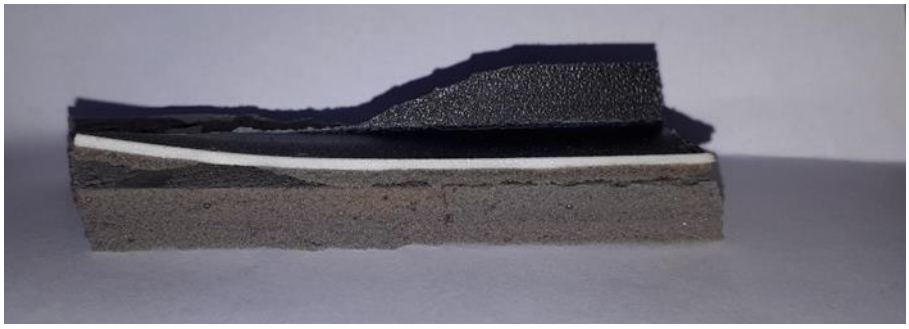

Figure 40 Composite structure of an Alfa Romeo dashboard.

The result is a characteristic curve shown in Figure 41 which is obtained with a compression test of the neat polyurethane foam used in this experimental campaign. It is possible distinguish three different regions:

i. Linear region: the curve has a linear correlation between stress and strain, comparable to the stretch of elastic deformation in the common traction curves.

ii. Steadily stress region: it can be more or less prolonged, the effort to increase the deformation remains constant.

iii. Exponential region: the stress starts to raise exponentially with the deformation.

the explanation of these three regions could be given by the following consideration: the shape of the air chamber inside the polymer lattice changing according to pressure stage governed process. In other words, the geometry of cells works as a metastable structure. The different stages could be for example: the lowest energy (p<pressure transition applied) and highest energy (p>p transition applied). The first stage is represented by the initial part of the graph (linearity). At this stage, the cell strut is subjected to linear deformation without a remarkable geometry variation. According to the test procedure, the pressure increases until pressure transition value (2.3x10-5 Pa). The geometry of cells, at this second stage, could not stand the pressure applied and a new geometry resulted from equilibrium configuration is established. After the collapsing of first cell structure in the new stable configuration suddenly the cells next to it started to collapse. The passing process from first stage geometry to second stage geometry causes energy absorption as friction and heat. This transition process is equivalent to the nucleation of gems. Moreover, Maxwell stress is defined as the value of applied stress, which is constant for all the whole process, until the transition is completed. Figure 41 also shows three digital image which shows this phenomenon. This model is coherent with the deformation tests coaxial to the growth direction of the foams [31].

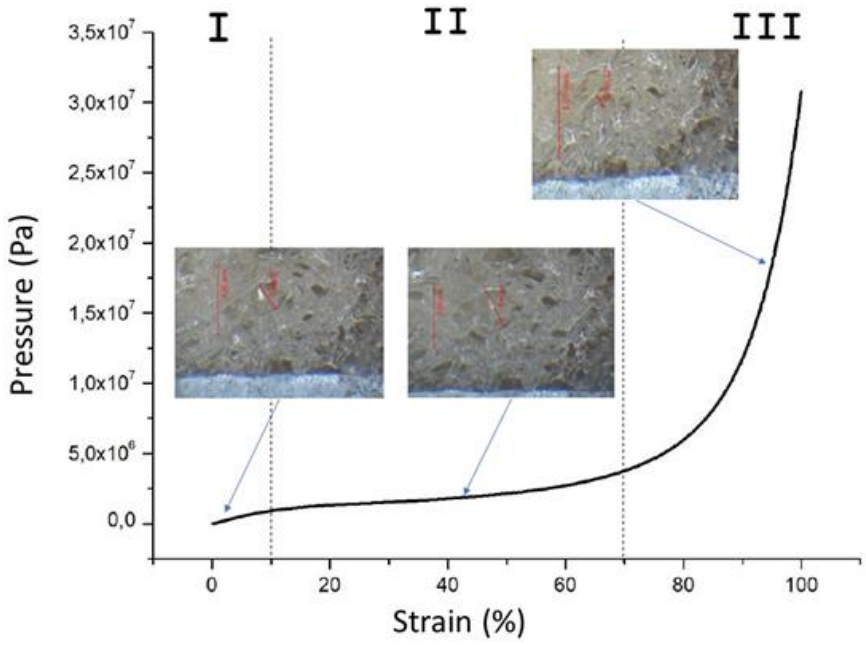

Figure 41 The typical stress-strain curve of the foam prepared with Lupranol® 2007/1 as polyol.

Figure 42 shows the results of mechanical pressure tests on the neat polyurethane foam compared to the foams obtained adding CNTs or CNT-COOH. The most rigid foam was obtained by adding 1,5 wt% of CNT-COOH at the polyol formulation. The 1% of CNTs added also shows an increasing in mechanical rigidity of the foam but weaker respect to CNT-COOH also with a lower concentration. The foam prepared with CNT-COOH always showed a strong mechanical reinforcement to the foam structure obtained with BASF product.

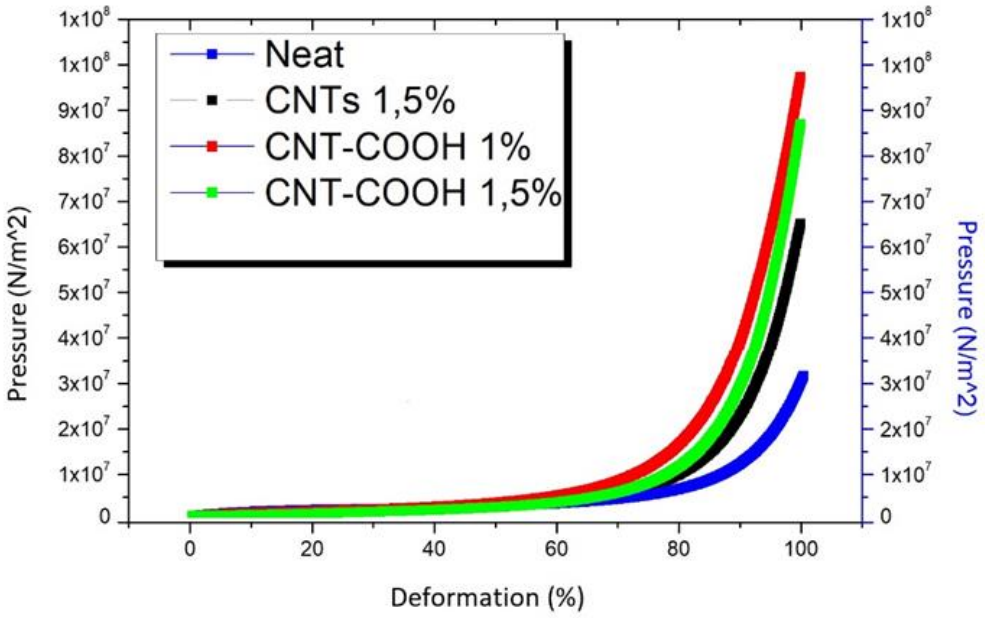

Figure 42 The line chart shows the results of mechanical compression of different foam prepared. All the foam with CNTs inside shows strong rigidity respect to the neat.

Table 4 shows the elastic modulus of the sample calculated in the plateau region. 1% of CNT added to the neat foam increases the rigidity while reduces the mechanical strength comparing to the CNT/COOH with a lower concentration. The foam prepared with CNT-COOH exhibited the highest elastic modulus comparing to the foam obtained with neat PU and PU/CNT 1.5 wt%.

Table 4 Comparison among the elastic's modulus of different sample with CNT concentration.

PU sample	$E_{plateau}$ [MPa]
Neat PU	31
PU/CNT 1.5%	42
PU/CNT-COOH 1%	45
PU/CNT-COOH 1.5%	52

4.1.2 SEM Images

SEM images of CNT's used for these experimental tests are shown in Figure 43. This interesting image allow us to observe the morphology of the nanoparticles (CNT agglomerates). Single Nanotubes could be seen also to 20.00KV, using secondary electrons at 10.000 X of magnification. The morphological image demonstrates high aspect ratio of CNTs that ensure percolation path also with lower filler concentration which is enough for the aim of this work. Moreover, the CNTs showed conductivity avoiding metal deposition and it was possible acquiring accurate images of their morphology.

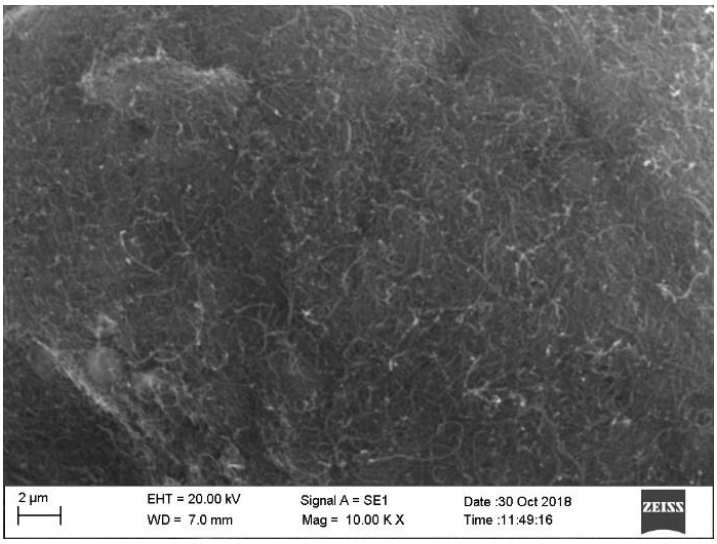

Figure 43 SEM image of CNTs powder.

Furthermore, the same analysis was performed on a neat sample the samples in order to have a reference for further images.

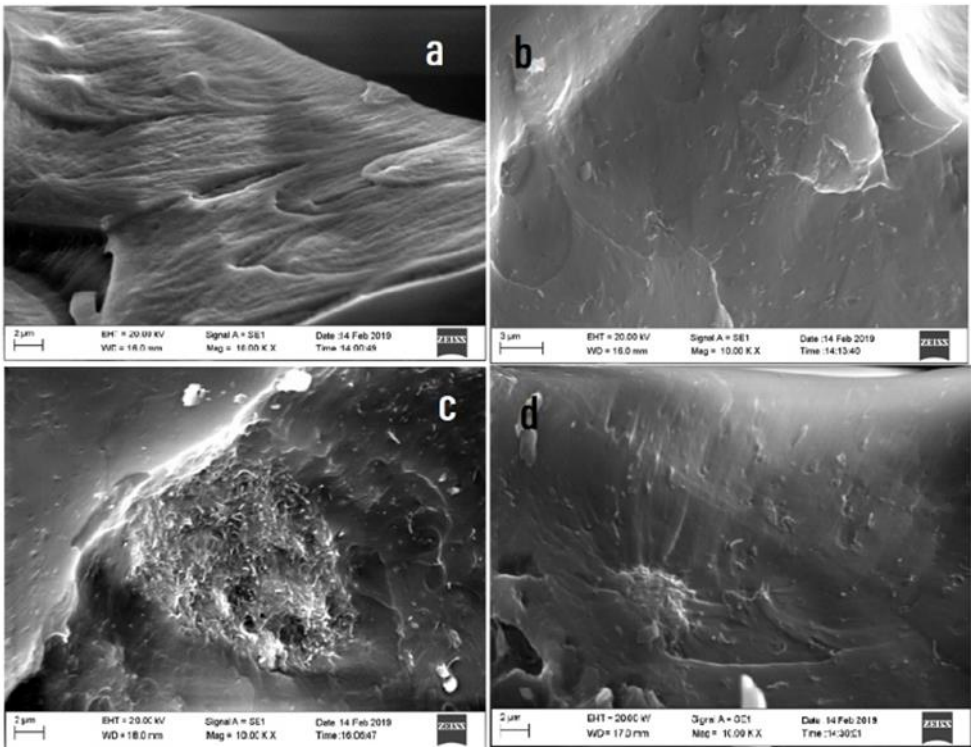

Figure 44 (a) SEM image at 10 Kx of the neat foam (b) SEM image at 10 Kx of the sample with 1,5% of CNTs (c) SEM image at 10 Kx of the sample prepared with 1% of CNT-COOH (d) SEM image at 10 Kx prepared with 1,5% of CNT-COOH.

Figure 44 shows the results of SEM analysis on the prepared PU/CNT samples. In particular, Figure 44a represents SEM image of the polyurethane foam without any filler, the surface appear smooth and regular without any visible particle. The Figure 44b is obtained with the PU/CNT 1,5% it is possible distinguish some dots that reveals the presence of CNT without agglomerates. The sample with CNT-COOH al 1% is shown in Figure 44c. This image shows an agglomerate of about 20 μm, all around the fracture the sample shows CNT-COOH agglomerates. The last image, Figure 44c, shows the bulk of PU/CNT-COOH 1,5%. This sample has different domain region in which CNT-COOH seems to be well distributed and the agglomerates are finer than PU/CNT-COOH 1% sample. This demonstrates that the CNT-COOH fillers have a strong covalent bond with the matrix, and they act as a reinforcement point of the foam structure. Moreover, samples with 1,5% of CNT did not show CNTs domain region. Commonly, the agglomerates suggesting a poorer dispersion mechanism and an entirely dissimilar interface between the matrix and the filler. Furthermore, SEM images allowed us to understand CNTs distribution and degree of dispersion inside the different nanocomposites. Moreover, SEM characterization together with the

electromechanical behaviour showed that the dispersion of CNTs is not the predominant parameter that affects the final properties of the foam.

4.1.3 TGA results

Figure 45 and Figure 46 reports the result of TGA analysis under Nitrogen and air flow, respectively. The degradation of the polymer starts from 280°C for all formulation. Under air flow, PU/CNT at 1,5 seems to be is more stable at high temperature then PU/CNT-COOH at 1,5% and the neat PU foam. Instead, the TGA under nitrogen flow shows that PU/CNT-COOH at 1,5% resulted the most stable respect other samples.

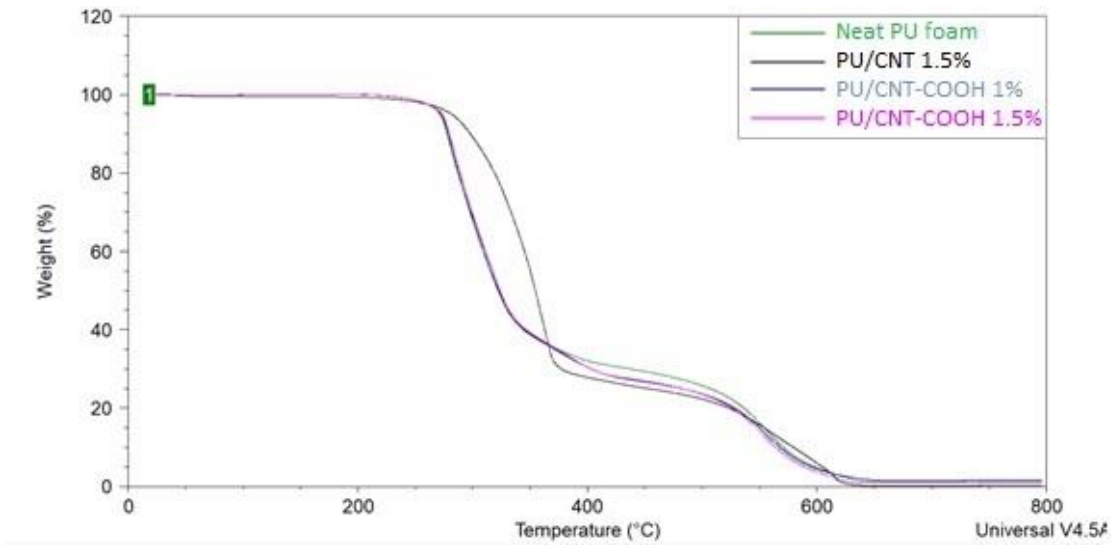

Figure 45 The line chart shows the weight loss in percentage on the temperature resulted on TGA nitrogen flux analysis.

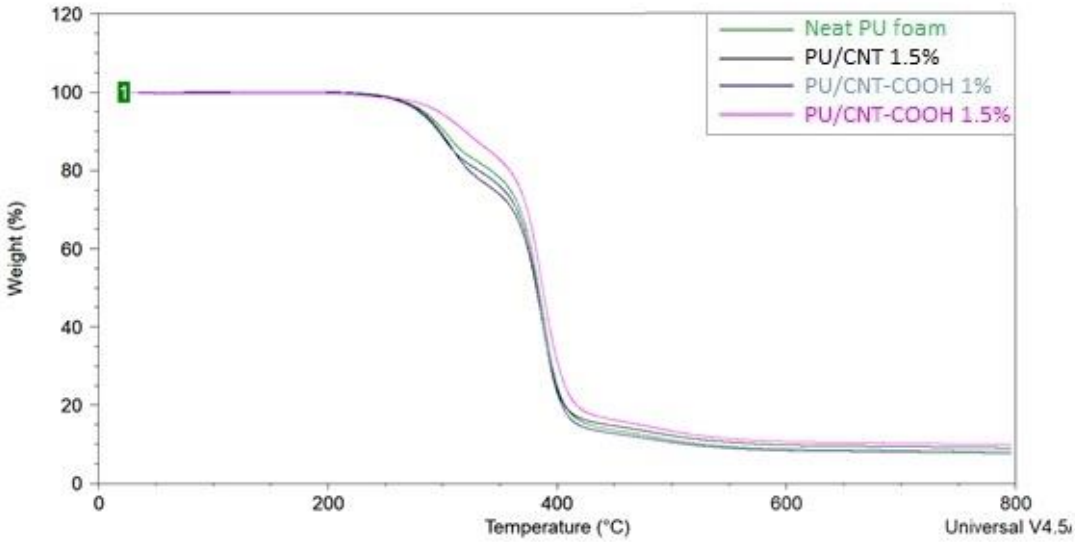

Figure 46 The line chart shows the weight loss in percentage on the temperature resulted on TGA nitrogen flux analysis.

Thermograms in nitrogen shows two steps of weight loss: the first step, from about 250°C is due to the breakup of urethane bond into isocyanates segments and polyols segments. With an increase of temperature, the polyols decompose into some kinds of aliphatic ether alcohol. In the temperature range of 350–500 °C, the dominant volatile products are primary amines, secondary amines, vinyl ethers and CO2. Under oxidative conditions, degradation, including ring fusion, occurs at a lower temperature than under non-oxidative conditions. [58–60]

4.1.4 Piezoresistive characterization

The polyurethane composite foams were compressed with a tensile testing machine (Instron 2kN) between two metal electrodes connected to Kithley multimeter. The multimeter acquired the electrical resistance during the compression test. The displacement and the resistance were acquired simultaneously with a data acquisition system (programmed with LabVIEW for the purpose) and plotted on a graph. the PU/CNT 1% samples showed a value of electrical conductivity above the threshold value of the instrument (120 MOhm) during all the compression tests. Figure 47 shows the most representative results for PU/CNT 1% sample, the electrical resistance was above the threshold value while the sample was compressed. The deformation rate was 10 mm/min with a maximum deformation of 5,5 mm.

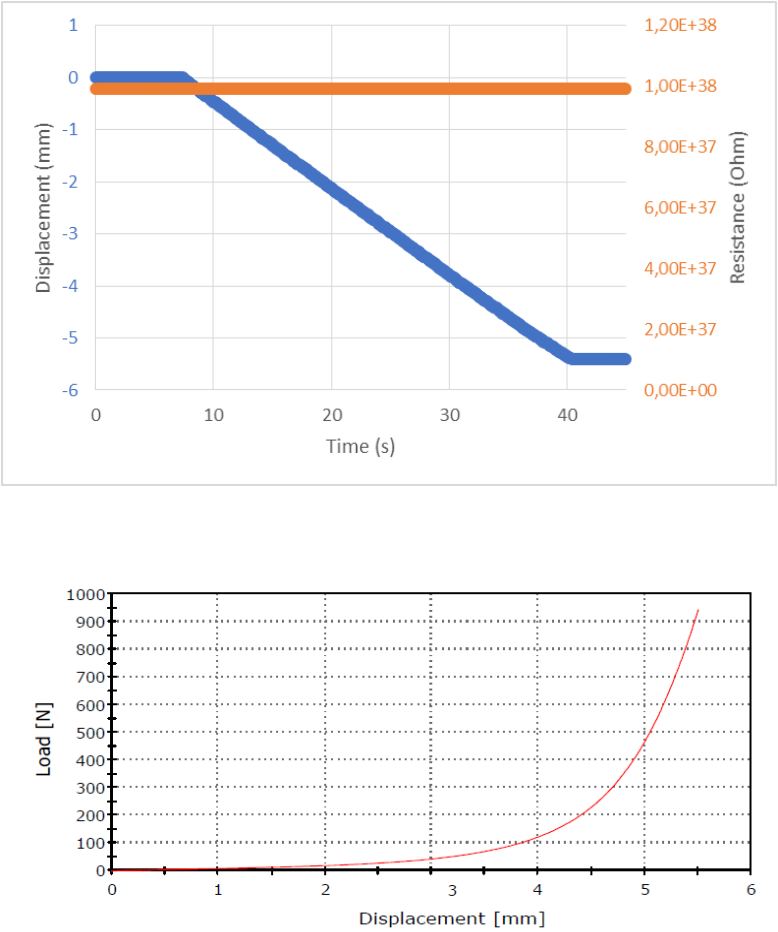

Figure 47 The first graph shows the compression (blue) imposed by the tensile testing machine and the electrical resistance (orange) measured during the test. The second graph shows the load displacement curve during the same test.

The polyurethane foam with the concentration of CNT under 1.5% did not show an electrical resistance sufficiently low to observe a value with our instrument set-up. The CNTs could not made a sufficiently conductive network to show a piezoresistive behaviour.

The PU/CNT 1.5% samples were cut and tested in the same way. The test conditions were the same of previous test: deformation rate of 10 mm/min and maximum deformation of 5,5 mm. The sample showed electrical conductivity before the compression tests. This means that the percolative network inside the sample are active and stable. Moreover, the sample showed also piezoresistivity and it was tested inside the piezoresistive facility compression test. Figure 48 shows the results of piezoresistive tests made on PU/CNT 1.5% sample. The sample was conductive also when the compression is not applied and has a resistance of 90MOhm. The lowest measured resistance of the sample was 80kOhm and is reached at the maximum deformation of 99%. The electrical resistance changes steadily with the compressive load through the whole test. The deformation rate was 10 mm/min with a maximum deformation of 5.5 mm.

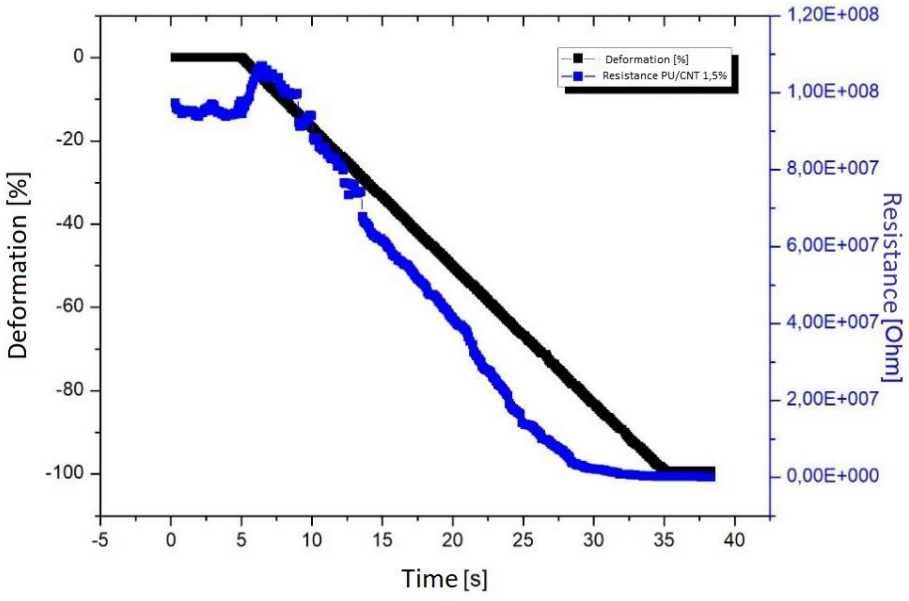

Figure 48 PU/CNT 1.5% during the compression test (black line) and the value of electrical resistance (blue line) acquired simultaneously.

Figure 49 shows the line graph acquired during the compression test of PU/CNT-COOH 1%. The foam did not show any CNT percolative network when the compression was less the 96%. Better to say that the electrical resistance was above the threshold value of the instrument (120 MOhm) during the initial compression. Unexpectedly, the sample started to be electrically conductive (insulator-conductor transition) at 94% of deformation with a resistance of 600kOhm. After this compression value the resistance started to reduce linearly with the mechanical compression. Reaching the lowest measured resistance value of about 60kOhm at the maximum acceptable deformation of 99%. The electrical resistance changes steadily with the imposed deformation from the 96% to the 99% of compression proving piezoresistivity effect.

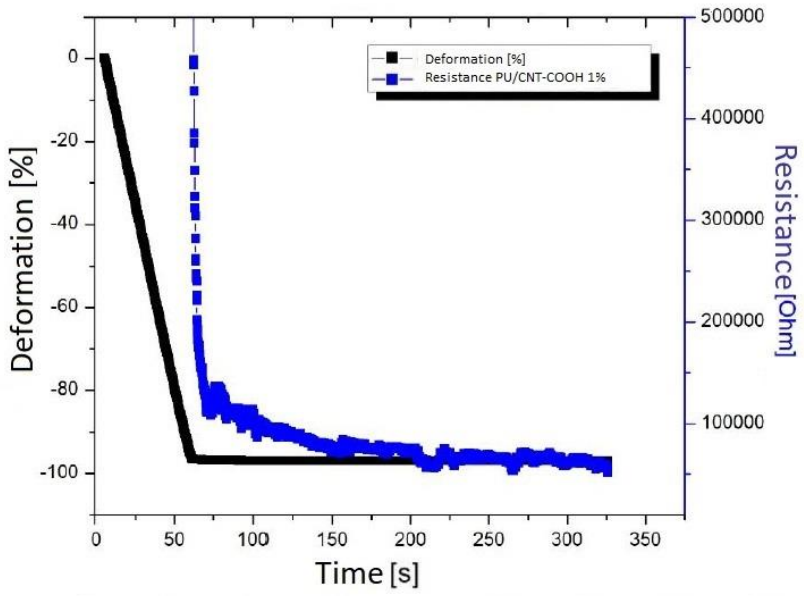

Figure 49 PU/CNT-COOH 1% during the compression test (black line) and the value of electrical resistance (blue line) acquired simultaneously.

Figure 50 displays the line graph acquired during the compression test of PU/CNT-COOH 1.5%. This result was very similar to the one obtained with PU/CNT-COOH 1% sample. The PU/CNT-COOH 1.5% disk was not conductive in the uncompressed configuration. Moreover, the sample starts to be conductive at 95% of deformation with a resistance of 400kOhm. The lowest measured resistance of the sample was 30kOhm

and is reached at the maximum deformation of 99%. The electrical resistance changes steadily with the imposed deformation from the 95.5% to the 99% of compression.

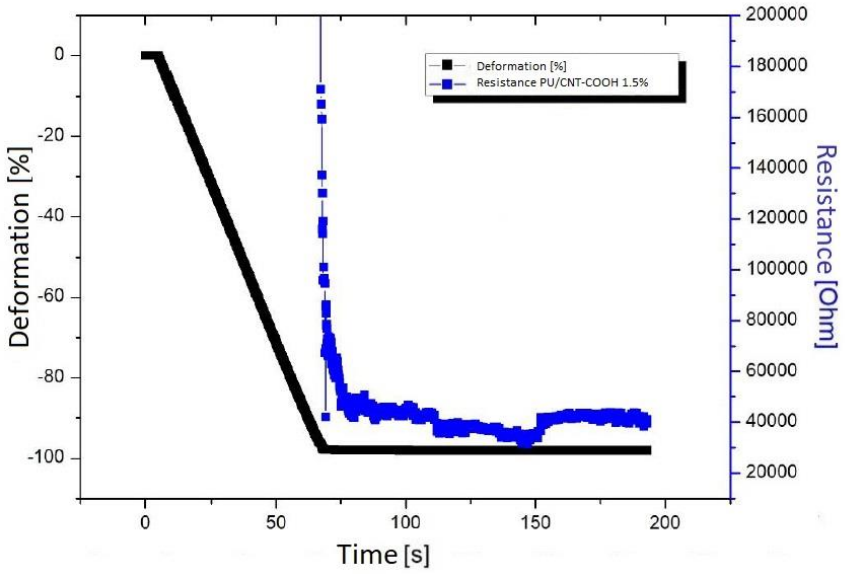

Figure 50 PU/CNT-COOH 1.5% during the compression test (black line) and the value of electrical resistance (blue line) acquired simultaneously.

4.1.4.1 Cyclic tests

The samples were subjected to cyclic test to understand the electromechanical behaviour to cyclic deformation. This test was aimed to characterize the foam as a switch application inside a hypothetical innovative smart dashboard. Figure 51 shows cycles of PU/CNT 1.5% the electrical resistance changes accordingly with the imposed compression, the acceptable deformation range is 10% of compression from 90 to 99,98% the corresponding value of resistance at this deformation are 80 kOhm and 2MOhm with a range of 2400% of resistance change. The starting value of 90% was chosen in order to compare the results with CNT-COOH sample.

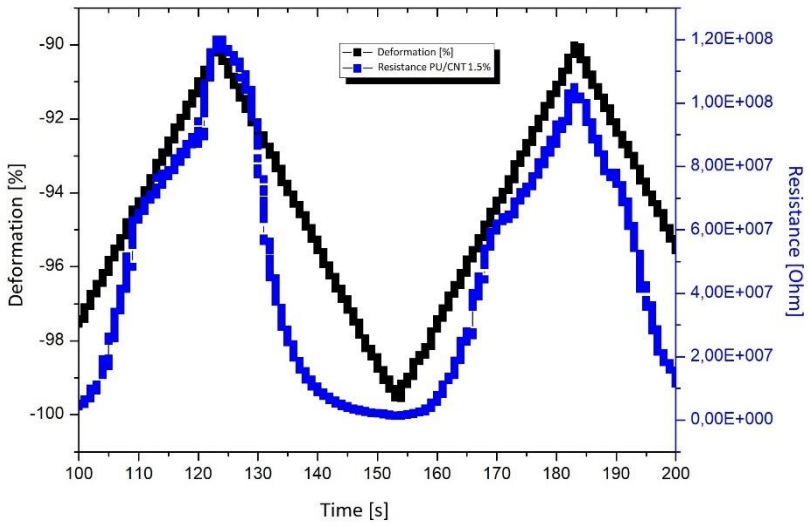

Figure 51 Cyclic test of PU/CNT 1.5% at 0.5 mm/min the deformation range (black line) is the 10 % of the sample height the electrical resistance (blue line) change with the deformation with a resistance variation of the 2400 of the initial resistance.

Figure 52 shows cycles of PU/CNT-COOH 1% the electrical resistance changes accordingly with the imposed compression, the acceptable deformation range is 5.5% of compression from 94 to 99.5% the corresponding value of resistance at this deformation are 20 kOhm and 240 kOhm with a range of 91% of resistance change.

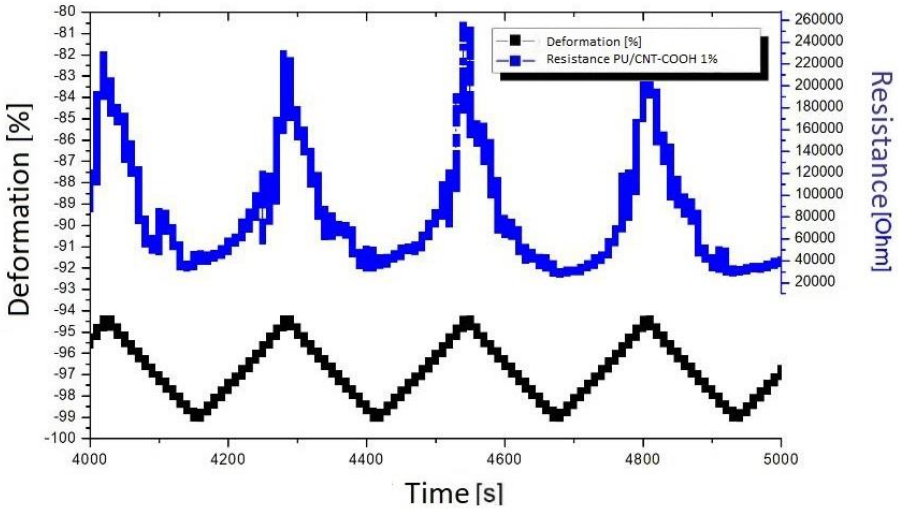

Figure 52 Cyclic test of PU/CNT-COOH 1% at 0.5 mm/min the deformation range (black line) is the 5.5 % of the sample height the electrical resistance (blue line) change with the deformation with a resistance variation of the 91% of the initial resistance.

Figure 53 shows cycles of PU/CNT-COOH 1.5% the electrical resistance changes accordingly with the imposed compression, the acceptable deformation range is 4.5% of compression from 95 to 99.5% the corresponding value of resistance at this deformation are 100 kOhm and 400 kOhm with a range of 75% of resistance change.

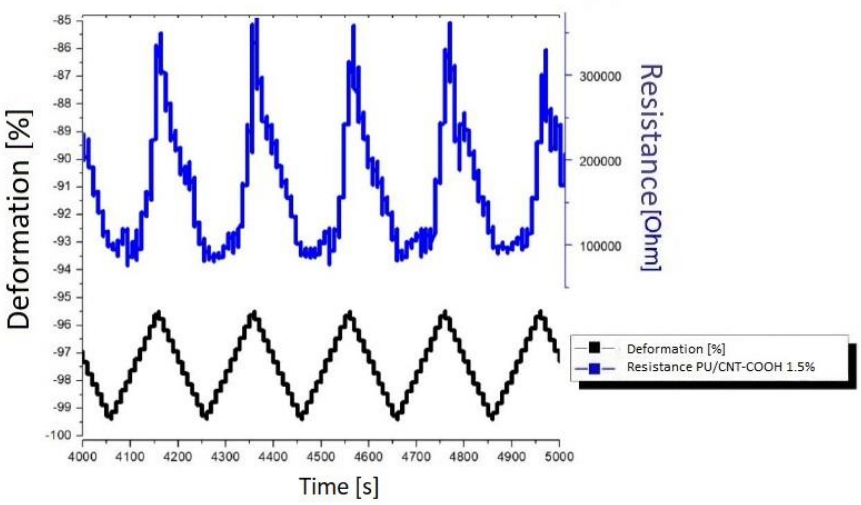

Figure 53 Cyclic test of PU/CNT-COOH 1.5% at 0.5 mm/min the deformation range (black line) is the 4.5 % of the sample height the electrical resistance (blue line) change with the deformation with a resistance variation of the 75% of the initial resistance.

Table 5 Deformation range, Initial resistance value and final resistance value of PU foams that exhibited insulator-conductor transition.

PU foam	Deformation range [%]	Initial resistance value [MOhm]	Final Resistance value [kOhm]
PU CNT-COOH 1%	95.5 – 99.8	>120[1]	618
PU CNT-COOH 1.5%	95.5 – 99.8	>120[1]	34

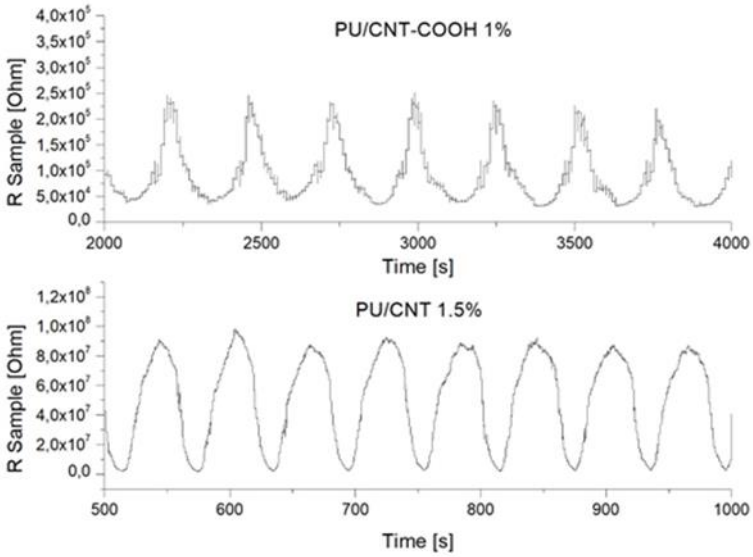

Figure 54 Details of durability piezoresistive tests on PU CNT-COOH 1% (first graph) and PU CNT 1.5% (second graph). (sample size: D 4.5 cm, thk 1 cm)

Table 6 The Gauge factor resulted from tested samples.

PU foam	Gauge Factor
PU CNT 1.5%	80
PU CNT-COOH 1%	33
PU CNT-COOH 1.5%	23

CNT and CNT-COOH were added to polyol solution as conductive particles in order to reach a percolative network in the final polymer. CNTs were added in an industrial polyol mixture named Lupranol produced by BASF. The utilized product is the same used in automotive production plant during the foaming process of dashboard. The formation of CNT distribution within a viscous solution is phenomenon governed by several factors [33–35]. The dispersion method together with the CNTs physical characteristics is the main parameter could affect the result. The major problem related to the network formation is related with the interface forces between CNT and the matrix. On one hand, CNTs tend to merge in agglomerate due

to strong Van Der Waals forces among them. On the other hand, the surface interaction area grows with a rate of 10^3 with the decreasing of CNT volume resulting in lowest CNT content to reach percolation path [34,35]. An important study discovered that high shear force imposed by the dispersion facilities are responsible for CNT breaking and damaging [35]. Moreover, our results show that the PU/CNT-COOH sample has less sensitivity (Gauge factor shows in Table 6) than PU/CNT sample. This could be due to CNT-COOH defect induced by the functionalization method amplified by the dispersion process [36]. Electrical conduction and piezoresistive behaviour of nanocomposite foams can be explained trough percolation theory [6,38]. Increasing the amount of fillers respect to a fixed weight of polymer causes the formation of a percolative conductive network inside the foam and an insulator-to-conductor transition could be clearly seen when a percolative path is established [39,40]. In other words, this specific weight ratio percentage of CNTs on insulating matrix is called percolation threshold. Similarly, studies on polymer/CNT composites have found that changing in percolative network structure, which could be due to a mechanical strain of the sample, affects the electric resistance of the composite. In other words, composite near to the percolation threshold nanocomposite with CNTs showed piezoresistivity [38,40,41]. The imposed strain on the sample leads to a structural change of the CNTs distribution explained with the possibility of polymer chain sliding that drags and shift the CNTs [41]. The result of this is a remarkable change of the nanocomposite electric resistance. The relationship between strain and resistance is different for PU/CNT and PU/CNT-COOH materials. In particular, the intensity and the insulator-conductor transition effect are different. Firstly, PU/CNT samples demonstrated lower value of resistance and they did not show any conductor-insulator transition. Secondly, the PU/CNT-COOH demonstrated highest value of resistance compared to CNT and it was possible to see a clear insulator-conductor transition effect caused by the imposed deformation. Moreover, after the 90% of compressive strain the CNT-COOH foams showed a resistance lower than 120 MOhm. The assumption is functional COOH group improve the compatibility between CNT and the polyol solution [42], in consequence of this CNT could intricately disseminate inside the final PU foam causing a drop down of the overall electric resistance [43]. However, alteration of CNT sp2 bonds [36] leads to a worsening of CNT electrical

properties because of breaking π bond during the formation reaction. The CNT with the functional group did not show a better distribution compared to CNT as confirmed by the SEM images. Moreover, CNT-COOH sample showed a lower value of percolation threshold suggesting smaller but more widespread agglomerations. PU/CNT sample showed highest performance in terms of conductivity and sensitivity. The correlation between PU/CNT foam resistance and applied strain resulted linear. This suggests a finer network and a better dispersion. Instead, PU/CNT-COOH sample showed conduction between agglomerate and the exponential behaviour of the resulting resistance-strain curve suggesting that the tunnelling resistance has a major role in the conduction mechanism of this sample according to Figure 54. Furthermore, the insulator-conductor transition (detailed documented in Table 5) of this sample is a more desirable feature for lees demanding application as command button (on/off). On the contrary, PU/CNT sample are more suitable for piezoresistve sensor and tuneable devices.

4.1.5 Characterization of thermoplastic polyurethane with reduced graphene nanoplatelets (TPU/GNP)

4.1.5.1 Tensile test of SN-1487-B with Deben

The tensile test was performed on the samples obtained by SN-1487-B sheet and prepared with the procedure described in previous section. The test was performed with DEBEN and the Kithley multimeters. The deformation rate was 1.5 mm/min and the coupon were elongate until breakage. The result of the test is shown in Figure 55.

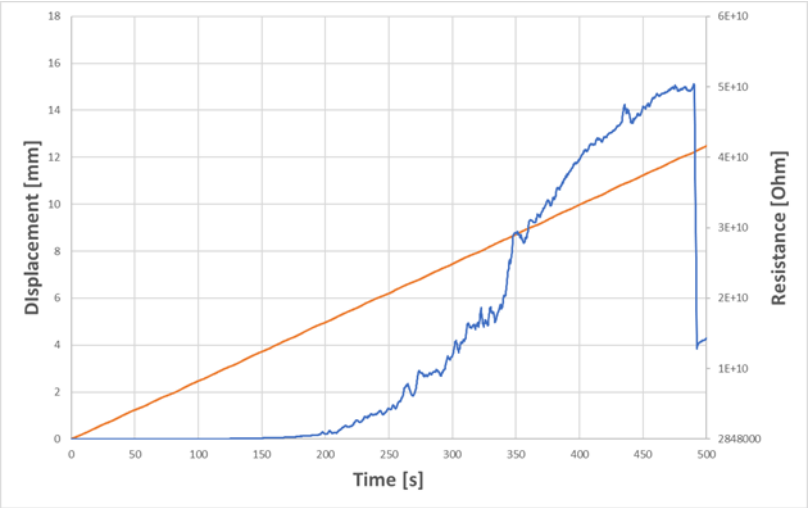

Figure 55 Results of tensile test performed on SN-1487-B. The orange line shows the displacement (mm) and the blue line shows the resistance (Ohm).

The material shows a good mechanical response and the sample returned at the same initial condition when the stress was not applied. This material also shows a good correlation between displacement and resistance change.

4.1.6 Cyclic piezoresistive characterization with MTS tensile testing machine

TTest-1

The TTest-1 has been done on the rod specimen 1 of SN-1487-B to test the electromechanical behaviour and to evaluate the best strategy for comparing the property of the SN-1487-B material with other material tested in CRF laboratory. The deformation rate of the test has been settled to 1.5 mm/min with any elongation limit.

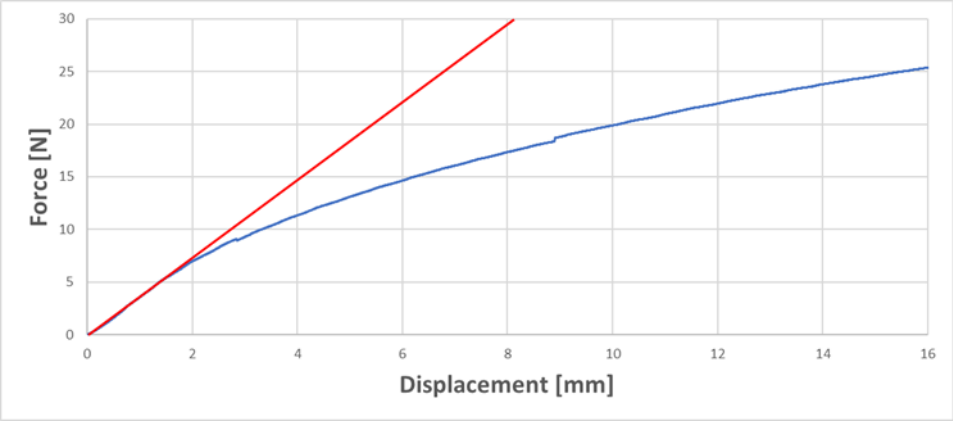

Figure 56 The load-displacement curve of the specimen 1 during TTest-1(blue) and the linear approximation (red).

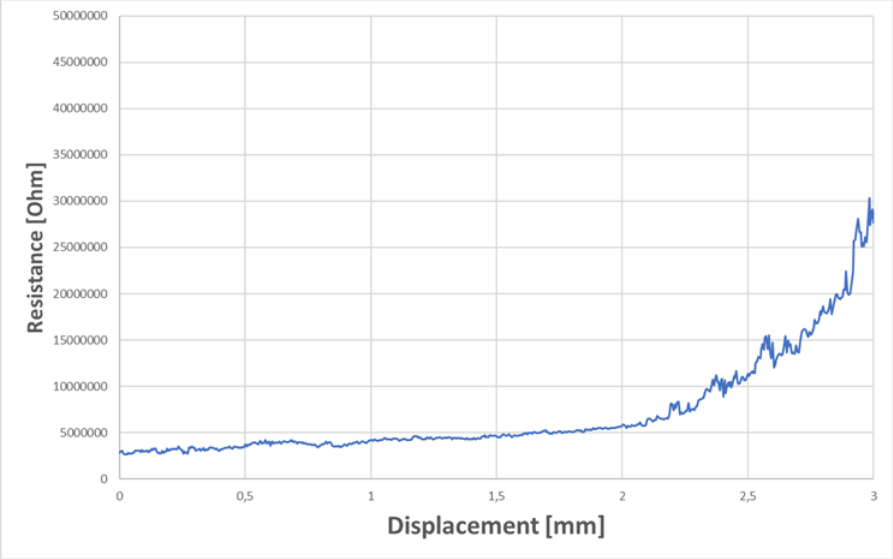

Figure 57 The electric resistance during TTest-1 of SN-1487-B.

Figure 56 and Figure 57 show the results of this test which demonstrates clearly a piezoresistive response of the material during the entire tensile deformation. The mechanical and electrical behaviour are linearly dependent from 0 mm of deformation to 2 mm of deformation. After this threshold value the mechanical (Load) and electrical signal (Resistance) start to increase sharply and their relations with the imposed displacement are no longer linear. The next experiment was aimed to investigate the linear range from 0 to 2 mm of displacement.

TTest-2

The second test was a cyclic test to understand the electromechanical behaviour after 100 cycles. The maximum deformation was placed to 1 mm and the deformation rate was 1 Hz. The electric signal of the material should be consistent with the increase in the number of cycles. In particular, the output does not have to drift consistently from its initial values. The noise of the signal does not should exceed a specific value in order to be useful for an electronic interface. Figure 58 shows the electric signal corresponding to the cyclic displacement imposed by the MTS tensile testing machine. The initial resistance of specimen when any deformation is applied was 74630□□

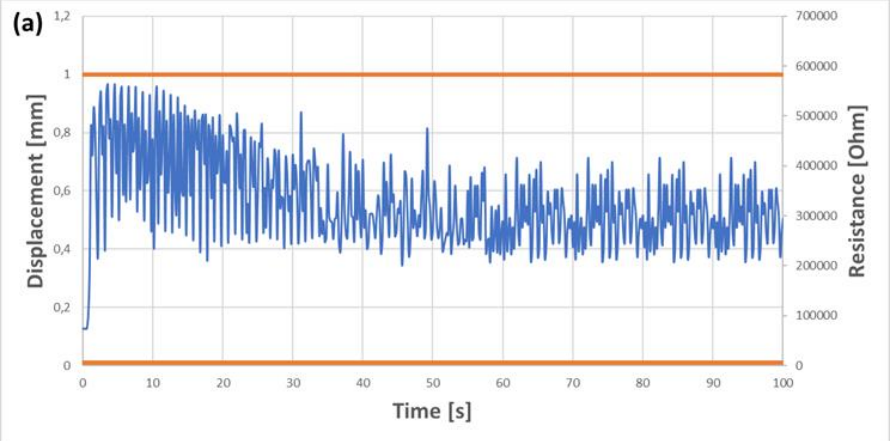

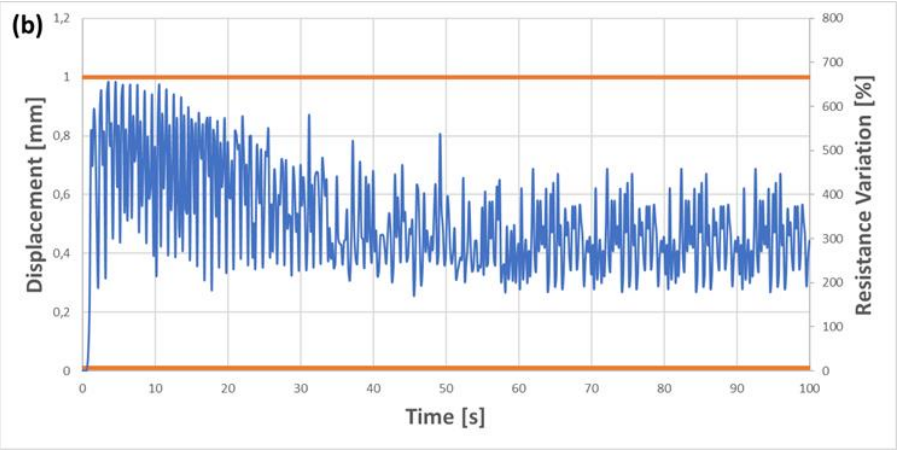

Figure 58 Results of TTest–2. The graph (a) shows the resistance (blue) and the maximum and minimum displacements (orange) while the specimen has been subjected to cyclic bending test. The graph (b) shows the resistance variation DR (blue) and the displacement (orange) during the same test.

The electrical resistance changes accordingly with the imposed displacement and the resistance variation range starts from 0% to 650%. Furthermore, the signal drifted from the first cycle according to the graph in Figure 58. The drift of the electrical resistance is not regular, and the electronic interface could have a problem to correlate this random variation to a specific deformation status. To evaluate the signal quality is useful to look at a small number of cycles. Figure 59 gives information about five cycles of TTest-2. The resistance does not simultaneously change with the mechanical deformation and it is very difficult to correlate a specific resistance value with a displacement of the specimens. The electric signal shows a strange peak in the descending phase of the cycle. The noise of the signal is not excessively high, and it should not be a problem for the electronic interface.

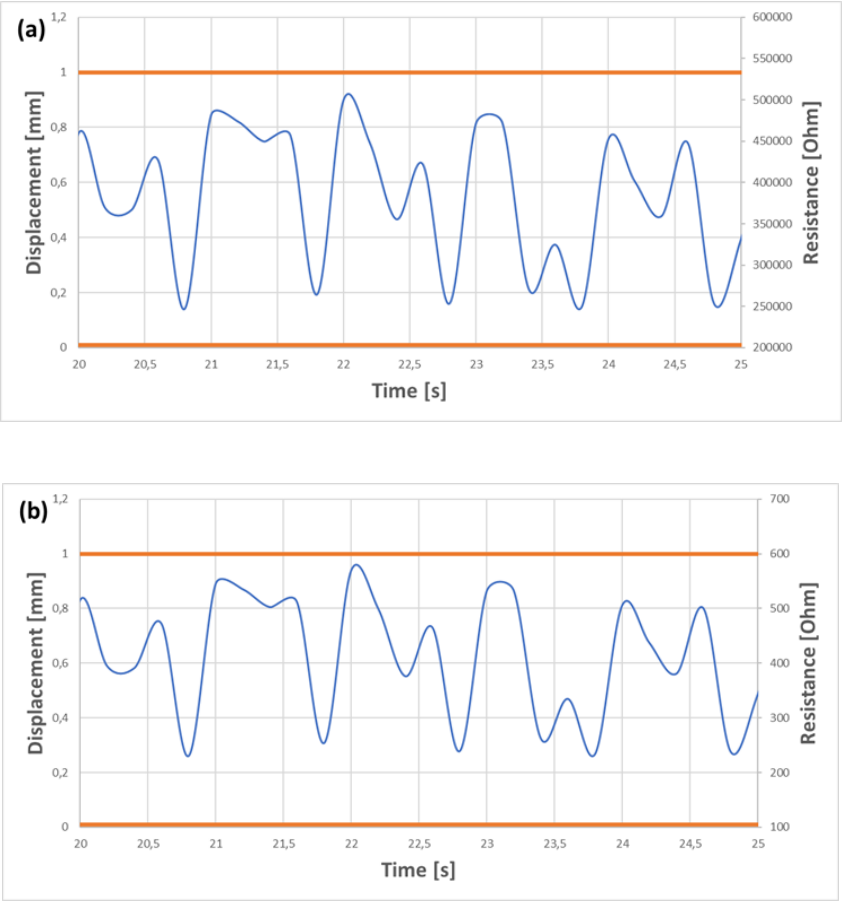

Figure 59 The detail of the results of TTest-2. The first graph shows five cycles of the graph (a)-Figure 58a and the second graph shows five cycles of the graph (b)- Figure 58b.

TTest-3

The Ttest-3 was a cyclic test to confirm the electromechanical behaviour of the material after 100 cycles. The maximum elongation of TTest-3 was the same of TTest-2 and the deformation cycle rate was 2 Hz. The output does not have to drift consistently from its initial values. Figure 60 shows the electric signal corresponding to the displacement imposed by the MTS tensile testing machine. The initial resistance of specimen when any deformation is applied was 117463 Ohm.

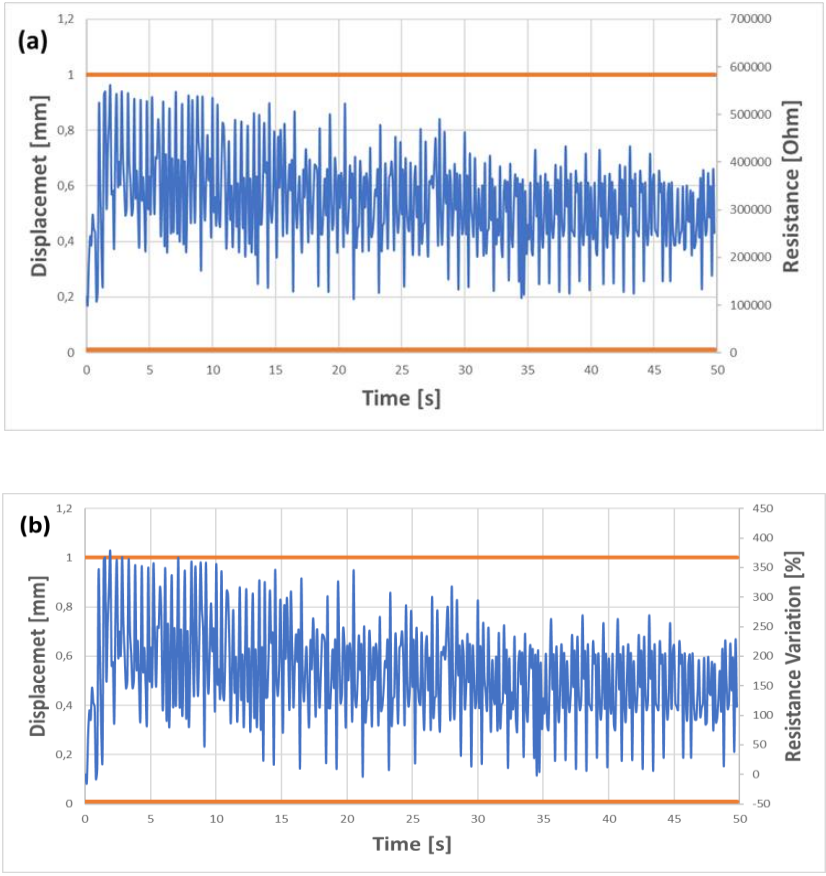

Figure 60 Results of TTest–3. The graph (a) shows the resistance (blue) and the maximum and minimum displacements (orange) while the specimen has been subjected to cyclic bending test. The graph (b) shows the resistance variation DR (blue) and the displacement (orange) during the same test.

The electrical resistance changes with the imposed displacement and the range of resistance variation starts from 0% to 350%. The signal shape of TTest-3 is quite similar to the trend obtained TTest-2. To evaluate the signal quality is useful to look at a small number of cycles like TTest-3. Figure 61 gives information about five cycles of TTest-3. The resistance does not simultaneously change with the mechanical deformation and it is very difficult to correlate a specific resistance value with a displacement of the specimens. The electric signal shows a strange peak in the descending phase of the cycle. The noise of the signal is not excessively high, and it should not be a problem for the electronic interface. The main problem, which it is clearly shown also in TTest-2, is the randomness of the signal.

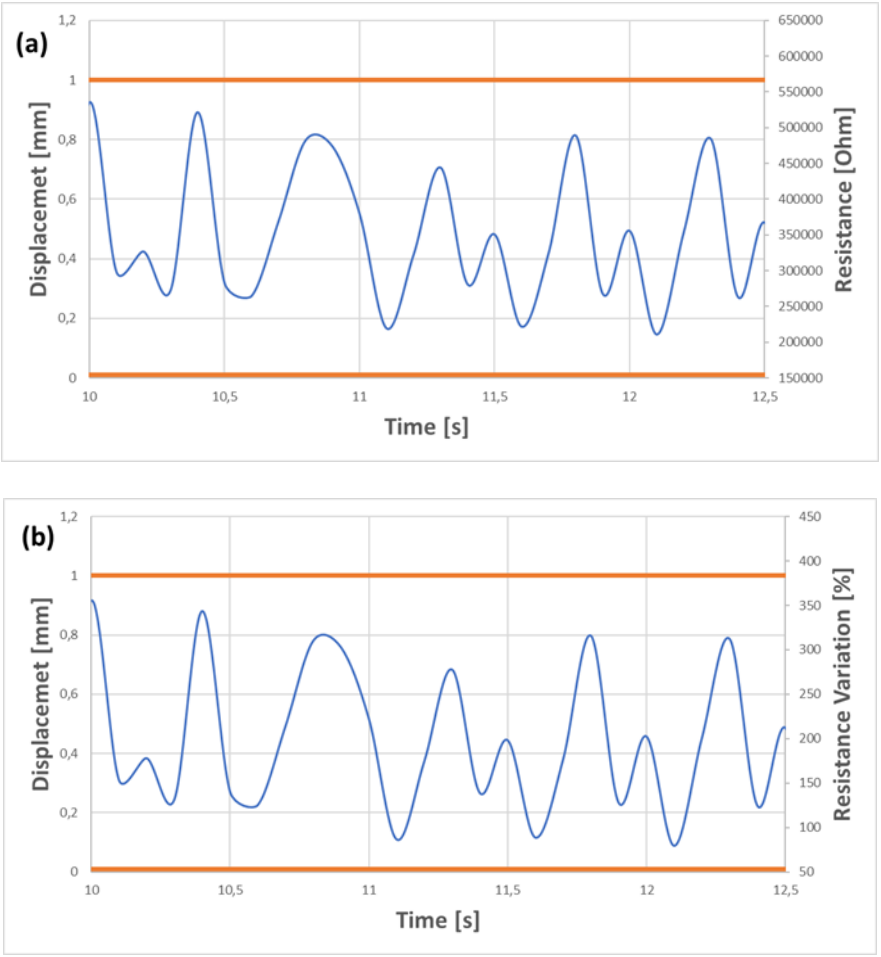

Figure 61 The detail of the results of TTest-3. The first graph shows five cycles of the graph (a)-Figure 60a and the second graph shows five cycles of the graph (b)- Figure 60b.

TTest-4

The TTest-4 was a cyclic test to explore the electromechanical behaviour of the material after 100 cycles by changing the deformation rate up to 0.5 Hz with the same deformation of previous test. The output does not have to drift consistently from its initial values. The noise of the signal does not should exceed a specific value in order to be useful for an electronic interface. Figure 62 shows the electric signal corresponding to the displacement imposed by the MTS tensile testing machine. The initial resistance of specimen when any deformation is applied was 27117Ohm.

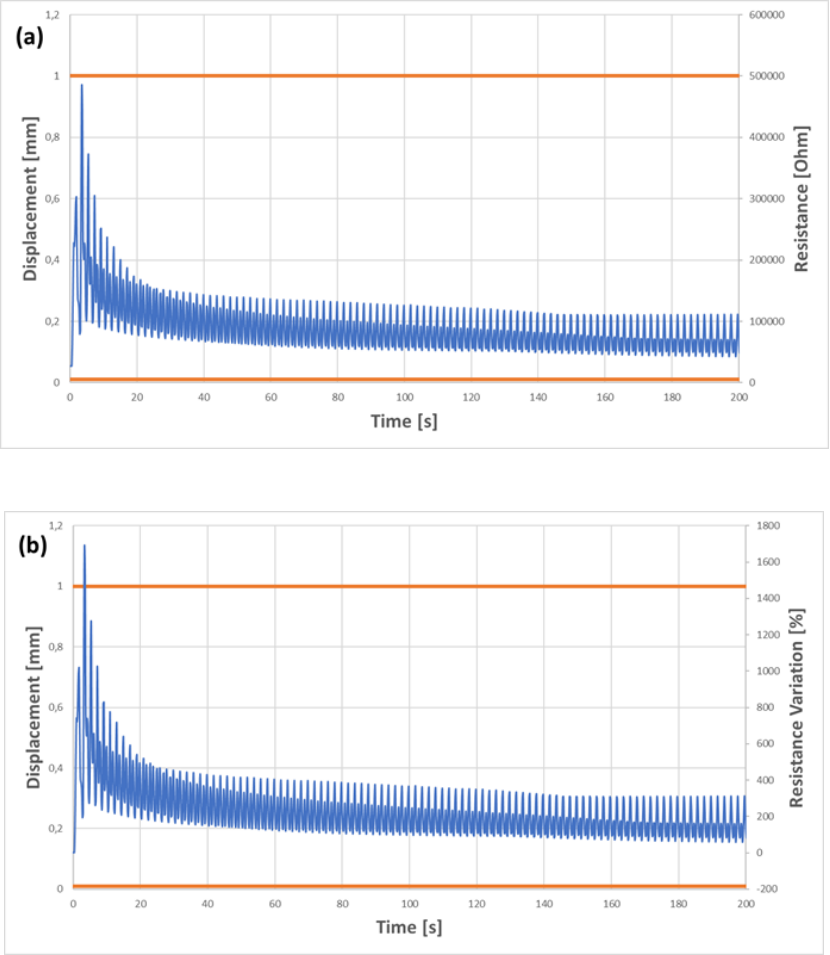

Figure 62 Results of TTest–4. The graph (a) shows the resistance (blue) and the maximum and minimum displacements (orange) while the specimen has been subjected to cyclic bending test. The graph (b) shows the resistance variation DR (blue) and the displacement (orange) during the same test.

The electrical resistance changes with the imposed displacement and the range of resistance variation starts from 0% to 1600%. Figure 63 gives information about five cycles of TTest-4. The resistance does not

simultaneously change with the mechanical deformation. The signal does not show any electrical noise. In this case, the signal responds regularly with the applied displacement different to the electrical behaviour of previous sample. However, the electric signal still shows a strange peak in the descending phase of the cycle.

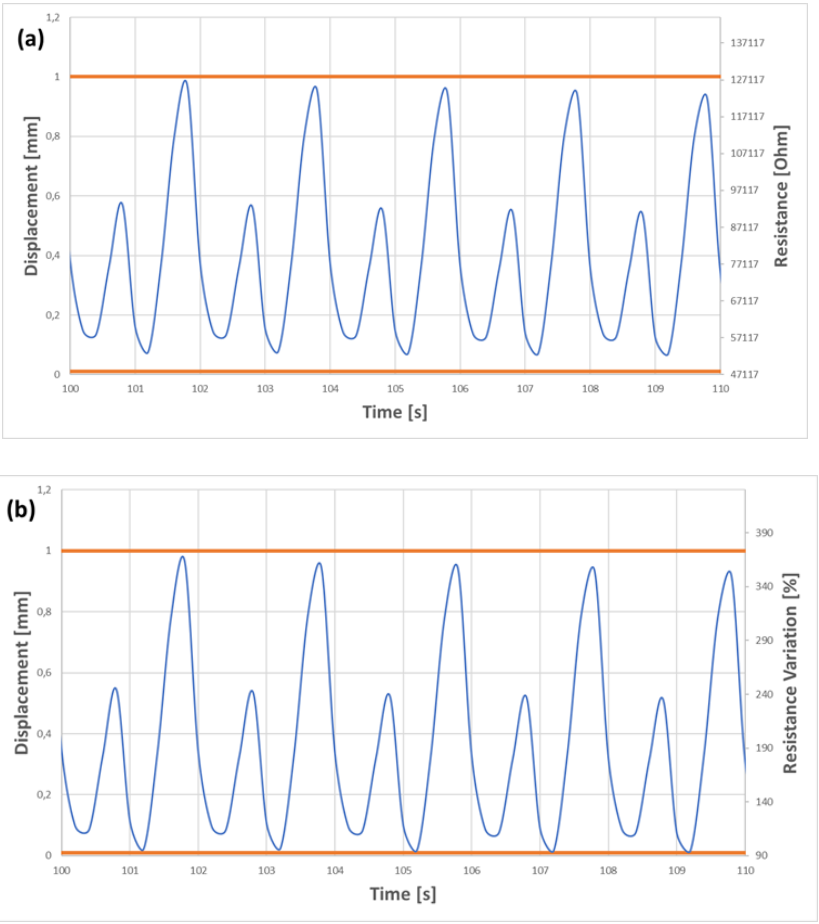

Figure 63 The detail of the results of TTest-4 The first graph shows five cycles of the graph (a)-Figure 62a and the second graph shows five cycles of the graph (b)- Figure 62b.

TTest-5

The TTest-5 was a cyclic test to explore the electromechanical behaviour of the material after 100 cycles by increasing the maximum deformation to 2 mm with the best deformation rate of 0.5 Hz. Figure 64 shows the electric signal corresponding to the displacement imposed by the MTS tensile testing machine. The initial resistance of specimen when any deformation is applied was 48403Ohm.

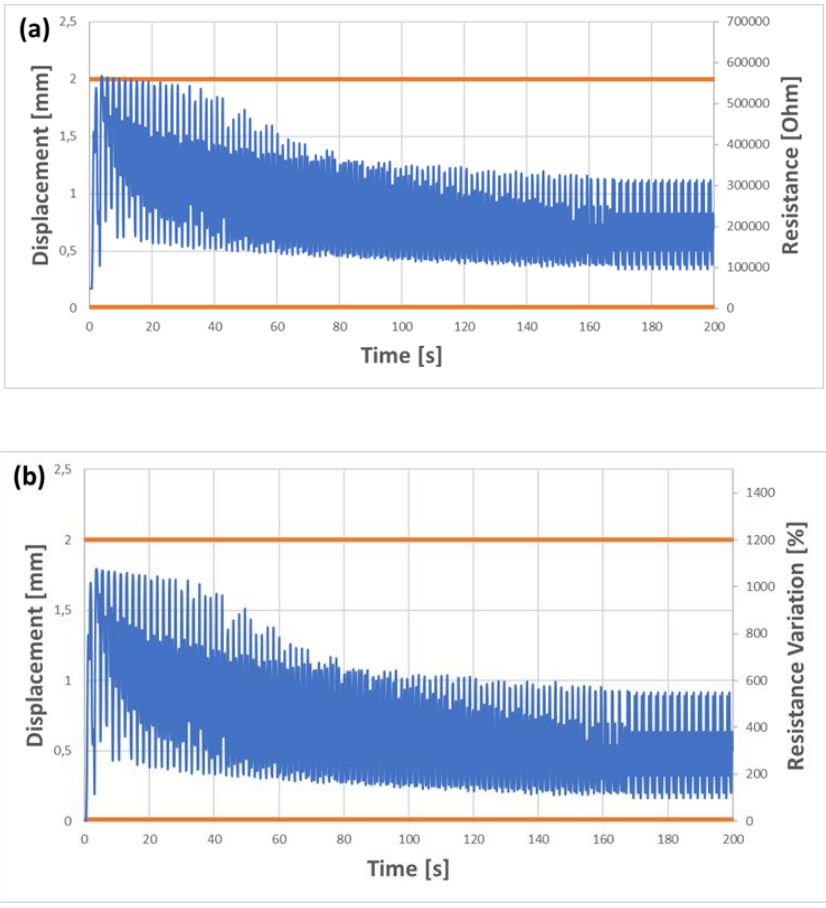

Figure 64 Results of TTest–5. The graph (a) shows the resistance (blue) and the maximum and minimum displacements (orange) while the specimen has been subjected to cyclic bending test. The graph (b) shows the resistance variation DR (blue) and the displacement (orange) during the same test.

The electrical resistance changes accordingly with the imposed displacement and the resistance variation range starts from 0% to 1200%. The signal shape of TTest-5 is mostly like the trend of TTest-4. The difference in resistance variation range could be due to the difference configuration of the fillers inside the TPU matrix, which changes the conductive network inside the specimens. Furthermore, the signal slightly drifted from the first cycle. Figure 65 gives information about five cycles of TTest-5. The resistance does not simultaneously change with the mechanical deformation, but it is possible to correlate a specific

resistance value with a displacement of the specimens. The noise of the signal is not excessively high, and it should not be a problem for the electronic interface. Similar to previous test, the signal responds regularly with the applied displacement. However, the electric signal still shows a strange peak in the descending phase of the cycle.

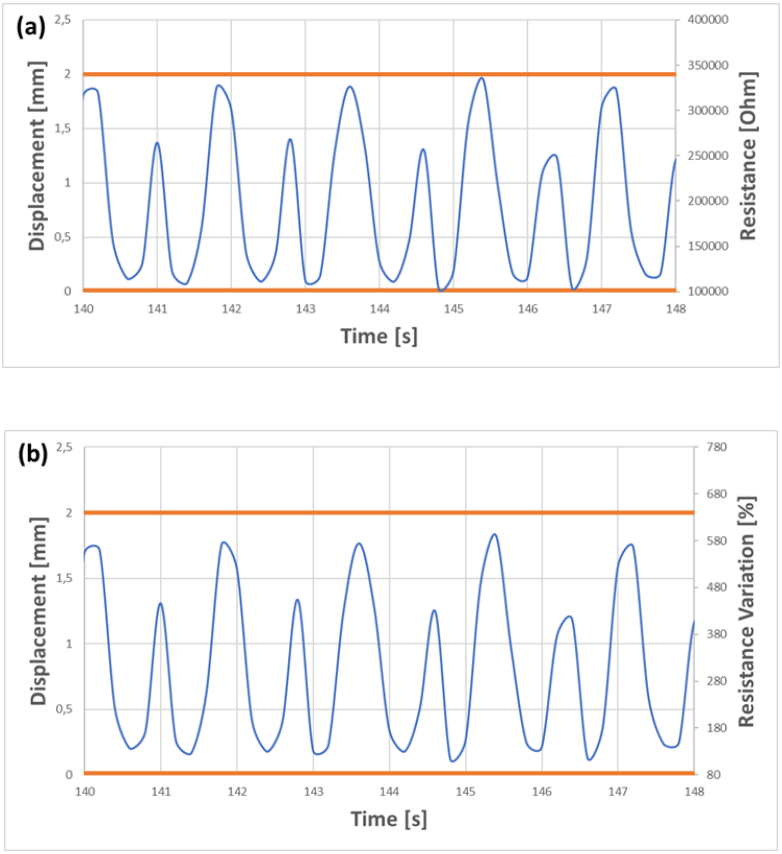

Figure 65 The detail of the results of TTest-5 The first graph shows five cycles of the graph (a)-Figure 64a and the second graph shows five cycles of the graph (b)- Figure 64b.

TTest-6

The TTest-6 was a cyclic test to explore the electromechanical behaviour of the material after 100 cycles by changing the maximum deformation value to 1 mm with the best deformation rate of 0.5 Hz obtained in previous test. The electric signal of the specimen should be like the signal obtained in previous tests with the same frequency. In particular, the output does not have to drift consistently from its initial values. Figure 66 shows the electric signal corresponding to the displacement imposed by the Instron tensile testing machine. The initial resistance of specimen when any deformation is applied was 31929Ohm.

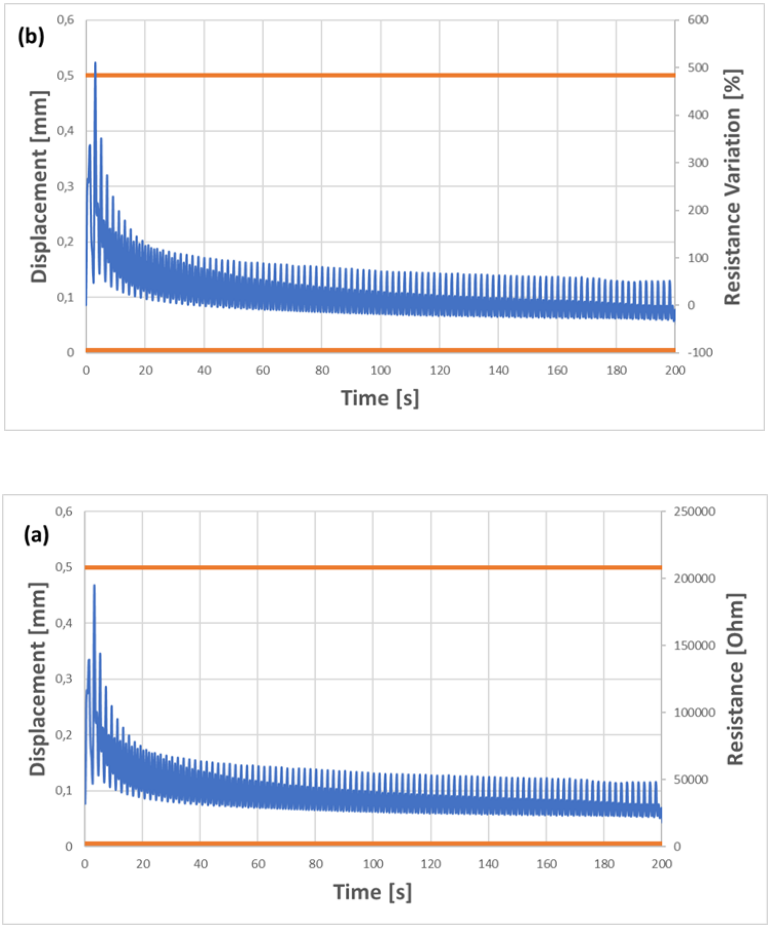

Figure 66 Results of TTest–6. The graph (a) shows the resistance (blue) and the maximum and minimum displacements (orange) while the specimen has been subjected to cyclic bending test. The graph (b) shows the resistance variation DR (blue) and the displacement (orange) during the same test.

The electrical resistance changes accordingly with the imposed displacement and the resistance variation range starts from 0% to 500%. The signal shape of TTest-5 is mostly like the trend of TTest-4 and TTest-5.

The difference in resistance variation range could be due to the difference configuration of the fillers inside the TPU matrix, which changes the conductive network inside the specimens.

Figure 67 gives information about five cycles of TTest-5. The resistance does not simultaneously change with the mechanical deformation, but it is possible to correlate a specific resistance value with a displacement of the specimens. The noise of the signal is not excessively high, and it should not be a problem for the electronic interface. Like previous test, the signal responds regularly with the applied displacement. However, the electric signal still shows a strange peak in the descending phase of the cycle.

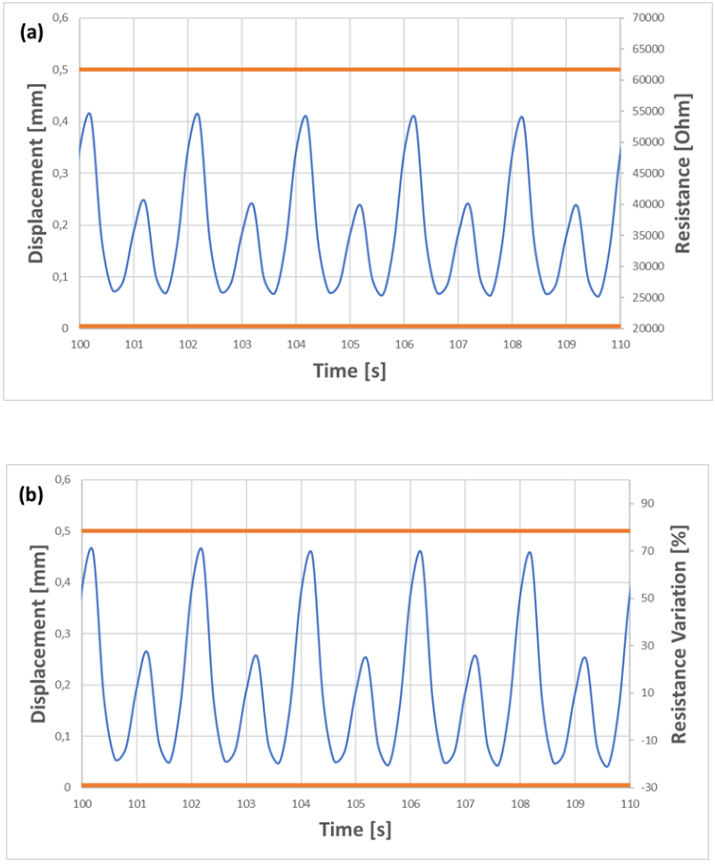

Figure 67 The detail of the results of TTest-6 The first graph shows five cycles of the graph (a)-Figure 66a and the second graph shows five cycles of the graph (b)-Figure 66b.

TTest-7

The TTest-7 was a cyclic test to explore the electromechanical behaviour of the material after 1000 cycles with the best maximum deformation value of 1 mm and the best deformation rate of 0.5 Hz obtained in previous tests. The output does not have to drift consistently from its initial values. The noise of the signal does not should exceed a specific value in order to be useful for an electronic interface. Figure 68 shows the electric signal corresponding to the displacement imposed by the MTS tensile testing machine. The initial resistance of specimen when any deformation is applied was 19946Ohm.

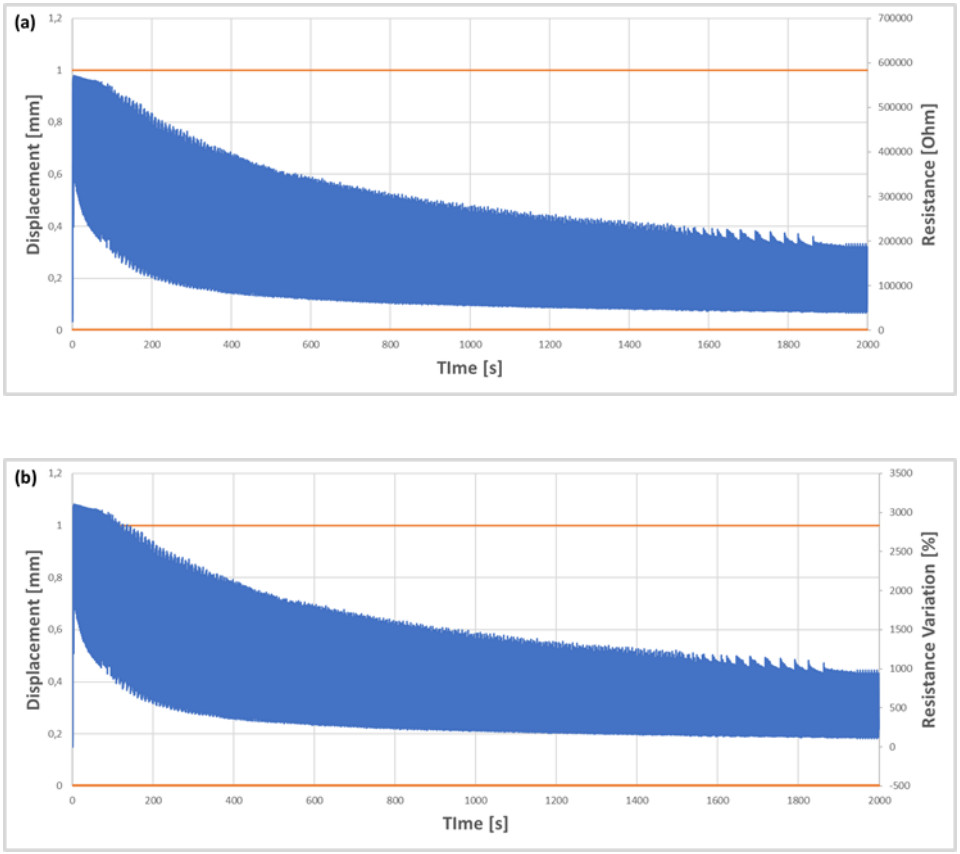

Figure 68 Results of TTest – 7 The graph (a) shows the resistance (blue) and the maximum and minimum displacements (orange) while the specimen has been subjected to cyclic bending test. The graph (b) shows the resistance variation ⍰R (blue) and the displacement (orange) during the same test.

The electrical resistance changes with the imposed displacement and the resistance variation range starts from 0% to 3000%. After the initial deformation, the sample seems to be more stable. The signal shape of TTest-7 is mostly like the trend of TTest-5. The signal slightly drifted from the first cycle according to the

graph in Figure 62. These results confirm a drift problem which can be solved taking this into account with the electronic acquisition system. To evaluate the signal quality is useful to look at a small number of cycles like previous results.

Figure 69 gives information about five cycles of TTest-7. The resistance does not change with the mechanical deformation and it is possible to correlate the resistance values with a displacement. The noise of the signal is quite low. The electrical resistance follows the imposed deformation. Like previous test, the signal responds regularly with the applied displacement. However, the electric signal still shows a strange peak in the descending phase of the cycle.

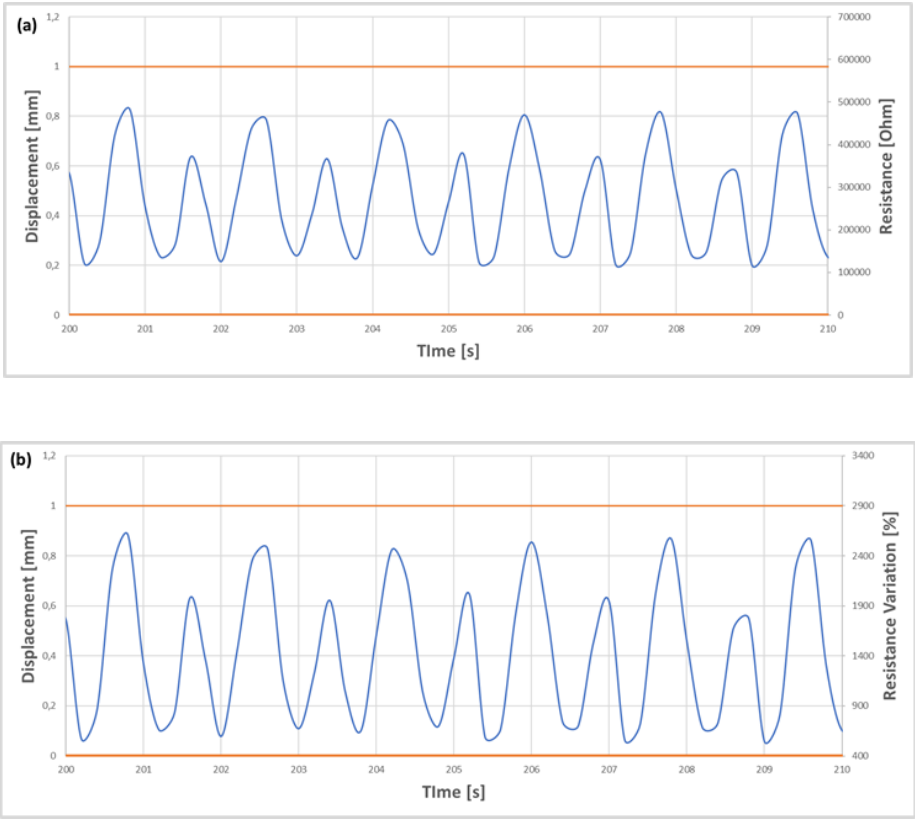

Figure 69 The detail of the results of TTest-7 the first graph shows five cycles of the graph (a)-Figure 68a and the second graph shows five cycles of the graph (b)- Figure 68b.

5 Conclusion and outlook

The purpose of this work was to fabricate and characterize a piezoresistive PU/CNT semi-rigid foam and TPU/graphene skin for automotive applications. In particular, the final application of this new kind of pressure sensors will be the total integration of components inside a mono-material dashboard. The first step concerned the dispersion of CNT inside the polyol commercial solution furnished by BASF. The investigated dispersion method was purely mechanical dispersion with a 4-blade mixer. Several attempts were tried, including change the working-hours and the speed rate, the optimized parameters for the CNTs dispersion have been resulted: 1500 rpm for 2 hours. The major problem resulted from the dispersion phase was the chemical degradation of the polyol mixture which showed thermal degradation and loss of volatile components. Sonication and extended in time dispersion procedures led to excessive degradation of the BASF polyol mixture. The second step was the adding of P-MDI to the polyol/CNT mixture and foaming the polyurethane inside a plastic cup. Samples with different CNT weight continent was produced in order to obtain a percolation curve but the only conductive samples were PU/CNT 1,5%, PU/CNT-COOH 1% and PU/CNT-COOH 1,5%. The composite foams were cut in disk shape of diameter 4 cm and 1 cm of thick and characterized in terms of mechanical and piezoresistive properties. PU/CNT 1.5% sample showed highest performance in terms of conductivity and sensitivity with a Gf of 80. Instead, PU/CNT-COOH 1.5% sample showed an insulator-conductor transition of about 80% of compressive strain but a very low sensitivity (Gf of 23). The two formulations showed also different conduction mechanisms. In fact, the PU/CNT-COOH resistance-strain curve showed exponential parts suggesting tunnelling resistance variation as prevalent physical effect for piezoresistive behaviour. This was proved also by SEM analysis which showed agglomerates inside the final composite foams. In parallel, thermoplastic polyurethane loaded with GNPs was studied and characterized in FORTH laboratories. The thermoplastic polyurethane produced by BASF was compounded with Graphene (GNP commercial quality) produced by AVANZARE. The samples with different graphene load were sanded to FORTH laboratories in Greece where the electromechanical characterization was carried out. The sample loaded with 12.5% and 15% of Graphene nanoplatelets (AVAFLG18) was characterized in order to understand the piezoresistive

behaviour of such material. Several cyclic tests were planned based on an initial characterization made with a micro-tensile tester (DEBEN). The results showed a nonlinear piezoresistive response of the sample and the best results in terms of noise and repeatability was obtained with the lowest frequency of 0.5 Hz and a displacement of 1 mm. The piezoresistive behaviour suggest a different strain distribution inside the material when subjected to load-unload cycle. The bulk of the sample seems to delay the piezoresistive response and a second lowest peak appear during the cycles. The final procedure was established among a variety of method described and suggested in the state-of-the-art paragraph. The materials were chosen considering industrial constraints and procedure. The final method was resulted from a series of attempts based on industrial application, facilities, and materials. Conductive fillers were chosen with the aim of reducing the complexities of dashboard components elements and assuring the high value of performances in terms of conductivities and piezoresistivitie properties. Moreover, high fillers quality ensures highest performance with lowest weight contents which also allows the lowest cost of the final smart components. The recyclability of complex component, which are for instance the steering wheel, dashboard etc., will be improved by removing different multi-materials elements with the engineered smart nanocomposites composed of only carbon-based materials. The developed approaches are based on polyurethanes as matrix and alternatively CNT or CNT-COOH as conductive fillers. The polyurethane is widely applied in the interior dashboard components and structure for structural and aesthetics reasons. In particular, the polyurethane foam closed for this study are applied all around finishes and protrusions of the car dashboard. The industrial application of the polyurethane foam is an important step of the dashboard production and allows us the possibility to exploit the process to introduce new smart functionalities and removing button and switches in further step. Furthermore, the proposed approach will allow to industrial car makers of reducing the production working time and the cost at the same time increasing the functionality and the customer perceived quality. In conclusion, the different piezoresistive behaviour of polyurethane foam loaded with CNT or CNT-COOH are interesting and could be applied for different purpose (e.g PU/CNT foam for sensitive application and PU/CNT for switch). Moreover, the TPU/graphene skin showed piezoresistive response in the automotive range of

applicability, but further improvement should be done in order to understand the mechanical behaviour of the nanocomposite. Numerical simulations should be done to better understand the double-peak shown in all piezoresistive graphs resulted from TPU/GNP skin characterization. Improvement could also be done in order to obtain a more uniform material with more reliable properties.

6 Reference

1. Cravanzola, S.; Haznedar, G.; Scarano, D.; Zecchina, A.; Cesano, F. Carbon-based piezoresistive polymer composites: Structure and electrical properties. *Carbon N. Y.* **2013**, *62*, 270–277, doi:10.1016/j.carbon.2013.05.064.

2. Padovano, E.; Bonelli, M.E.; Veca, A.; De Meo, E.; Badini, C. Effect of long-term mechanical cycling and laser surface treatment on piezoresistive properties of SEBS-CNTs composites. *React. Funct. Polym.* **2020**, *152*, 104601, doi:https://doi.org/10.1016/j.reactfunctpolym.2020.104601.

3. Yang, S.Y.; Lin, W.N.; Huang, Y.L.; Tien, H.W.; Wang, J.Y.; Ma, C.C.M.; Li, S.M.; Wang, Y.S. Synergetic effects of graphene platelets and carbon nanotubes on the mechanical and thermal properties of epoxy composites. *Carbon N. Y.* **2011**, *49*, 793–803, doi:10.1016/j.carbon.2010.10.014.

4. Yu, J.; Choi, H.K.; Kim, H.S.; Kim, S.Y. Synergistic effect of hybrid graphene nanoplatelet and multi-walled carbon nanotube fillers on the thermal conductivity of polymer composites and theoretical modeling of the synergistic effect. *Compos. Part A Appl. Sci. Manuf.* **2016**, *88*, 79–85, doi:10.1016/j.compositesa.2016.05.022.

5. Ke, K.; Bonab, V.S.; Yuan, D.; Manas-zloczower, I. Piezoresistive thermoplastic polyurethane nanocomposites with carbon nanostructures. *Carbon N. Y.* **2018**, *139*, 52–58, doi:10.1016/j.carbon.2018.06.037.

6. Yan, D.-X.; Dai, K.; Xiang, Z.-D.; Li, Z.-M.; Ji, X.; Zhang, W.-Q. Electrical conductivity and major mechanical and thermal properties of carbon nanotube-filled polyurethane foams. *J. Appl. Polym. Sci.* **2011**, *120*, 3014–3019, doi:doi:10.1002/app.33437.

7. Caradonna, A.; Badini, C.; Padovano, E.; Veca, A.; De Meo, E.; Pietroluongo, M. Laser Treatments for Improving Electrical Conductivity and Piezoresistive Behavior of Polymer–Carbon Nanofiller Composites. *Micromachines* **2019**, *10*, 63, doi:10.3390/mi10010063.

8. Wang, X.H.; Mu, Y.H.; Tang, Q.; Li, C.Q. Preparation and Performance of PVC/CNT Nanocomposite. *Adv. Polym. Technol.* **2018**, *37*, 358–364, doi:10.1002/adv.21674.

9. Ke, K.; Solouki Bonab, V.; Yuan, D.; Manas-Zloczower, I. Piezoresistive thermoplastic polyurethane nanocomposites with carbon nanostructures. *Carbon N. Y.* **2018**, *139*, 52–58, doi:10.1016/j.carbon.2018.06.037.

10. Sang, Z.; Ke, K.; Manas-Zloczower, I. Effect of carbon nanotube morphology on properties in thermoplastic elastomer composites for strain sensors. *Compos. Part A Appl. Sci. Manuf.* **2019**, *121*, 207–212, doi:10.1016/j.compositesa.2019.03.007.

11. Bardelli, F.; Application, F.; Data, P.; Cesano, F.; Civera, P.; Demarchi, D.; Galli, R.; Scarano, D. PROCESSES FOR PRODUCING CONDUCTIVE AND/OR PIEZORESISTIVE TRACES 0N POLYMERIC SUBSTRATES 2013, US 20130255997Al.

12. Marchesan, S.; Prato, M. Nanomaterials for (Nano)medicine. *ACS Med. Chem. Lett.* **2013**, 2012–2014, doi:10.1021/ml3003742.

13. Cardinal, M.F.; Mcanally, M.O.; Duyne, R.P. Van; Ende, E. Vander; Hackler, R.A.; Stair, P.C.; Schatz, G.C. Chem Soc Rev Expanding applications of SERS through versatile nanomaterials engineering. **2017**, 3886–3903, doi:10.1039/c7cs00207f.

14. Abishera, R.; Velmurugan, R.; Nagendra Gopal, K. V. Reversible plasticity shape memory

effect in carbon nanotube/epoxy nanocomposites: Shape recovery studies for torsional and bending deformations. *Polym. Eng. Sci.* **2018**, *58*, E189–E198, doi:10.1002/pen.24861.

15. Avil, F.; Cen-puc, M. Piezoresistivity , Strain , and Damage Self-Sensing of Polymer Composites Filled with Carbon Nanostructures. *Adv. Eng. Mater.* **2018**, *1701159*, 1–23, doi:10.1002/adem.201701159.

16. Garima, Q. Journal of Industrial and Engineering Chemistry A review on carbon nanotubes and graphene as fillers in reinforced polymer nanocomposites. *J. Ind. Eng. Chem.* **2014**, doi:10.1016/j.jiec.2014.03.022.

17. Chen, Y.; Li, Y.; Xu, D.; Zhai, W. thermoplastic polyurethane / graphene composites. *RSC Adv.* **2015**, 82034–82041, doi:10.1039/c5ra12515d.

18. Liu, H.; Gao, J.; Huang, W.; Dai, K.; Zheng, G.; Liu, C.; Shen, C.; Yan, X.; Guo, J.; Guo, Z. Electrically conductive strain sensing polyurethane nanocomposites with synergistic carbon nanotubes and graphene bifillers. *Nanoscale* **2016**, *8*, 12977–12989, doi:10.1039/c6nr02216b.

19. Santamaria, A.; Garci, J.L. 1 , 1 0 -binaphthylphosphazene R / S Random Copolymer. *Physics (College. Park. Md).* **2010**, *48*, 2215–2221, doi:10.1002/POLB.

20. Simmons, J.G. Generalized Formula for the Electric Tunnel Effect between Similar Electrodes Separated by a Thin Insulating Film. *J. Appl. Phys.* **1963**, *34*, 6, doi:10.1063/1.1702682.

21. Nag, A.; Mitra, A.; Chandra, S. Sensors and Actuators A : Physical Graphene and its sensor-based applications : A review. *Sensors Actuators A. Phys.* **2018**, *270*, 177–194, doi:10.1016/j.sna.2017.12.028.

22. Milazzo, M.; Gallone, G.; Marcello, E.; Mariniello, M.D.; Bruschini, L.; Roy, I.; Danti, S. Biodegradable Polymeric Micro / Nano-Structures with Intrinsic Antifouling / Antimicrobial Properties : Relevance in Damaged Skin and Other Biomedical Applications. **2020**, 1–20.

23. Theodosiou, T.C.; Saravanos, D.A. Numerical investigation of mechanisms affecting the piezoresistive properties of CNT-doped polymers using multi-scale models. *Compos. Sci. Technol.* **2010**, *70*, 1312–1320, doi:10.1016/j.compscitech.2010.04.003.

24. Tewari, A.; Gandla, S.; Bohm, S.; McNeill, C.R.; Gupta, D. Highly Exfoliated MWNT-rGO Ink-Wrapped Polyurethane Foam for Piezoresistive Pressure Sensor Applications. *ACS Appl. Mater. Interfaces* **2018**, *10*, 5185–5195, doi:10.1021/acsami.7b15252.

25. Maryam Bandarian, Akbar Shojaeia, A.M.R. Thermal , mechanical and acoustic damping properties of flexible open-cell polyurethane / multi-walled carbon nanotube foams : effect of surface functionality of nanotubes Maryam Bandarian , a Akbar Shojaei a ∗ and Ali Morad Rashidi b. *Polym Int 2011* **2011**, *60*, 475–482, doi:10.1002/pi.2971.

26. Liu, S.; Chevali, V.S.; Xu, Z.; Hui, D.; Wang, H. A review of extending performance of epoxy resins using carbon nanomaterials. *Compos. Part B* **2018**, *136*, 197–214, doi:10.1016/j.compositesb.2017.08.020.

27. Guo, P.S.; Sun, Z.; Chen, Y.W.; Zheng, Z.H. A novel approach to mass synthesis of raw CNTs for printed field emission cathodes by chemical vapour deposition. **2006**, *60*, 966–969, doi:10.1016/j.matlet.2005.10.079.

28. Chhowalla, M.; Teo, K.B.K.; Ducati, C.; Rupesinghe, N.L.; Amaratunga, G.A.J. Growth process conditions of vertically aligned carbon nanotubes using plasma enhanced chemical vapor deposition. **2001**, *90*, 5308–5317, doi:10.1063/1.1410322.

29. Sánchez-romate, X.F.; Artigas, J.; Jiménez-suárez, A.; Sánchez, M.; Güemes, A.; Ureña, A. Critical parameters of carbon nanotube reinforced composites for structural health monitoring applications : Empirical results versus theoretical predictions. *Compos. Sci. Technol.* **2019**, *171*, 44–53, doi:10.1016/j.compscitech.2018.12.010.

30. Wang, X.; Li, Q.; Xie, J.; Jin, Z.; Wang, J.; Li, Y.; Jiang, K.; Fan, S. Fabrication of Ultralong and Electrically Uniform Single-Walled Carbon Nanotubes on Clean Substrates. **2009**, 1–5.

31. Tuloup, C.; Harizi, W.; Aboura, Z.; Meyer, Y.; Khellil, K.; Lachat, R. On the use of in-situ piezoelectric sensors for the manufacturing and structural health monitoring of polymer-matrix composites : A literature review. *Compos. Struct.* **2019**, *215*, 127–149, doi:10.1016/j.compstruct.2019.02.046.

32. Yu, A.M.; Lourie, O.; Dyer, M.J.; Moloni, K.; Kelly, T.F.; Ruoff, R.S.; Yu, M.; Lourie, O.; Dyer, M.J.; Moloni, K.; et al. Strength and Breaking Mechanism of Multiwalled Carbon Nanotubes Under Tensile Load. **2000**, *287*, 637–640.

33. Filleter, T.; Bernal, R.; Li, S.; Espinosa, H.D. Ultrahigh Strength and Stiffness in Cross-Linked Hierarchical Carbon Nanotube Bundles., doi:10.1002/adma.201100547.

34. Hamada, N.; Sawada, S.; Oshiyama, A. New one-dimensional conductors : Graphitic microtubules. **1992**, doi:10.1103/PhysRevLett.68.1579.

35. Electronics, N. A flexible approach to mobility. **2007**, *2*, 207–208.

36. Charlier, J. Electronic and transport properties of nanotubes. **2007**, *79*, 677–732, doi:10.1103/RevModPhys.79.677.

37. Broadbent, S.R.; Hammersley, J.M. Percolation processes: I. Crystals and mazes. *Math. Proc. Cambridge Philos. Soc.* **2020**, *53*, 629–641.

38. Dietrich Stauffer, A.A. *Introduction to PERCOLATION THEORY*; London, Ed.; 2nd Editio.; Taylor & Francis, 1992; ISBN 9781315274386.

39. Kirkpatrick, S.; Thomas, I.B.M.; Heights, Y.; York, N. THE NATURE OF PERCOLATION 'CHANNELS.' *Solid State Commun.* **1973**, *12*, 1279–1283.

40. Hu, N.; Fukunaga, H.; Atobe, S.; Liu, Y.; Li, J. Piezoresistive Strain Sensors Made from Carbon Nanotubes. *sensors* **2011**, *11*, 10691–10723, doi:10.3390/s111110691.

41. Tewari, A.; Gandla, S.; Bohm, S.; Mcneill, C.R.; Gupta, D. Highly Exfoliated MWNT − rGO Ink-Wrapped Polyurethane Foam for Piezoresistive Pressure Sensor Applications. *Appl. Mater. interfaces* **2018**, *10*, 5185–5195, doi:10.1021/acsami.7b15252.

42. Xu, X.-B.; Li, Z.-M.; Shi, L.; Bian, X.-C.; Xiang, Z.-D. Ultralight Conductive Carbon-Nanotube–Polymer Composite. *Small* **2007**, *3*, 408–411, doi:10.1002/smll.200600348.

43. Zhai, T.; Li, D.; Fei, G.; Xia, H. Piezoresistive and compression resistance relaxation behavior of water blown carbon nanotube/polyurethane composite foam. *Compos. Part A Appl. Sci. Manuf.* **2015**, *72*, 108–114, doi:10.1016/j.compositesa.2015.02.003.

44. Sensitive, H.; Sensor, P.; Nanoplatelets, G. A Flexible and Highly Sensitive Pressure

Sensor Graphene Nanoplatelets. **2016**, doi:10.3390/s16122148.

45. Asadi, A.; Alari, I.M.; Ali, V.; Nguyen, H.M. Ultrasonics - Sonochemistry An experimental investigation on the e ff ects of ultrasonication time on stability and thermal conductivity of MWCNT-water nano fl uid : Finding the optimum ultrasonication time. **2019**, *58*, doi:10.1016/j.ultsonch.2019.104639.

46. Ma, P.; Siddiqui, N.A.; Marom, G.; Kim, J. Dispersion and functionalization of carbon nanotubes for polymer-based nanocomposites : A review. *Compos. Part A* **2010**, *41*, 1345–1367, doi:10.1016/j.compositesa.2010.07.003.

47. Properties, C. Dispersion of Carbon Nanotubes: Mixing, Sonication, Stabilization, and Composite Properties. *Polymers (Basel).* **2012**, *4(1)*, 275–295, doi:10.3390/polym4010275.

48. Foundation, A.; Blaedel, W.J.; Wang, J.; Rochon, A.M.; Gesser, H.D.; Aubert, J.H.; Rand, P.B.; Arnold, C.; Clough, L.R.; Clough, R.L.; et al. Mechanical Damage of Carbon Nanotubes by Ultrasound. *Carbon (New York, NY)* **1996**, *34*, 814–816.

49. High, M.; Fluid, S.; Panagiotou, T.; Bernard, J.M.; Mesite, S.V.; Rd, O. Deagglomeration and Dispersion of Carbon Nanotubes Using Microfluidizer® High Shear Fluid Processors. *NSTI-Nanotech 2008* **2008**, *1*, 39–42.

50. Benali, M.; Gerbaud, V.; Hemati, M. Effect of operating conditions and physico – chemical properties on the wet granulation kinetics in high shear mixer. *Powder Technol.* **2009**, *190*, 160–169, doi:10.1016/j.powtec.2008.04.082.

51. Jiménez-suárez, A.; Campo, M.; Gaztelumendi, I.; Markaide, N.; Sánchez, M.; Ureña, A. The influence of mechanical dispersion of MWCNT in epoxy matrix by calendering method : Batch method versus time controlled. *Compos. Part B* **2013**, *48*, 88–94, doi:10.1016/j.compositesb.2012.12.011.

52. Chatterjee, S.; Nafezarefi, F.; Tai, N.H.; Schlagenhauf, L.; Nüesch, F.A.; Chu, B.T.T. Size and synergy effects of nanofiller hybrids including graphene nanoplatelets and carbon nanotubes in mechanical properties of epoxy composites. *Carbon N. Y.* **2012**, *50*, 5380–5386, doi:10.1016/j.carbon.2012.07.021.

53. Pötschke, P.; Krause, B.; Buschhorn, S.T.; Köpke, U.; Müller, M.T.; Villmow, T.; Schulte, K. Improvement of carbon nanotube dispersion in thermoplastic composites using a three roll mill at elevated temperatures. **2013**, *74*, 78–84, doi:10.1016/j.compscitech.2012.10.010.

54. Thostenson, E.T.; Chou, T. Processing-structure-multi-functional property relationship in carbon nanotube / epoxy composites. *Carbon N. Y.* **2006**, *44*, 3022–3029, doi:10.1016/j.carbon.2006.05.014.

55. Li, Y.B.; Wei, B.Q.; Liang, J.; Yu, Q.; Wu, D.H. Transformation of carbon nanotubes to nanoparticles by ball milling process. *Carbon N. Y.* **1999**, *37*, 493–497, doi:10.1016/S0008-6223(98)00218-8.

56. Sahoo, N.G.; Jung, Y.C.; Yoo, H.J.; Cho, J.W. Effect of Functionalized Carbon Nanotubes on Molecular Interaction and Properties of Polyurethane Composites. *Macromol. Chem. Phys.* **2006**, *207*, 1773–1780, doi:10.1002/macp.200600266.

57. Sui, G.; Liu, D.; Liu, Y.; Ji, W.; Zhang, Q.; Fu, Q. The dispersion of CNT in TPU matrix with different preparation methods : solution mixing vs melt mixing. *Polymer (Guildf).*

2019, *182*, 121838, doi:10.1016/j.polymer.2019.121838.

58. Gaboriaud, F.; Vantelon, J.P.; Chimie, G.D.R. De Mechanism of Thermal Degradation of Polyurethane Based on MDI and Propoxylated Trimethylol Propane. **1982**, *20*, 2063–2071.

59. Herrera, M.; Matuschek, G.; Kettrup, A. Thermal degradation of thermoplastic polyurethane elastomers (TPU) based on MDI. *Polym. Degrad. Stab.* **2002**, *78*, 323–331.

60. Karlsson, D.; Dahlin, J.; Skarping, G.; Dalene, M. Determination of isocyanates , aminoisocyanates and amines in air formed during the thermal degradation of polyurethane. *J. Environ. Monit* **2002**, *4*, 216–222, doi:10.1039/b110593k.

7 Summary of the activities performed during PhD

7.1 First Year

Courses completed successfully: Electrochemical energy storage and conversion systems, bioinspired materials, artificial photosynthesis: mimicking nature to produces the energy of the future, solid state NMR: basics and applications, Raman Day 2018 (PHD school for improving knowledge of the methodology).

PhD School: XXXIX Scuola AIM "Mario Farina" 2018, Italy, 13/05/18 – 18/05/18.

Seminars Conferences Attended: Recent advances in biosensor Technologies 22/11/17.
Cu Based zeolites, versatile materials for redox catalysis 20/07/2018.

7.2 Second year

Courses completed successfully: Introduction to Scientific Programming (in Python), Introduction to Crystallography, BC3-Elctron Diffraction, Instrument for X-Ray Diffraction, X-Ray diffraction, X-Ray diffraction Methods: Polycrystalline, Safety measurements for workers and researchers.

PhD School: Crystallography School, Turin (Italy), 27 May – 14 June 2019.
Innovative Catalysis and Sustainability: Scientific and Socio-Economic Aspects, Bardonecchia (Italy), 7th – 11th January 2019.
Seminars, Conferences Attended: Proplast plastics innovation pole ECCP – 2nd edition, Turin 23/10/2018.
PhD Workshop 2018, Turin 24-25 September 2018.

7.3 Third year

Courses completed successfully: Chemical Sensors for Scientific Research and Everyday Life.

Presentations: Oral presentation: "Laser Induced Selective Activation (LISA) Improves Electrical and Piezoresistive behaviour of Polymer Nanocomposites." – E. De Meo, A. Veca, V. Brunella, M. Zanetti – LSP 2020 – Webinar, 3-5 September 2020.

Poster presentation: "Laser Induced Selective Activation (LISA) Improves Electrical and Piezoresistive behaviour of Polymer Nanocomposites." – E. De Meo, A. Veca, V. Brunella, M. Zanetti – NanoInnovation 2020 – Rome,15-18 September 2020.

Papers:

- De Meo, E.; Agnelli, S.; Veca, A.; Brunella, V.; Zanetti, M; Piezoresistive and mechanical Behavior of CNT based polyurethane foam, J. Compos. Sci. 2020, Carbon-Based Polymer Nanocomposites, 4, 131.
- Valorosi, F.; De Meo, E.; Blanco-varela, T.; Martorana, B.; Veca, A.; et al. "Graphene and related materials in hierarchical fiber composites: Production techniques and key industrial benefits.", Compos. Sci. Technol. 2020, 185, 107848.
- Padovano, E.; Bonelli, M.E.; Veca, A.; De Meo, E.; Badini, C., "Effect of long-term mechanical cycling and laser surface treatment on piezoresistive properties of SEBS-CNTs composites.", React. Funct. Polym. 2020, 152, 104601.

Università degli Studi di Torino

Doctoral School of the University of Torino

PhD Programme in Chemical and Materials Sciences XXXIII cycle

Development of multifunctional materials for aesthetical and smart automotive components

Candidate: **Enea De Meo**

Supervisor: Prof. **Marco Zanetti**
Dott. Antonino Domenico Veca

Jury Members: Prof. **Maria Giovanna Pastore Carbone**
University of Patra (FORTH)
Department of chemical engineering sciences

Prof. **Andrea Raso**
Laboratori SFC Solutions Italy s.r.l.

Prof. **Pierangiola Bracco**
University of Turin
Department of Chemistry

Head of the Doctoral School: Prof. Alberto Rizzuti
PhD Programme Coordinator: Prof. Bartolome Civalleri

Torino, 2020